



EURONU-WP6-11-34

EUROnu-WP6 2010 Report

The EUROnu Working Package 6 (Physics)

S. K. Agarwalla¹, E. Akhmedov², M. Blennow³, P. Coloma^{4,5}, A. Donini^{1,5} (editor), E. Fernández Martínez³, C. Giunti⁶, J. J. Gómez Cadenas¹, M.C. González García^{7,8,9}, P. Hernández¹ (editor), P. Huber¹⁰, M. Laveder¹¹, T. Li¹², A. Longhin^{13,14}, J. López Pavón⁵, M. Maltoni⁵, D. Meloni¹⁵, O. Mena¹, J. Menéndez^{5,16,17}, M. Mezzetto¹¹, P. Migliozzi¹⁸, T. Ohlsson¹⁹, C. Orme¹², S. Pascoli¹², J. Salvado⁸, T. Schwetz², L. Scotto-Lavina^{20,21}, J. Tang¹⁵, F. Terranova¹⁴, W. Winter¹⁵ and H. Zhang¹⁹

September 14, 2012

- ¹ *Instituto de Física Corpuscular (IFIC), CSIC/UEVEG, Edificio Investigación Paterna, Apartado 22085, 46071 Valencia, Spain*
- ² *Max-Planck-Institut für Kernphysik, PO Box 103980, 69029 Heidelberg, Germany*
- ³ *Max-Planck-Institut für Physik (Werner-Heisenberg-Institut), Fohringer Ring 6, D-80805 Munich, Germany*
- ⁴ *Departamento de Física Teórica, Universidad Autónoma de Madrid, Cantoblanco, E-28049, Madrid, Spain*
- ⁵ *Instituto de Física Teórica, UAM/CSIC, Cantoblanco, E-28049, Madrid, Spain*
- ⁶ *Istituto Nazionale di Fisica Nucleare, Sezione di Torino, Via P. Giuria 1, I-10125 Torino, Italy*
- ⁷ *Institució Catalana de Recerca i Estudis Avançats (ICREA)*
- ⁸ *Departament d'Estructura i Constituents de la Matèria and Institut de Ciències del Cosmos, Universitat de Barcelona, Diagonal 647, E-08028 Barcelona, Spain*
- ⁹ *C.N. Yang Institute for Theoretical Physics, State University of New York at Stony Brook, Stony Brook, NY 11794-3840, USA*
- ¹⁰ *Center for Neutrino Physics, Virginia Tech, Blacksburg, VA 24061, USA*
- ¹¹ *Dipartimento di Fisica G. Galilei, Università di Padova and Istituto Nazionale di Fisica Nucleare, Sezione di Padova, Via Marzolo 8, I-35131, Padova, Italy*
- ¹² *Institute for Particle Physics Phenomenology, Department of Physics, University of Durham, Science Laboratories, South Rd, Durham, DH1 3LE, UK*
- ¹³ *Institut de Recherche sur les lois Fondamentales de l'Univers, CEA-Saclay, 91191 Gif-sur-Yvette, France*
- ¹⁴ *Istituto Nazionale di Fisica Nucleare, Laboratori Nazionali di Frascati, Frascati, Italy*
- ¹⁵ *Institut für Theoretische Physik und Astrophysik, Universität Würzburg, D-97074 Würzburg, Germany*
- ¹⁶ *Institut für Kernphysik, Technische Universität Darmstadt, 64289 Darmstadt, Germany*
- ¹⁷ *ExtreMe Matter Institute EMMI, GSI Helmholtzzentrum für Schwerionenforschung GmbH, 64291 Darmstadt, Germany*
- ¹⁸ *Istituto Nazionale di Fisica Nucleare, Sezione di Napoli, Italy*
- ¹⁹ *Department of Theoretical Physics, School of Engineering Sciences, KTH Royal Institute of Technology, AlbaNova University Center, Roslagstullsbacken 21, 106 91 Stockholm, Sweden*
- ²⁰ *University of Zurich, Physik-Institut, CH-8057 Zurich, Switzerland*
- ²¹ *Laboratoire SUBATECH, 4 rue Alfred Kastler, 44307 Nantes cedex 3, France*

Contents

1. Executive summary	2
2. The Physics case	4
2.1. The leptonic flavour sector [1]	5
2.2. θ_{13} : phenomenology, present status and prospect [2]	14
2.3. Direct Determination of the Solar Neutrino Fluxes from Neutrino Data [3]	19
3. A new design for the SPL-Fréjus Super-Beam [4]	23
4. Beta-Beams	25
4.1. Performances of Beta-Beam setups as of January 2011 [5]	25
4.2. Atmospheric neutrino events at ICAL@INO and high Q β -beam [6]	29
4.3. A minimal Beta Beam with high-Q ions to address leptonic CP violation [7]	31
4.4. Update on the physics of Electron Capture neutrino beams [8]	33
4.5. High- γ Beta Beams within the LAGUNA design study [9]	36
5. Physics at the Neutrino Factory	39
5.1. Neutrino Factory in stages [10]	39
5.2. LENF Overview [11]	41
5.3. The τ -contamination of the golden muon sample at the Neutrino Factory [12]	43
6. Physics beyond three-family oscillations	48
6.1. Neutrinoless double beta decay in seesaw models	48
6.2. Short-Baseline $\bar{\nu}_\mu \rightarrow \bar{\nu}_e$ Oscillations [13]	51
6.3. MiniBooNE/LSND data: NSI's in a (3+1)-scheme vs. (3+2)-oscillations [14]	53
6.4. Sterile neutrinos beyond LSND at the Neutrino Factory [15]	55
6.5. NSI's vs. non-unitary lepton flavor mixing at a neutrino factory [16]	57
6.6. Non-standard neutrino interactions in the Zee-Babu model [17]	60
7. Physics potential of EUROnu facilities as of April 2011 [18]	63
8. Summary of the NuFlavour workshop [19]	65
8.1. LFV from GUT see-saw models and from TeV see-saw models	65
8.2. Neutrino physics and the cosmology/astroparticle physics complementarity	65
8.3. A theoretical perspective on lepton flavor physics at the TeV scale within i) SUSY models ii) extra-dimension models	66
8.4. Leptogenesis in the context of neutrino mass models: model dependent versus model independent considerations	66
8.5. Interplay between neutrino masses and other phenomenological signatures	67
8.6. Discussion on performance indicators in long baseline experiments	67

8.7. Conclusions

67

References

68

1. Executive summary

The phenomenon of neutrino oscillations, arguably the most significant advance in particle physics over the past decade, has been established through measurements on neutrinos and anti-neutrinos produced in the sun, by cosmic-ray interactions in the atmosphere, nuclear reactors, and beams produced by high-energy particle accelerators. In consequence, we know that the Standard Model is incomplete and must be extended to include neutrino mass, mixing among the three neutrino flavours, and therefore lepton-flavour non conservation. These observations have profound implications for the ultimate theory of particle interactions and for the description of the structure and evolution of the Universe.

These exciting possibilities justify an energetic and far reaching programme, an essential part of which is to make precision measurements of the oscillation parameters. Assuming the three flavours and the unitary neutrino-mixing matrix that is presently favoured, oscillation measurements can be used to determine the three mixing angles and the critical phase parameter that can provide a new source of CP-invariance violation. Neutrino oscillation measurements can also be used to determine the two (signed) mass differences. This programme is similar to the long-standing investigations of quark mixing via the CKM matrix and it would now seem to be clear that an understanding of the flavour problem will definitely need precision measurements in both quark and lepton sectors.

Not all the properties of the neutrino can be determined by oscillation experiments. Equally important is the determination of the Majorana or Dirac nature of the neutrino which requires the ongoing and planned neutrinoless double beta decay experiments. In addition, although oscillation measurements determine the mass differences, they are insensitive to the absolute mass, m_1 , of the lightest mass state. The determination of m_1 requires a very precise measurement of the end-point of the electron spectrum in beta decay.

Coordination and Outreach

The members of WP6 have held meetings during the general meeting at Strasbourg in June 2010, at the CERN workshop NuThemes in September 2010 and at the Rutherford lab during the IDS-NF meeting also in September 2010. A summary of the EURONU-WP6 workshop held at from 8-10 June 2009 at Cosener's House, Abingdon, UK on the subject "Flavour physics in the era of precision neutrino experiments" has been included in this report.

The group has kept close contact with the IDS-NF concerning the physics of the neutrino factory, with WP4 as regards the scenarios for the beta-beam and with WP5 as regards detector performance and systematic errors. During 2010, the WP6 results of the first year of the project (2009) were summarized in a report that was submitted to the archives to inform the wider community [20].

Global analysis and interpretation of present data

The members of WP6 have carried out a number of important studies for the EURONU project. The first is a revision of the global analysis of neutrino oscillation data including the latest results, such as those from MiniBOONE and MINOS, as well as new cosmological data. The values of the atmospheric and solar parameters and the bounds on the angle θ_{13} are of course essential for the physics optimization of future facilities. Obviously if there is physics beyond the standard three-neutrino scenario, for example the presence of new sterile species, this could also change drastically the optimization of baseline and energy of the neutrino beam.

Evaluation of physics performance, optimization and comparison

A number of studies of the physics potential of the future facilities as regards the standard three-neutrino oscillation scenario, as well as new physics, have been performed during the past year. The results have been published in peer-review journals and are also listed as EURONU documents, or will be presented here as internal documents. Between these, the report contains a new design of the SPL-Fréjus Super-Beam is included (see Ref. [4] for more details), the study of the potential of high- γ electron-capture beta-beams in the context of the LAGUNA european project has also been reviewed [9], a review of all beta-beam setups that have been discussed in the literature in the past [5] and a dedicated study of atmospheric neutrino backgrounds at the ICAL@INO detector exposed to a high- γ β -beam [6].

Tools for physics studies

A new release of the GLOBES package including migration matrices for signal and background was made available during 2010.

2. The Physics case

The main motivation of a future neutrino physics programme is to unveil what the new physics associated to neutrino masses is. We know for sure that new degrees of freedom must be added to the Standard Model (e.g. right-handed neutrinos) at some energy scale Λ . If Λ is much larger than the electroweak scale, there is a natural explanation of why neutrinos are so light. Indeed the effects of *any* such new physics must be generically well described at low energies by an effective Lagrangian which contains the Standard Model, plus a tower of higher dimensional operators constructed with the SM fields and satisfying all the gauge symmetries:

$$\mathcal{L} = \mathcal{L}_{SM} + \sum_i \frac{\alpha_i}{\Lambda} \mathcal{O}_i^{d=5} + \sum_i \frac{\beta_i}{\Lambda^2} \mathcal{O}_i^{d=6} + \dots \quad (1)$$

The effective operators, \mathcal{O}_i , are ordered by their mass dimension, since the higher the dimension, the higher the power of Λ that suppresses them. The dominant operator is therefore the lowest dimensional one, with $d = 5$, which is precisely the Weinberg's operator:

$$\mathcal{O}^{d=5} = \bar{L}^c \Phi \Phi L, \quad (2)$$

which, as is well known, induces three new ingredients to the minimal SM:

- Neutrino masses
- Lepton mixing
- Lepton number violation

In this context, neutrino masses are very small, because they come from an effective operator which is suppressed by a high energy scale. If we go to operators of $d = 6$, that are suppressed by two powers of Λ , these will generically induce new physics in dipole moments, rare decays, etc. Beyond $d = 6$ we would find operators inducing non-standard neutrino interactions (NSI).

It is also possible that the scale Λ is at or below the electroweak scale, or in other words that neutrino masses are linked to light degrees of freedom, *i.e.* a *hidden* sector which we have not detected yet, because it is weakly interacting. Such scenarios do not offer an explanation of why neutrinos are light, but neutrinos are the natural messengers with such hidden sectors, since they are the only particles in the SM carrying no conserved charge. Such new physics could be related to other fundamental problems in particle physics such as the origin of dark matter and dark energy.

Even though it is not guaranteed that we can fully understand the new physics associated to neutrino masses by measuring them, it is quite clear that we have a good chance to learn something more about it by testing the Standard scenario of 3ν mixing with future and more precise neutrino experiments. In particular we should be able to measure all the fundamental parameters: three mass eigenstates (m_1^2, m_2^2, m_3^2), three angles ($\theta_{12}, \theta_{13}, \theta_{23}$) and one or three CP-violating phases ($\delta, \alpha_1, \alpha_2$). But, also, it will be very important to search for new physics beyond neutrino masses and mixings, in particular for those effects that are generic in many models of neutrino masses, such as violations of unitarity, non-standard interactions or the presence of light sterile species. To some extent these searches can also be improved in future facilities and this should be evaluated. Typically such analyses imply

dealing with a much larger parameter space, which calls for new tools to perform the fits, in particular Montecarlo methods.

Many studies in the last ten years have shown that we can measure θ_{13} , discover leptonic CP violation and determine the neutrino hierarchy in more precise neutrino oscillation experiments, searching for the subleading channel $\nu_e \leftrightarrow \nu_\mu$ or its CP-conjugate channel $\nu_\mu \leftrightarrow \nu_e$ in the atmospheric range. In this first section, we present the results obtained within the work of EUROnu-WP6 in 2010 concerning: the status of leptonic mixing global fits [1]; the prospects for θ_{13} searches [2]; and, the direct determination of solar neutrino fluxes from solar neutrino data [3].

2.1. The leptonic flavour sector [1]

It is now an established fact that neutrinos are massive and leptonic flavors are not symmetries of Nature [21, 22]. In the last decade this picture has become fully proved thanks to the upcoming of a set of precise experiments. In particular, the results obtained with solar [23–32] and atmospheric neutrinos [33, 34] have been confirmed in experiments using terrestrial beams: neutrinos produced in nuclear reactors [35, 36] and accelerators [37–40] facilities have been detected at distances of the order of hundreds of kilometers [41].

The minimum joint description of all the neutrino data requires mixing among all the three known neutrinos (ν_e, ν_μ, ν_τ), which can be expressed as quantum superpositions of three massive states ν_i ($i = 1, 2, 3$) with masses m_i . This implies the presence of a leptonic mixing matrix in the weak charged current interactions [42, 43] which can be parametrized as:

$$U = \begin{pmatrix} 1 & 0 & 0 \\ 0 & c_{23} & s_{23} \\ 0 & -s_{23} & c_{23} \end{pmatrix} \cdot \begin{pmatrix} c_{13} & 0 & s_{13}e^{-i\delta_{\text{CP}}} \\ 0 & 1 & 0 \\ -s_{13}e^{i\delta_{\text{CP}}} & 0 & c_{13} \end{pmatrix} \cdot \begin{pmatrix} c_{21} & s_{12} & 0 \\ -s_{12} & c_{12} & 0 \\ 0 & 0 & 1 \end{pmatrix} \cdot \begin{pmatrix} e^{i\eta_1} & 0 & 0 \\ 0 & e^{i\eta_2} & 0 \\ 0 & 0 & 1 \end{pmatrix}, \quad (3)$$

where $c_{ij} \equiv \cos \theta_{ij}$ and $s_{ij} \equiv \sin \theta_{ij}$. In addition to the Dirac-type phase δ_{CP} , analogous to that of the quark sector, there are two physical phases η_i associated to the Majorana character of neutrinos and which are not relevant for neutrino oscillations [44, 45].

Given the observed hierarchy between the solar and atmospheric mass-squared splittings there are two possible non-equivalent orderings for the mass eigenvalues, which are conventionally chosen as

$$m_1 < m_2 < m_3 \quad \text{with} \quad \Delta m_{21}^2 \ll |\Delta m_{31}^2 \simeq \Delta m_{32}^2| \quad \text{and} \quad \Delta m_{31}^2 > 0; \quad (4)$$

$$m_3 < m_1 < m_2 \quad \text{with} \quad \Delta m_{21}^2 \ll |\Delta m_{31}^2 \simeq \Delta m_{32}^2| \quad \text{and} \quad \Delta m_{31}^2 < 0. \quad (5)$$

As it is customary we refer to the first option, Eq. (4), as the *normal* (N) scheme, and to the second one, Eq. (5), as the *inverted* (I) scheme; in this form they correspond to the two possible choices of the sign of Δm_{31}^2 . In this convention the angles θ_{ij} can be taken without loss of generality to lie in the first quadrant, $\theta_{ij} \in [0, \pi/2]$, and the phases $\delta_{\text{CP}}, \eta_i \in [0, 2\pi]$.

Thanks to the synergy amongst a variety of experiments involving solar and atmospheric neutrinos, as well as man-made neutrinos at nuclear power plants and accelerators, we have now a relatively detailed picture of the parameters describing three-flavor neutrino oscillations [1, 46–48].

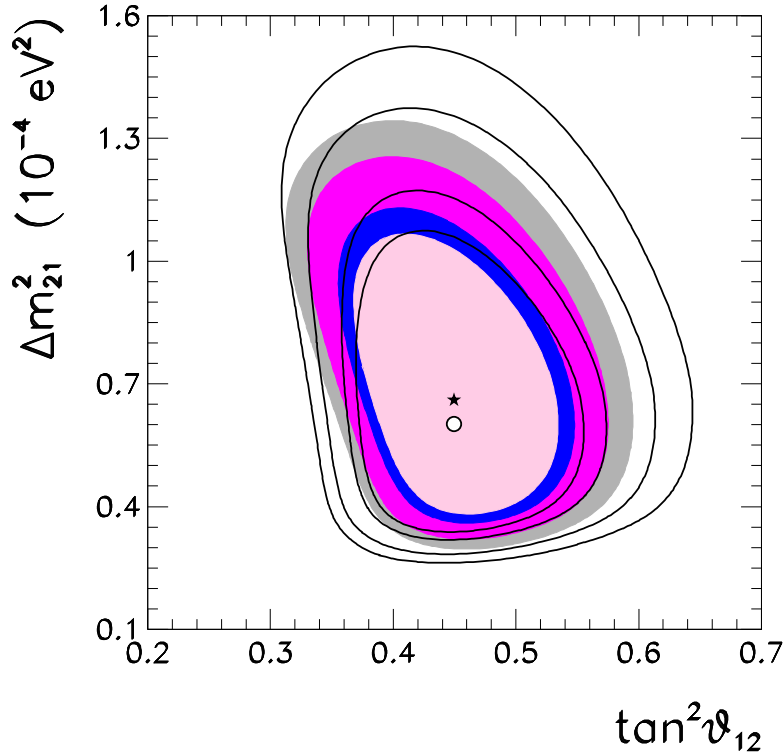


Figure 1. Allowed parameter regions (at 90%, 95%, 99% and 99.73% CL for 2 d.o.f.) from the combined analysis of solar data for $\theta_{13} = 0$. The best-fit point is marked with a star. For comparison we also show as empty regions (the best-fit is marked by a circle) the results prior to the inclusion of the latest Ga capture rate of SAGE [25], the energy spectrum of Borexino [31, 32] and the low energy threshold analysis of the combined SNO phase I and phase II [30]. In both analysis we use as inputs the GS98 solar model fluxes and the Gallium capture cross-section of Bahcall [49].

2.1.1. Leading Δm_{21}^2 oscillations: solar and KamLAND data

In the analysis of solar neutrino experiments we include the total rates from the radiochemical experiments Chlorine [23], Gallex/GNO [24] and SAGE [25]. For real-time experiments we include the 44 data points of the electron scattering (ES) Super-Kamiokande phase I (SK-I) energy-zenith spectrum [26] and the data from the three phases of SNO [27–29], including the results on the low energy threshold analysis of the combined SNO phase I and phase II [30] (which we label SNO-LETA). We also include the main set of the 192 days of Borexino data [31] (which we label Borexino-LE) as well as their high-energy spectrum from 246 live days [32] (Borexino-HE).

In Fig. 1 we show the present determination of the leading parameters Δm_{21}^2 and θ_{12} from the updated oscillation analysis of the solar neutrino data described above in the context of the GS98 solar model. For comparison we also show the results obtained prior to the inclusion of the latest Ga capture rate of SAGE [25], the energy spectrum of Borexino [31, 32] and the SNO-LETA results [30] for the same solar model. As seen in this figure, the inclusion of these results lead to an improvement on

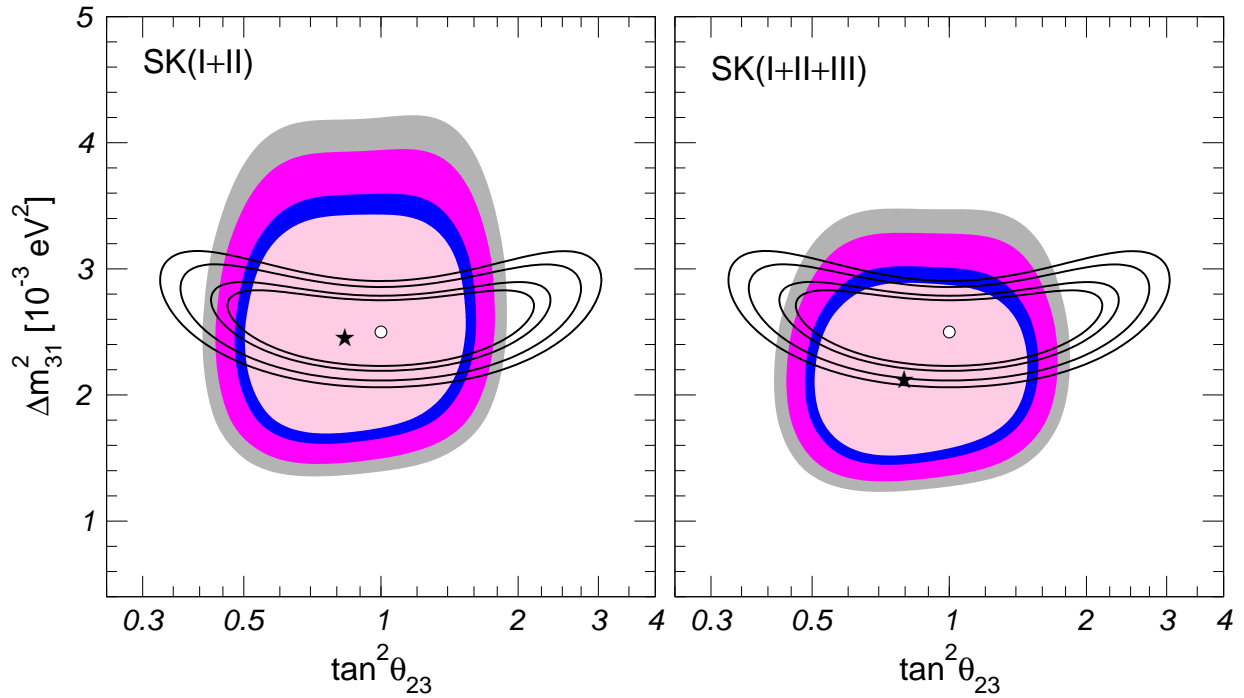


Figure 2. Allowed parameter regions (at 90%, 95%, 99% and 99.73% CL for 2 d.o.f.) from the analysis of atmospheric data (full regions, best-fit marked with a star) and LBL data (void regions, best-fit marked by a circle) for $\theta_{13} = 0$ and $\Delta m_{21}^2 = 7.6 \times 10^{-5} \text{ eV}^2$.

the determination of both θ_{12} and Δm_{21}^2 and for this last one the best-fit value slightly increases. The most quantitatively relevant new information arises from the inclusion of the SNO-LETA results. The inclusion of Borexino tends to shift the region towards slightly lower values of θ_{12} angle. Conversely, if the analysis is done in the context of the AGSS09 model the region is shifted towards slightly larger θ_{12} .

2.1.2. Leading Δm_{31}^2 oscillations: atmospheric and accelerator data

In this section we present two different analyses of the atmospheric data. The first one is very similar to the one detailed in Ref. [41], and includes the results from the first run of Super-Kamiokande, which accumulated data from May 1996 to July 2001 (1489 day exposure) and is usually referred as SK-I [33], as well as the data obtained with the partial coverage after the 2001 accident (804 day exposure), the so-called SK-II period [50]. We will refer to this analysis as SK(I+II). The second one is based on the new analysis recently presented by the Super-Kamiokande collaboration including also the data taken from December 2005 to June 2007, usually referred as SK-III [34]. Apart from the inclusion of these new event rates, in this data release the selection criteria and the corresponding estimate of uncertainties for the SK-I and SK-II periods have been changed with respect to the previous SK(I+II) analysis. We have therefore performed a reanalysis of the new combined samples from phases I, II

and III as presented in [34]. We refer to the results of this analysis as SK(I+II+III). It is important to point out that already since SK-II the Super-Kamiokande collaboration has been presenting its experimental results in terms of a large number of data samples. The rates for some of those samples cannot be theoretically predicted (and therefore include in a statistical analysis) without a detailed simulation of the detector which can only be made by the experimental collaboration itself. Thus our results represent the most up-to-date analysis of the atmospheric neutrino data which can be performed outside the collaboration. For details on our simulation of the data samples and the statistical analysis see the Appendix of Ref. [41].

For what concerns LBL accelerator experiments, we combine the results on ν_μ disappearance from K2K [37] with those obtained by MINOS at a baseline of 735 km after a two-year exposure to the Fermilab NuMI beam, corresponding to a total of 3.36×10^{20} protons on target [38]. We also include the recent results on $\nu_\mu \rightarrow \nu_e$ transitions based on an exposure of 7×10^{20} protons on target [51, 52].

In order to test the description of the present data in the absence of θ_{13} -induced effects we show in Fig. 2 the present determination of the leading parameters Δm_{31}^2 and θ_{23} for $\theta_{13} = 0$ and $\Delta m_{21}^2 = 7.6 \times 10^{-5} \text{ eV}^2$ from the two atmospheric neutrino analyses and the LBL accelerator results. For concreteness we plot only normal ordering; the case of inverted ordering gives practically identical results as long as $\theta_{13} = 0$. This figure illustrates how the bounds on the oscillation parameters θ_{23} and Δm_{31}^2 emerges from a complementarity of atmospheric and accelerator neutrino data: $|\Delta m_{31}^2|$ is determined by the spectral data from MINOS, whereas the mixing angle θ_{23} is still largely dominated by atmospheric data from Super-Kamiokande with a best-fit point close to maximal mixing. It is interesting to note that there is a very good agreement in the location of the best-fit points from SK(I+II) and MINOS. This is not the case for SK(I+II+III) for which the best-fit point in $|\Delta m_{31}^2|$ is now lower than the one obtained from LBL.

2.1.3. Status of θ_{13} from global data in 2010

The third mixing angle θ_{13} is of crucial importance for future oscillations experiments. Fig. 3 summarizes the information on θ_{13} from present data, which emerges from an interplay of different data sets. An important contribution to the bound comes, of course, from the CHOOZ reactor experiment [54] combined with the determination of $|\Delta m_{31}^2|$ from atmospheric and long-baseline experiments. Using this set of data, a possible hint for a non-zero θ_{13} from atmospheric data has been found in Refs. [55, 56]. The origin of such a hint has been investigated in some detail in Ref. [48], and more recently in [1, 57]. From these results one may conclude that the statistical relevance of the hint for non-zero θ_{13} from atmospheric data depends strongly on the details of the rate calculations and of the χ^2 analysis. Furthermore, the origin of that effect might be traced back to a small excess (at the 1σ level) in the multi-GeV e -like data sample in SK-I, which however is no longer present in the combined SK(I+II) data and is extremely weak in SK(I+II+III) data. A very recent analysis (neglecting subleading Δm_{21}^2 effects) from the Super-Kamiokande collaboration finds no evidence of such a hint [34].

Another fragile indication of non-zero θ_{13} arises from the results of the MINOS experiment. In Ref. [39] the first results on the search for $\nu_\mu \rightarrow \nu_e$ transitions were reported, based on an exposure of 3.14×10^{20} protons-on-target in the Fermilab NuMI beam. The collaboration observed 35 events in the Far Detector with a background of 27 ± 5 (stat) ± 2 (syst), corresponding to a 1.5σ excess which could be explained by a non-zero value of θ_{13} . Recently a new analysis with double statistics (exposure of 7×10^{20}) has been presented [51, 52]. The MINOS collaboration reported the observation of 54 events with an expected background of 49.1 ± 7.0 (stat) ± 2.7 (syst), thus reducing the excess above background to 0.7σ .

An important piece of information on θ_{13} comes from solar and KamLAND data. The relevant survival probabilities are given by

$$P_{ee} \approx \begin{cases} \cos^4 \theta_{13} (1 - \sin^2 2\theta_{12} \langle \sin^2 \phi \rangle) & \text{solar, low energies / KamLAND} \\ \cos^4 \theta_{13} \sin^2 \theta_{12} & \text{solar, high energies} \end{cases} \quad (6)$$

where $\phi = \Delta m_{21}^2 L/4E$ and $\langle \sin^2 \phi \rangle \approx 1/2$ for solar neutrinos. Eq. (6) implies an anti-correlation of $\sin^2 \theta_{13}$ and $\sin^2 \theta_{12}$ for KamLAND and low energy solar neutrinos. In contrast, for the high energy part of the spectrum, which undergoes the adiabatic MSW conversion inside the sun and which is subject to the SNO CC/NC measurement, a positive correlation of $\sin^2 \theta_{13}$ and $\sin^2 \theta_{12}$ emerges. As discussed already in [58, 59], this complementarity leads to a non-trivial constraint on θ_{13} and it allows to understand the hint for a non-zero value of θ_{13} , which helps to reconcile the slightly different best fit points for θ_{12} as well as for Δm_{21}^2 for solar and KamLAND separately [41, 56, 59–61].

We found that the inclusion of the new solar data, and in particular of the SNO-LETA results tends to lower the statistical significance of $\theta_{13} \neq 0$ while the results from ν_e appearance from MINOS increases it. Within the context of the solar model with higher metallicities (GS98) and for the original Ga capture cross-section [49], we conclude that the significance of $\theta_{13} \neq 0$ from solar+KamLAND data is 79% (1.26σ) which increases to 81% (1.31σ) after inclusion of the atmospheric, CHOOZ and LBL data. We also found that using the solar neutrino fluxes required to fit the lower metallicity data (AGSS09) and/or the modified (lower) cross-section for neutrino capture in Ga lowers the best fit value of θ_{13} and its statistical significance. So when using the AGSS09 fluxes and the lower Ga cross-section the significance of $\theta_{13} \neq 0$ from solar+KamLAND data is 70% (1.05σ) and 76% (1.17σ) for adding atmospheric, CHOOZ and LBL data.

2.1.4. Tritium beta decay experiments

The neutrino mass scale is constrained in laboratory experiments searching for its kinematic effects in Tritium β decay which are sensitive to the so-called effective electron neutrino mass [62–64]

$$m_{\nu_e}^2 \equiv \sum_i m_i^2 |U_{ei}|^2 = c_{13}^2 c_{12}^2 m_1^2 + c_{13}^2 s_{12}^2 m_2^2 + s_{13}^2 m_3^2, \quad (7)$$

At present the most precise determination from the Mainz [65] and Troitsk [66] experiments give no indication in favor of $m_{\nu_e} \neq 0$ and one sets an upper limit

$$m_{\nu_e} < 2.2 \text{ eV}, \quad (8)$$

at 95% confidence level (CL). A new experimental project, KATRIN [67], is under construction with an estimated sensitivity limit: $m_{\nu_e} \sim 0.2 \text{ eV}$.

2.1.5. Neutrinoless double-beta decay experiments

Direct information on neutrino masses can also be obtained from neutrinoless double beta decay ($0\nu\beta\beta$) searches provided they are Majorana particles. In the absence of other sources of lepton number violation in the low energy Lagrangian, the $0\nu\beta\beta$ decay amplitude is proportional to the effective Majorana mass of ν_e , m_{ee} ,

$$m_{ee} = \left| \sum_i m_i U_{ei}^2 \right| = \left| c_{13}^2 c_{12}^2 m_1 e^{i\eta_1} + c_{13}^2 s_{12}^2 m_2 e^{i\eta_2} + s_{13}^2 m_3 e^{-i\delta_{\text{CP}}} \right|, \quad (9)$$

which, in addition to the masses and mixing parameters that affect the tritium beta decay spectrum, depends also on the phases in the leptonic mixing matrix. The strongest bound from $0\nu\beta\beta$ decay was imposed by the Heidelberg-Moscow group [68]

$$m_{ee} < 0.26 \text{ (0.34) eV} \quad \text{at 68\% (90\%) CL}, \quad (10)$$

which holds for a given prediction of the nuclear matrix element. However, there are large uncertainties in those predictions which may considerably weaken the bound [69]. A series of new experiments is planned with sensitivity of up to $m_{ee} \sim 0.01 \text{ eV}$ [70].

2.1.6. The impact of cosmological fits

Neutrino oscillation data provides as unique information on the absolute neutrino mass scale a lower bound

$$\Sigma_\nu \equiv \sum_i m_i \gtrsim \begin{cases} \sqrt{|\Delta m_{31}^2|} & \text{for Normal hierarchy,} \\ 2\sqrt{|\Delta m_{31}^2|} & \text{for Inverted hierarchy.} \end{cases} \quad (11)$$

Furthermore, neutrinos, like any other particles, contribute to the total energy density of the Universe. Furthermore within what we presently know of their masses, the three Standard Model (SM) neutrinos are relativistic through most of the evolution of the Universe and they are very weakly interacting which means that they decoupled early in cosmic history. Depending on their exact masses they can impact the CMB spectra, in particular by altering the value of the redshift for matter-radiation equality. More importantly, their free streaming suppresses the growth of structures on scales smaller

than the horizon at the time when they become non-relativistic and therefore affects the matter power spectrum which is probed from surveys of the LSS distribution (see [71] for a detailed review of cosmological effects of neutrino mass).

Within their present precision, cosmological observations are sensitive to neutrinos only via their contribution to the energy density in our Universe, $\Omega_\nu h^2$ (where h is the Hubble constant normalized to $H_0 = 100 \text{ km s}^{-1} \text{ Mpc}^{-1}$). $\Omega_\nu h^2$ is related to the total mass in the form of neutrinos

$$\Omega_\nu h^2 = \Sigma_\nu / (94 \text{ eV}). \quad (12)$$

Therefore cosmological data mostly gives information on the sum of the neutrino masses and has very little to say on their mixing structure and on the ordering of the mass states (see Ref. [72] for a recent update on the sensitivity of future cosmological observations to the mass ordering.)

In Ref. [73] we have studied the information on the absolute value of the neutrino mass which can be obtained from the analysis of the cosmological data in $\omega\text{CDM} + \Delta N_{\text{rel}} + m_\nu$ cosmologies where, besides neutrino masses, one allows for non-vanishing curvature, dark energy with equation of state with $\omega \neq -1$ together with the presence of new particle physics whose effect on the present cosmological observations can be parametrized in terms of additional relativistic degrees of freedom. To break the degeneracies in these models, at least the information from four different cosmological probes must be combined. Thus we have performed analysis including the data from CMB experiments, the present day Hubble constant H_0 , measurement, the high-redshift Type-I SN results and the information from large scale LSS surveys.

In Fig. 4 we plot the 95% allowed regions (for 2 dof) in the planes (m_{ν_e}, Σ_ν) and (m_{ee}, Σ_ν) . In the figure we also show superimposed the single parameter 95% bounds on Σ_ν from different cosmological analysis. The figure illustrates the well-known fact that currently for either mass ordering the results from neutrino oscillation experiments imply a lower bound on m_{ν_e} . On the contrary m_{ee} is only bounded from below for the case of the normal ordering while full cancellation due to the unknown Majorana phases is still allowed for the inverted ordering. These results show that, even for the most restrictive analysis including LSSPS, part of the allowed ranges for m_{ν_e} in the context of the $\omega\text{CDM} + \Delta N_{\text{rel}} + m_\nu$ cosmologies are within the reach of the KATRIN experiment. This is not the case for $\Lambda\text{CDM} + m_\nu$ models unless only the information of CMB and BAO (or SN) is included. We also find that near future neutrinoless double beta decay can test some of the allowed ranges in all these scenarios. This will be complementary to the improvement on the expected sensitivity from upcoming cosmological probes such as the Planck mission [74].

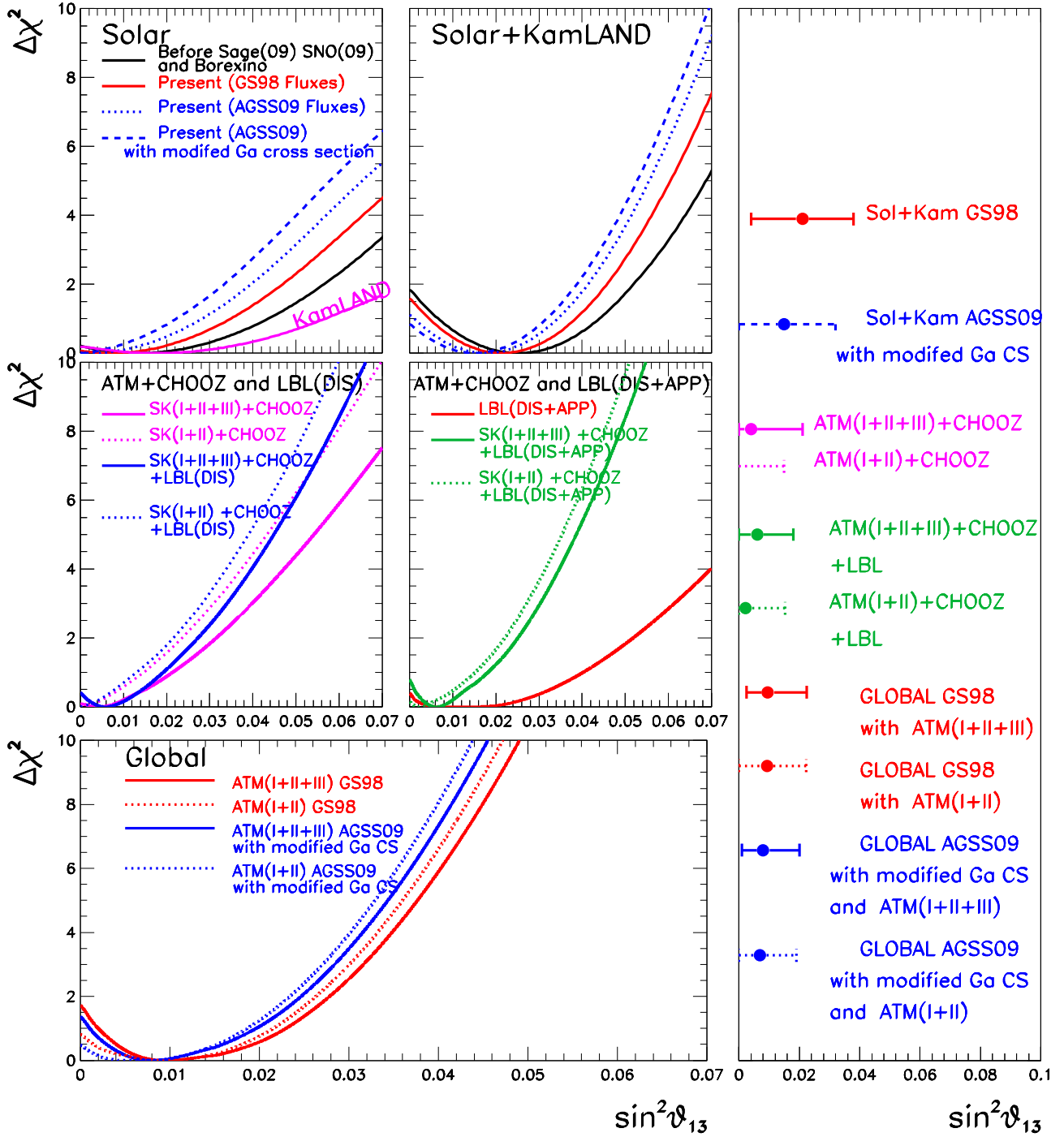


Figure 3. $\Delta\chi^2$ dependence on $\sin^2\theta_{13}$ from various data sets as labeled in the figure. The right panel shows 1σ ranges [1]. AGSS09 and GS98 refer to low and high metallicity solar models, respectively [53].

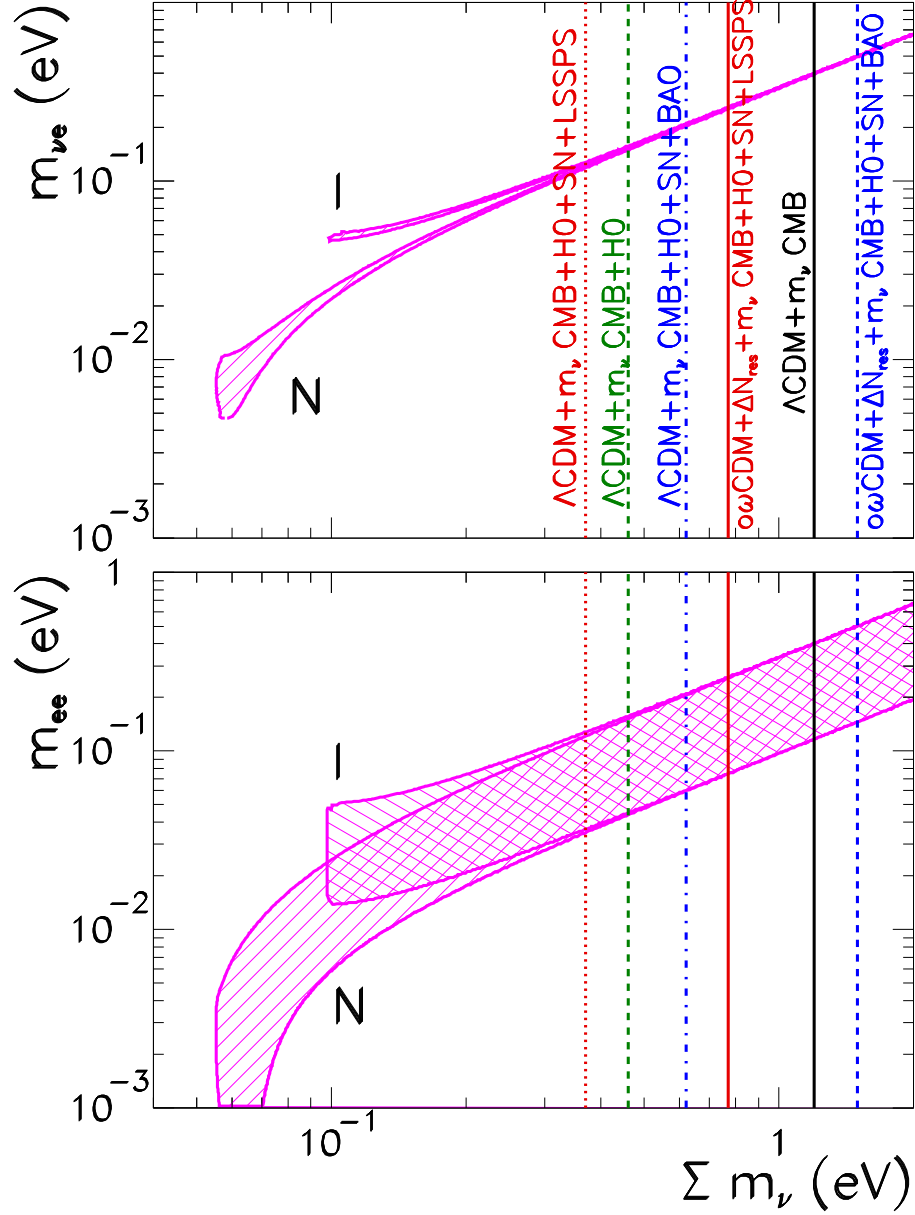


Figure 4. 95% allowed regions (for 2 dof) in the planes $(m_{\nu e}, \Sigma_\nu)$ and (m_{ee}, Σ_ν) from the global analysis of oscillation data (full regions). We also show superimposed the 95% upper bounds on Σ_ν from cosmological constraints for the different analysis as labeled in the figure.

2.2. θ_{13} : phenomenology, present status and prospect [2]

The leptonic mixing angle θ_{13} is currently a high-priority topic in the field of neutrino physics, with five experiments under way, searching for neutrino oscillations induced by this angle: the reactor neutrino experiments Daya Bay [75], Double Chooz [76], RENO [77] and the accelerator experiments NO ν A [78] and T2K [79]. The results of these experiments will be essential for the planning towards a possible next generation of long-baseline neutrino experiments able to address leptonic CP violation and the neutrino mass hierarchy.

On the theoretical side, the determination of θ_{13} will provide important information on the mechanism of neutrino mass generation and the flavour structure in the lepton sector. Considering neutrino mass models without any flavour structure, so-called anarchical models, one does expect a value of θ_{13} close to the present bound [80]. If on the contrary experiments would indicate a very tiny value for θ_{13} one might wish to have a symmetry reason as an explanation. For example, rather symmetric patterns for the mixing matrix are the tri-bimaximal [81] or the bimaximal [82] mixing matrices.

The present situation obtained in the global fit of all relevant oscillation data, can be summarized according to the updated analysis of [47]. The following bounds at 90% (3) CL are obtained:

$$\sin^2 \theta_{13} \leq \begin{cases} 0.053(0.078) & \text{solar + KamLAND} \\ 0.033(0.058) & \text{CHOOZ + atm + K2K + MINOS} \\ 0.031(0.047) & \text{global data} \end{cases} \quad (13)$$

The hint for $\theta_{13} > 0$ coming from the different data sets can be quantified by considering the $\Delta\chi^2$ for $\theta_{13} = 0$:

$$\sin^2 \theta_{13} \leq \begin{cases} 2.2(1.5) & \text{solar + KamLAND} \\ 0.8(0.9) & \text{CHOOZ + atm + K2K + MINOS} \\ 0.6(0.7) & \text{MINOS } \nu_e \text{ appearance} \\ 1.8(1.3) & \text{global data} \end{cases} \quad (14)$$

In table I are compared the best-fit values for $\sin^2 \theta_{13}$ and the significance of the hint for $\theta_{13} > 0$ from the global fits to neutrino oscillation data from three different groups. All groups find a non-zero best-fit point in the range $\sin^2 \theta_{13} = 0.01 - 0.02$. While it is premature to draw strong conclusions from these results, upcoming experiments will answer very soon the question whether θ_{13} is indeed in the range indicated by present global analyses. Reactor experiments see a large signal of $\bar{\nu}_e$ events, and search for a small deviation from the non-oscillation prediction due to θ_{13} -induced $\bar{\nu}_e$ disappearance. These are a precision experiment, whose success relies on statistical as well as systematic errors below the percent level. Table II summarises a few key parameters of reactor experiments. Accelerator experiments look for the appearance of the ν_e flavour in an almost pure ν_μ beam, due to oscillations.

The T2K (TokaitoKamioka) experiment [79] will use a high intensity off-axis (2.5°) neutrino beam, with a peak energy of 700 MeV, generated by a 30 GeV proton beam at J-PARC (Japan Proton

reference	best-fit and 1σ errors	significance
Fogli et al. [57]	$\sin^2 \theta_{13} = 0.02 \pm 0.01$	2σ
Gonzalez-Garcia et al. [1] (GS98)	$\sin^2 \theta_{13} = 0.0095_{-0.007}^{+0.013}$	1.3σ
Gonzalez-Garcia et al. [1] (AGSS09)	$\sin^2 \theta_{13} = 0.008_{-0.007}^{+0.012}$	1.1σ
Schwetz et al. [47] (GS98)	$\sin^2 \theta_{13} = 0.013_{-0.010}^{+0.013}$	1.5σ
Schwetz et al. [47] (AGSS09)	$\sin^2 \theta_{13} = 0.010_{-0.008}^{+0.013}$	1.3σ

Table I. Comparison of the best-fit values for $\sin^2 \theta_{13}$ and the significance of the hint for $\theta_{13} > 0$ from different global fits to neutrino oscillation data. The numbers from [1] and [47] include 7×10^{20} pot ν_e appearance data from MINOS, whereas [57] is based on 3.14×10^{20} pot. AGSS09 and GS98 refer to low and high metallicity solar models, respectively [53].

Setup	P_{Th} [GW]	L [m]	m_{Det} [t]	Events/year	Backgrounds/day
Daya Bay [75]	17.4	1700	80	$10 \cdot 10^4$	0.4
Double Chooz [76]	8.6	1050	8.3	$1.5 \cdot 10^4$	3.6
RENO [77]	16.4	1400	15.4	$3 \cdot 10^4$	2.6

Table II. Summary of experimental key parameters of upcoming reactor neutrino experiments. We give the thermal reactor power, the approximate distance between reactors and far detector, and detector mass, neutrino events per year, and background events per day, all for the far detector. RENO backgrounds are the sum of correlated backgrounds as computed in [77] and uncorrelated backgrounds as estimated in [83].

Accelerator Research Complex) fired to the Super Kamiokande detector, located 295 km from the proton beam target.

The NO ν A experiment [78] will run at an upgraded NuMI neutrino beam expected to deliver 6.5×10^{20} pot/year, corresponding to a beam power of 700 kW, generating a neutrino beam with an average energy $E_\nu \sim 2$ GeV and a ν_e contamination less than 0.5%. The far detector, placed at baseline of 810 km, 14 mrad (0.8°) off-axis, will be a totally active tracking liquid scintillator, constructed from liquid scintillator contained inside extruded PVC cells.

Fig. 5 shows the θ_{13} discovery reach of the five upcoming experiments expected in 2018. It is clear from the figure that the discovery potential of the appearance experiments strongly depends on the CP-phase as well as on the neutrino mass hierarchy. We observe that the inverted hierarchy gives a weaker sensitivity. Hence, in case no appearance signal is found the final θ_{13} limit will be set by the IH. The different shape of the IH curve for NO ν A results from the anti-neutrino running included in the NO ν A run plan. As evident from the figure, reactor experiments are neither sensitive to the value of δ nor to the mass hierarchy.

The sensitivity of the different experiments to θ_{13} can be discussed using two different performance indicators: the θ_{13} sensitivity limit and the θ_{13} discovery potential. The θ_{13} sensitivity limit describes the ability of an experiment to constrain θ_{13} if no signal is seen. It is basically determined by the

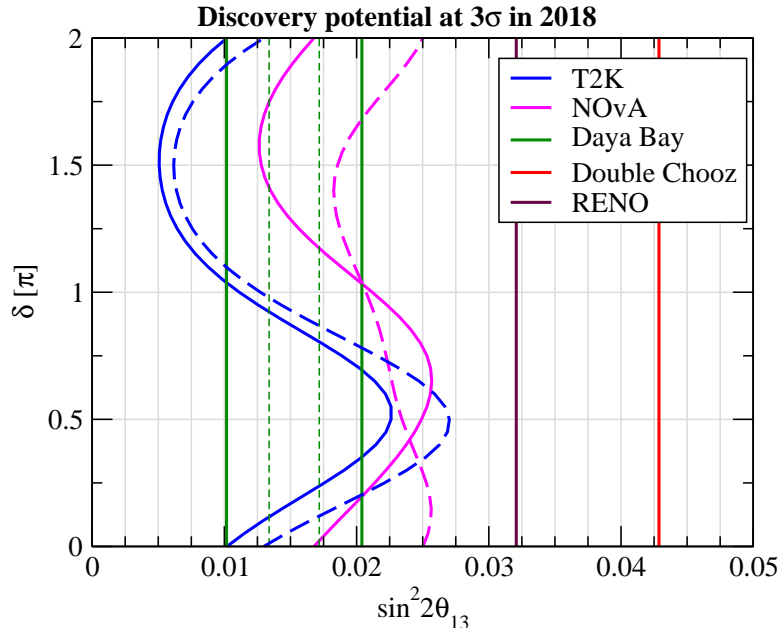


Figure 5. Discovery potential of the five upcoming experiments in the plane of $\sin^2 2\theta_{13}$ and δ expected in 2018, see section 5.3 of Ref. [2] for our assumptions on exposure. To the right of the curves a non-zero value of θ_{13} can be established at 3σ . For the beam experiments we show normal (solid) and inverted (dashed) hierarchies, while reactor experiments are independent of the hierarchy. The four lines for Daya Bay correspond to different assumptions on the achieved systematic uncertainty, from weakest to strongest sensitivity: 0.6% correlated among detector modules at one site, 0.38% correlated, 0.38% uncorrelated among modules, 0.18% uncorrelated.

worst case parameter combination which may fake the simulated $\theta_{13} = 0$. The θ_{13} sensitivity limit time evolution is shown in Fig. 6. We observe that the global sensitivity limit will be dominated by reactor experiments.

In case of no signal, the θ_{13} limit from beam experiments suffers from the marginalization over the CP phase and the mass hierarchy. This situation is very different in case of the discovery potential, since there a favourable value of δ can greatly enhance the sensitivity of the appearance experiments. The θ_{13} discovery potentials are shown in Fig. 7 as a function of time. For the beam experiments, the dependence on the true value of δ is reflected by the interval between the solid curves for a given time (shaded regions). The dashed curves for T2K and NO ν A correspond to a fixed value for the CP phase of $\delta = 0$.¹ The reactor experiments are not affected by the true δ ; the various curves for Daya Bay again correspond to the different assumptions concerning systematics as described above. The comparison of Figs. 7 and 6 shows that suitable values of δ may significantly improve the discovery potential of beams compared to their sensitivity limit. Indeed, T2K may discover θ_{13} for smaller θ_{13} than Daya Bay in a significant fraction of the parameter space, depending on the achieved systematics in Daya Bay. The NO ν A band becomes more narrow due to the complementary information from the

¹ Evolution of sensitivities under this condition have been shown recently in [84, 85].

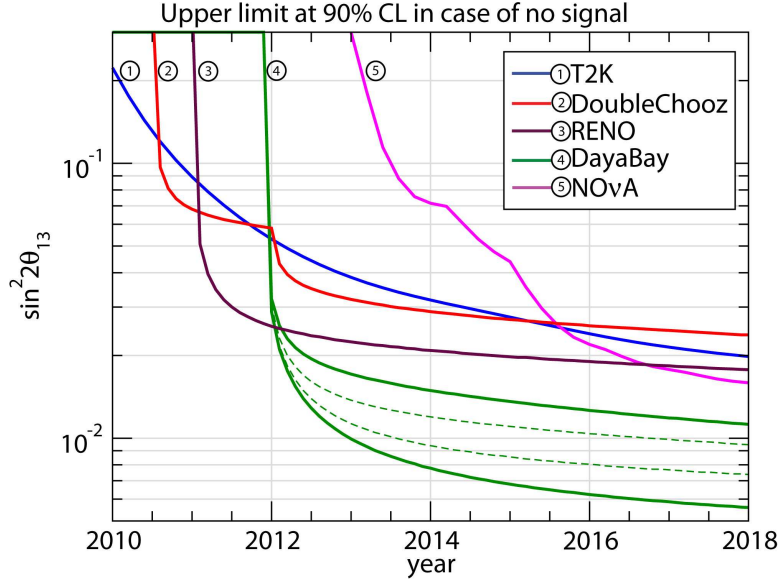


Figure 6. Evolution of the θ_{13} sensitivity limit as a function of time (90% CL), i.e., the 90% CL limit which will be obtained if the true θ_{13} is zero. The four curves for Daya Bay correspond to different assumptions on the achieved systematic uncertainty, from weakest to strongest sensitivity: 0.6% correlated among detector modules at one site, 0.38% correlated, 0.38% uncorrelated among modules, 0.18% uncorrelated.

anti-neutrino running, with the clear disadvantage of being somewhat late.

In figure 7 is also illustrated how the world sensitivity to θ_{13} could look like under the assumptions of the above schedules and that at each point in time a combined analysis of all available data is performed. The discovery reach will be set roughly by the optimal sensitivity of T2K, where the reactor experiments play an important role in providing sensitivity for the values of δ unfavourable for T2K. This plot nicely illustrates the interplay between reactor and beam experiments and shows that the global reach can be enhanced significantly if experiments of both types are available simultaneously with comparable sensitivities.

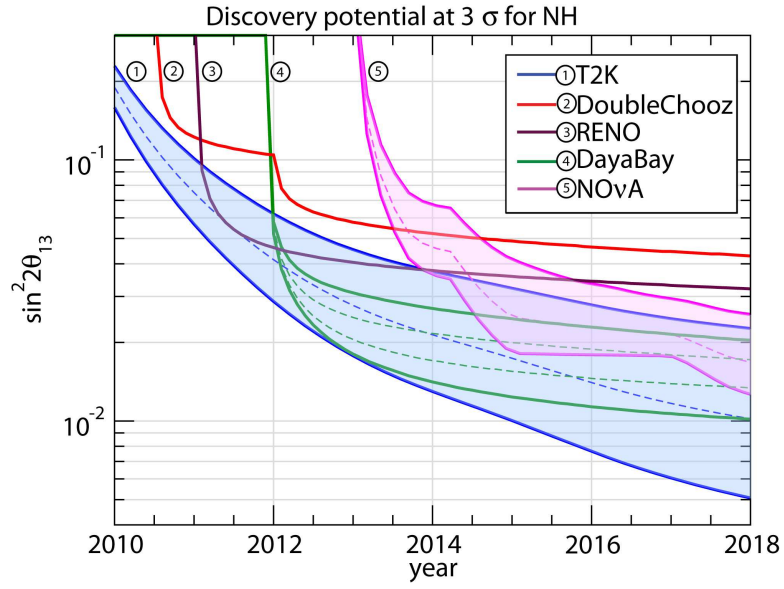


Figure 7. Evolution of the θ_{13} discovery potential as a function of time (3σ CL) for NH, showing the global sensitivity reach. The bands for the beams and the global reach reflect the (unknown) true value of δ . For Daya Bay it is assumed a systematical uncertainty of 0.38% correlated among detector modules at one site.

2.3. Direct Determination of the Solar Neutrino Fluxes from Neutrino Data [3]

In 1939, Hans Bethe described in an epochal paper [86] two nuclear fusion mechanisms by which main sequence stars like the Sun could produce the energy necessary to power their observed luminosities. The two mechanisms have become known as the pp-chain and the CNO-cycle [87]. In order to precisely determine the rates of the different reactions in the two chains, which are responsible for the final neutrino fluxes and their energy spectrum, a detailed knowledge of the Sun and its evolution is needed. Standard Solar Models (SSM's) [53, 88–93] describe the properties of the Sun and its evolution after entering the main sequence.

Till recently SSM's have had notable successes in predicting other observations. In particular, quantities measured by helioseismology such as the radial distributions of sound speed and density [90–93] showed good agreement with the predictions of the SSM calculations and provided accurate information on the solar interior. A key element to this agreement is the input value of the abundances of heavy elements on the surface of the Sun [94]. However, recent determinations of these abundances point towards substantially lower values than previously expected [95, 96]. A SSM which incorporates such lower metallicities fails at explaining the helioseismological observations [97], and changes in the Sun modeling (in particular of the less known convective zone) are not able to account for this discrepancy [98, 99].

So far there has not been a successful solution of this puzzle. Thus the situation is that, at present, there is no fully consistent SSM. This led to the construction of two different sets of SSM's, one (labeled “GS”) based on the older solar abundances [94] implying high metallicity, and one (labeled “AGS”) assuming lower metallicity as inferred from more recent determinations of the solar abundances [95, 96]. In Ref. [53] the solar fluxes corresponding to such two models were detailed, based on updated versions of the solar model calculations presented in Ref. [93].

Alternatively one may attempt to directly determine the solar neutrino fluxes from the solar neutrino data itself. In here we summarize the results of the most up-to-day extraction of the solar neutrino fluxes directly from the solar neutrino data from Ref. [3] in the framework of three-neutrino oscillations. The data included comprises the total rates from the radiochemical experiments Chlorine [23], Gallex/GNO [100] and SAGE [25, 100]. For real-time experiments in the energy range of ${}^8\text{B}$ neutrinos we include the 44 data points of the electron scattering (ES) Super-Kamiokande phase I (SK-I) energy-zenith spectrum [26], the 34 data points of the day-night spectrum from SNO-I [27], the separate day and night rates for neutral current (NC) and ES events and the day-night energy-spectrum for charge current (CC) events from SNO-II (a total of 38 data points) [28], the three rates for CC, ES and NC from SNO-III [29], and the 6 points of the high-energy spectrum from the 246 live days of Borexino [32]. Finally, we include the main set of the 192 days of Borexino data [31]. Besides solar experiments, we also include the latest results from the long baseline reactor experiment KamLAND [35, 41], which in the framework of three neutrino mixing also yield information on the parameters Δm_{21}^2 , θ_{12} , and θ_{13} . In addition, we include the information on θ_{13} obtained after marginalizing over Δm_{31}^2 , θ_{23} and δ_{CP} the results from the complete SK-I and SK-II atmospheric neutrino data sets (see the Appendix

of Ref. [41] for full details on our analysis), the CHOOZ reactor experiment [36], K2K [37], the latest MINOS ν_μ disappearance data corresponding to an exposure of 3.4×10^{20} p.o.t. [38], and the first MINOS $\nu_\mu \rightarrow \nu_e$ appearance data presented in Ref. [101].

We do a Bayesian analysis in order to produce the posterior probability distribution for the parameters $(\Delta m_{21}^2, \theta_{12}, \theta_{13}, f_{\text{pp}}, f_{7\text{Be}}, f_{\text{pep}}, f_{13\text{N}}, f_{15\text{O}}, f_{17\text{F}}, f_{8\text{B}}, f_{\text{hep}})$. In this model independent analysis we assume a uniform prior probability over which we impose a set of constraints, such as the luminosity constraint which relates the number of neutrinos produced with the total Sun luminosity [102], as well as those needed to ensure consistency in the pp-chain and CNO-cycle, and some relations from nuclear physics. For details on the normalization of the fluxes and the nuclear constraints see [3]. An important one arises from the

Our results for the analysis with luminosity constraint are displayed in Fig. 8, where we show the marginalized one-dimensional probability distributions for the eight solar neutrino fluxes as well as the 90% and 99% CL two-dimensional allowed regions. The corresponding ranges at 1σ (and at the 99% CL in square brackets) on the oscillation parameters are:

$$\begin{aligned}\Delta m_{21}^2 &= 7.6 \pm 0.2 [\pm 0.5] \times 10^{-5} \text{ eV}^2, \\ \sin^2 \theta_{12} &= 0.33 \pm 0.02 [\pm 0.05], \\ \sin^2 \theta_{13} &= 0.02 \pm 0.012 [{}^{+0.03}_{-0.02}],\end{aligned}\tag{15}$$

while for the solar neutrino fluxes are (in units of $\text{cm}^{-2} \text{s}^{-1}$):

$$\begin{aligned}\Phi_{\text{pp}} &= 5.910_{-0.063}^{+0.057} [{}^{+0.14}_{-0.16}] \times 10^{10}, & \Phi_{7\text{Be}} &= 5.08_{-0.43}^{+0.52} [{}^{+1.3}_{-1.0}] \times 10^9, \\ \Phi_{\text{pep}} &= 1.407_{-0.020}^{+0.019} [{}^{+0.054}_{-0.057}] \times 10^8, & \Phi_{13\text{N}} &= 7.8_{-3.4}^{+5.0} [{}^{+16}_{-7.0}] \times 10^8, \\ \Phi_{15\text{O}} &= 4.0_{-1.9}^{+1.8} [{}^{+4.8}_{-3.8}] \times 10^8, & \Phi_{17\text{F}} &\leq 5.9 [43] \times 10^7, \\ \Phi_{8\text{B}} &= 5.02_{-0.17}^{+0.18} [{}^{+0.45}_{-0.42}] \times 10^6, & \Phi_{\text{hep}} &= 1.3 \pm 1.0 [{}^{+3.0}_{-1.3}] \times 10^4.\end{aligned}\tag{16}$$

All these results imply the following share of the energy production between the pp-chain and the CNO-cycle

$$\frac{L_{\text{pp-chain}}}{L_\odot} = 0.986_{-0.006}^{+0.005} [{}^{+0.011}_{-0.014}] \iff \frac{L_{\text{CNO}}}{L_\odot} = 0.014_{-0.005}^{+0.006} [{}^{+0.014}_{-0.011}],\tag{17}$$

in perfect agreement with the SSM's which predict $L_{\text{CNO}}/L_\odot \leq 1\%$ at the 3σ level.

As seen in Figs. 8 the inclusion of Borexino has a very important impact on the determination of the ${}^7\text{Be}$, pep and CNO fluxes, and indirectly on the pp flux.

In order to statistically compare our results with the SSM's predictions we perform two different significance tests. First we do the analysis without assuming gaussianity constructing an statistical estimator t from the likelihood, where we found that the GS model has a lower t , $t_{\text{GS}} = 8.5$, while $t_{\text{AGS}} = 11.0$ which corresponds to $P_{\text{GS}}^{\text{agr}} = 43\%$ and $P_{\text{AGS}}^{\text{agr}} = 20\%$.

In the second case we use an estimation of the covariance matrix from the posterior probability distribution and we do a chi-square test, we found $\chi_{\text{GS}}^2 = 5.2 (P_{\text{GS}}^{\text{agr}} = 74\%)$ versus $\chi_{\text{AGS}}^2 = 7.4 (P_{\text{AGS}}^{\text{agr}} = 50\%)$.

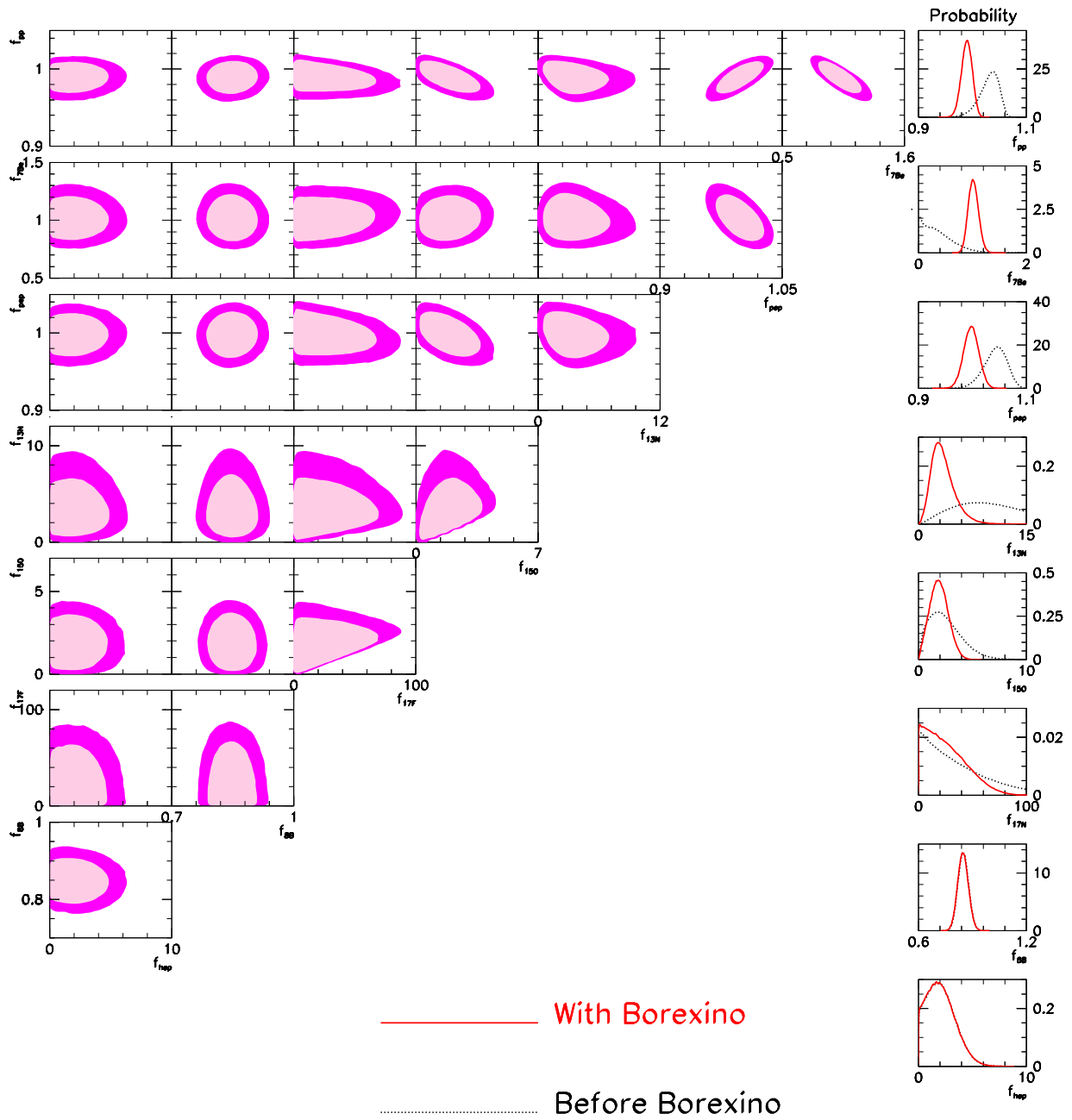


Figure 8. Constraints from our global analysis on the solar neutrino fluxes. The curves in the rightmost panels show the marginalized one-dimensional probability distributions, before and after the inclusion of the Borexino spectral data. The rest of the panels show the 90% and 99% CL two-dimensional credibility regions (see text for details).

From these results we conclude that, while the fit shows a slightly better agreement with the GS model corresponding to higher metallicities, the difference between the two is not statistically significant. This is partly due to the lack of precision of present data. But we also notice that, while the measurements of SNO and SK favor a lower ^8B flux as predicted by the low metallicity models, the determination of the ^7Be flux in Borexino and the corresponding determination of the pp flux from the luminosity constraint show better agreement with the GS predictions.

Finally in order to check the consistency of our results we have performed the same analysis without imposing the luminosity constraint. This allow us to test the relation between the luminosity of the Sun as directly measured with the one infered from the determination of the solar fluxes.

$$\frac{L_{\odot}(\text{neutrino-inferred})}{L_{\odot}} = 1.00 \pm 0.14^{[+0.37]}_{[-0.34]}. \quad (18)$$

Thus at present, the neutrino inferred luminosity perfectly agrees with the one directly determined and this agreement is known with a 1σ uncertainty of 15%.

3. A new design for the SPL-Fréjus Super-Beam [4]

In this study we consider a graphite target: this choice constitutes a proven technology in existing neutrino beams (i.e. T2K and CNGS). We assume a cylindrical shape with $r = 1.5$ cm, $L = 78$ cm and $\rho = 1.85$ g/cm³. A granular Ti target with the same geometry will also be discussed.

A new horn model inspired by the one used for the MiniBooNE beam, having a large acceptance for forward produced pions, has been adopted giving a reduced contamination from wrong-charge pions. The generic layout of the horn is shown in Fig. 9 (Left). Taking advantage of the small transversal

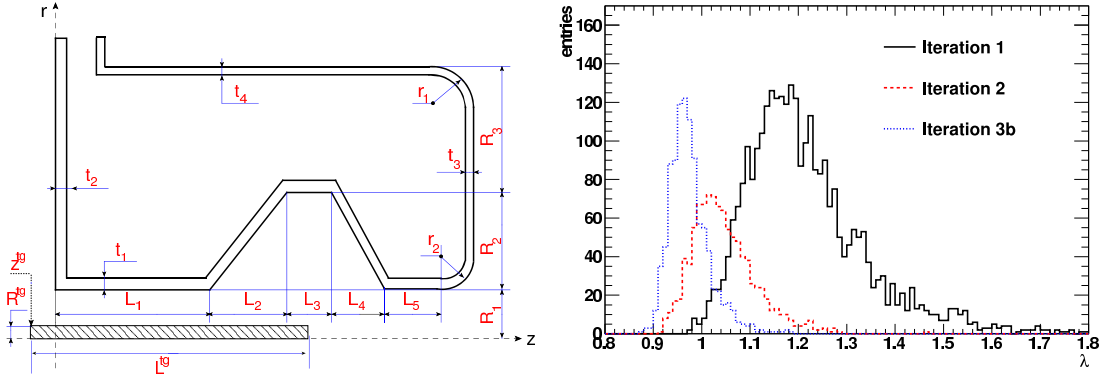


Figure 9. Left: parametrization of the forward-closed horn. Right: distribution of the figure of merit λ . See the text for the definition of the samples.

dimensions, the idea of using a battery of four horns in parallel has been proposed. This arrangement allows reduced stress on the targets thanks to the lower frequency pulsing (12.5 Hz) which brings the average beam power on each target to a level which is currently considered as a viable upper limit for solid targets operations (~ 1 MW). We have verified that placing the horns as central as possible (i.e. in mutual contact) causes a minor loss of ν_μ of the order of 1-2% with a mild loss as a function of the radial displacement.

The approach which was followed in the optimization of the forward-closed horn and the decay tunnel uses the final $\sin^2 2\theta_{13}$ sensitivity, as a guiding principle in the ranking of the system. Given the well known dependence on the $\sin^2 2\theta_{13}$ limit on the δ_{CP} phase, we introduced the figure of merit of the focusing system λ defined as the δ_{CP} -averaged 99 % C.L. sensitivity limit on $\sin^2 2\theta_{13}$ in units of 10^{-3} . In a first stage the parameters of the forward-closed horn and of the tunnel were sampled with uniform probability distributions within large ranges. The maximal length and radius of the horn were limited to 2.5 m and 80 cm in order to maintain a compact design suitable for the operation of four horns in parallel. Moreover, the inner radius R_1 was limited in $[1.2, 4]$ cm, the lower limit corresponding to the “integrated target” limit. At this level the target geometry and the current were not varied ($I = 300$ kA). The obtained distribution for λ is shown in the continuous histogram of Fig. 9 (Right). A second scan was performed after fixing the horn inner radius at 1.2 cm and restricting the ranges of variation of a set of relevant parameters[4]. The distribution of λ for this sample is shown by

the dashed histogram of Fig. 9. Finally the horn shape was fixed and a further tuning of the tunnel length and radius was performed. The dependence of λ on the tunnel variables can be reasonably fitted with a quadratic function: $\lambda = 0.94 + 2.1 \cdot 10^{-4}(L^{\text{tun}}[\text{m}] - 31.8)^2 + 2.4 \cdot 10^{-2}(R^{\text{tun}}[\text{m}] - 2.9)^2$. The distributions of λ for L^{tun} and R^{tun} in the neighborhood of the minimum, is shown by the dotted histogram of Fig. 9: an improvement of 25-30 % is obtained with respect to the initial sample. Since the minimum is relatively broad we chose $L^{\text{tun}} = 25$ m and $R^{\text{tun}} = 2$ m as central values based on practical considerations related to the excavation and shielding of large volumes. This compares to the previous values of 40 m of length and 2 m of radius.

We have also observed that an increase in the current (between 300 and 400 kA) tends to systematically produce better sensitivity limits. Data are well fitted by a linear function in (I, R_1) : $\lambda = (9.2 - 0.81 \cdot I[100 \text{ kA}]) / (7.3 - 0.37 \cdot R_1[\text{cm}])$. The effect of increasing the current, i.e. a stronger magnetic field in the vicinity of the target, is physically equivalent to decreasing the minimum horn inner radius. In this way, using a constant $I/R_1 (\propto B)$, allows to roughly work at fixed sensitivity.

The fractions of ν_μ , $\bar{\nu}_\mu$, ν_e and $\bar{\nu}_e$ with respect to the total are (98.0%, 1.6%, 0.42%, 0.015%) and (95.3%, 4.4%, 0.28%, 0.05%) for the positive and negative focusing modes respectively. In positive (negative) focusing mode the ν_e ($\bar{\nu}_e$) fluxes are dominated by muon decays: 82% (90%). The c.c. fluxes receive instead a large contribution from K 3-body decays (81 % and 75 % in "+" and "-" focusing respectively) with μ decays from the decay chain of "wrong charge" π at low energy contributing for the rest. These fluxes are available on the internet [4].

The discovery potential for $\theta_{13} \neq 0$ and CP violation improves with respect to the previous design. The uncertainty on hadro-production has also been addressed, for the graphite target, at the level of sensitivities by exploiting the data of the HARP experiment and different models (FLUKA and GEANT4-QGSP). More detailed information on the subject can be found in [4].

As undergoing studies in the context of the EUROnu design study have shown technical challenges for a solution with an integrated horn-target system, we studied the performances of two additional configurations assuming: 1) a graphite target separated from the horn (ST); 2) a granular target composed of titanium spheres with diameters of $\mathcal{O}(\text{mm})$ (PB); while keeping the target geometry unchanged. In both cases we set for the inner radius of the horn (R_1) a value of 3 cm and for the current a value of 350 kA. The 1.5 cm gap between the target and the horn is intended to accommodate the cooling infrastructure. Thanks to the favorable surface to volume ratio and the possibility to flow transversely the coolant within the interstices of the spheres (i.e. a high pressure flow of He gas) the granular target is expected to have a good behaviour even under extreme irradiation conditions.

The discovery potentials for $\theta_{13} \neq 0$ and CP violation for these two configurations are compared to the ones obtained with the former design based on a mercury target (HG) and to the performance with the integrated target (IT) in Fig. 10. With respect to the IT design the solution with a separated monolithic graphite target and increased current gives limits which are only slightly worsened; the PB solution gives practically unchanged performance for $\delta > \pi$ and some improvement for $\delta < \pi$. The granular Ti-target in association with the optimized horn represents then possibly the most appealing solution in terms of both physics performance and engineering.

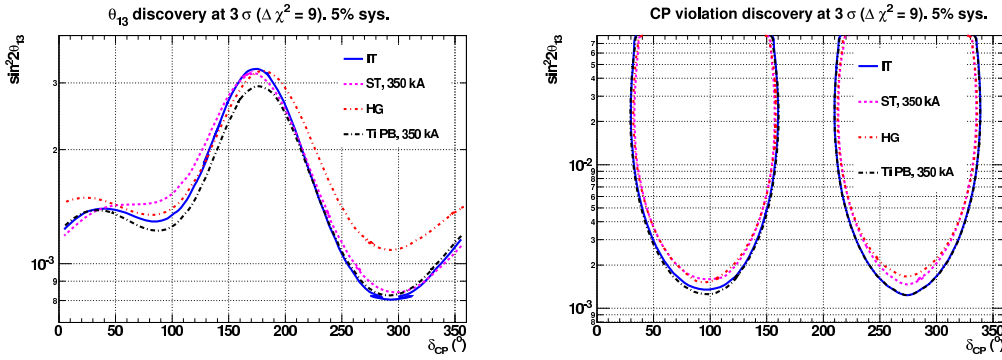


Figure 10. The θ_{13} (Left) and CP violation discovery potential (Right) at 3σ . Known parameters were included in the fit assuming a prior knowledge with an accuracy of 10% for θ_{12} , θ_{23} , 5% for Δm_{31}^2 and 3% for Δm_{12}^2 at 1σ level. The running time is $(2\nu+8\bar{\nu})$ years. Curves are calculated with GLoBES 3.0.14. The parametrization of the MEMPHYS Water Cherenkov detector is implemented in the publicly distributed AEDL file SPL.glb.

4. Beta-Beams

Beta-beams are one of the two new beam technologies that have been proposed in the last decade to produce intense neutrino beams aiming at distant detectors. Many different beta-beams proposals have been studied in recent years. The physics performances of most of them are summarized in Sect. ???. The rest of the section covers: atmospheric ν_μ background at ICAL@INO for a high- γ beta-beam from CERN [6]; minimal beta-beams that exploit at most existing european infrastructures [7]; an update of the physics potential of electron-capture beta-beams [8]; and, the physics potential of a high- γ beta-beam within the EU LAGUNA project [9].

4.1. Performances of Beta-Beam setups as of January 2011 [5]

In this short EUROnu-WP6 internal note, we review the physics potential of several beta-beam setups that have been proposed in recent years, comparing their performances in the sensitivity to $\sin^2 2\theta_{13}$, the CP discovery potential and the sensitivity to the neutrino mass hierarchy. Combination of these facilities with other facilities (as the proposed synergy of the SPL super-beam and the $\gamma = 100$ beta-beam aiming at the Fréjus underground laboratory) and/or with atmospheric neutrino oscillation data collected at the same detector of the beta-beam setup under study [103] are not considered in this review.

4.1.1. “Low”- γ : $\gamma = 100$

Belong to this category all the setups that use existing CERN facilities to boost the ions up to the desired energy. In particular, the reference setup is the $\gamma = 100$ ${}^6\text{He}/{}^{18}\text{Ne}$ beam aiming at a 1 Mton class water Čerenkov detector located in the Fréjus underground laboratory [104, 105], with a baseline

Setup	γ	Ions	Fluxes [10^{18}]	Years	Baseline	Detector Technology
CERN-Fréjus, 1	100	${}^6\text{He}$	2.9	5	130 km	440 Kton WC
		${}^{18}\text{Ne}$	1.1	5		
CERN-Fréjus, 2	100	${}^6\text{He}$	2.9×2	2	130 km	440 Kton WC
		${}^{18}\text{Ne}$	1.1/2	8		
CERN-Fréjus, 3	100	${}^6\text{He}$	2.9×2	2	130 km	440 Kton WC
		${}^{18}\text{Ne}$	1.1/5	8		
CERN-Canfranc, 4	100	${}^8\text{Li}$	2.9	5	650 km	440 Kton WC
		${}^8\text{B}$	1.1	5		
CERN-Canfranc, 5	100	${}^8\text{Li}$	2.9×2	5	650 km	440 Kton WC
		${}^8\text{B}$	1.1×2	5		
CERN-Canfranc, 6	100	${}^8\text{Li}$	2.9×5	5	650 km	440 Kton WC
		${}^8\text{B}$	1.1×5	5		
CERN-Canfranc, 4	100	${}^8\text{Li}$	2.9	3	650 km	440 Kton WC
		${}^8\text{B}$	1.1	5		
		${}^6\text{He}$	2.9	2		
CERN-Canfranc, 5	100	${}^8\text{Li}$	2.9×2	3	650 km	440 Kton WC
		${}^8\text{B}$	1.1×2	5		
		${}^6\text{He}$	2.9×2	2		
CERN-Canfranc, 6	100	${}^8\text{Li}$	2.9×5	3	650 km	440 Kton WC
		${}^8\text{B}$	1.1×5	5		
		${}^6\text{He}$	2.9×5	2		

Table III. Summary of the characteristics of the $\gamma = 100$ beta-beam setups that have been shown in the literature (for a review, see Ref. [109]).

$L = 130$ Km. Three options have been considered for this setup, depending on the achievable ion rates. A second possibility using the same infrastructures at CERN (i.e., the PS and the SPS) is to change the stored ions, going from low- Q ones such as ${}^6\text{He}/{}^{18}\text{Ne}$ to high- Q ones, such as ${}^8\text{Li}/{}^8\text{B}$. This possibility was advanced in Refs. [106, 107]. Also in this case, several options depending on the achievable ion rates have been considered. In addition to that, it is conceivable to store a mixture of low- and high- Q ions aiming at the same baseline, in order to use the first- and second-peak of the oscillation probability, as in Ref. [108]. The characteristics of the low- γ setups are summarized in Tab. III.

In Tab. IV we compare the performances of the $\gamma = 100$ beta-beam setups defined above in terms of three observables: (1) the minimum value of $\sin^2 2\theta_{13}$ that can be excluded at 3σ in case of a null result of a given experiment (sensitivity to θ_{13}); (2) the fraction of the δ -parameter space (known as the CP-fraction) for which a non-vanishing δ can be distinguished by $\delta = 0, \pi$ at 3σ (CP discovery potential), computed for² $\sin^2 2\theta_{13} = 0.1$; and, (3) the fraction of the δ -parameter space for which a true positive Δm_{13}^2 can be distinguished by a negative Δm_{13}^2 at 3σ (sensitivity to the neutrino mass

² This value is approximately consistent with the recent measurement of θ_{13} by reactor experiments [110–112].

Setup	$(\sin^2 2\theta_{13})_{\min}$	CP discovery potential	
		CP – fraction for $\sin^2 2\theta_{13} = 0.1$	Sensitivity to $\text{sign}(\Delta m_{13}^2)$ CP – fraction for $\sin^2 2\theta_{13} = 0.1$
CERN-Fréjus, 1	5×10^{-4}	70%	NO
CERN-Fréjus, 2	6×10^{-4}	70%	NO
CERN-Fréjus, 3	1×10^{-3}	61%	NO
CERN-Canfranc, 1	1.5×10^{-3}	58%	51%
CERN-Canfranc, 2	7×10^{-4}	72%	61%
CERN-Canfranc, 3	2×10^{-4}	78%	100%
CERN-Canfranc, 4	1.7×10^{-3}	66%	100%
CERN-Canfranc, 5	7×10^{-4}	71%	100%
CERN-Canfranc, 6	3×10^{-4}	79%	100%

Table IV. Summary of the performances of the $\gamma = 100$ beta-beam setups at 3σ in terms of: sensitivity to θ_{13} ; CP discovery potential; sensitivity to the neutrino mass hierarchy. From Ref. [109].

hierarchy), computed for $\sin^2 2\theta_{13} = 0.1$. Notice that in all cases we have considered no atmospheric neutrino background. This means that we have always assumed that the duty cycle at which the beta-beam is operated is tight enough to make this background negligible. The duty cycle for which this approximation is valid differs depending on the setup. How the performance are deteriorated when the duty cycle is relaxed is not shown in this table. The impact of the atmospheric neutrino background on the beta-beam performance has been studied in Ref. [109] for the low- γ case. See Sect. 4.2 in this report for an estimate of the effect of atmospheric neutrino background for high- γ setups.

4.1.2. “High”- γ : $\gamma \geq 350$

In Ref. [113, 114], the possibility of using an upgrade of the SPS³ to boost radioactive ions up to higher γ values. In particular, it was shown that the sensitivity to θ_{13} and the CP discovery potential of a beta-beam with ${}^6\text{He}/{}^{18}\text{Ne}$ ions boosted at $\gamma = 350$ was extremely good and competitive with the Neutrino Factory in some part of the parameter space. As for the $\gamma = 100$ option, the beam was directed towards a 1 Mton class water Čerenkov detector, located this time at the underground laboratory of Canfranc ($L = 650$ Km from CERN). This option was later adapted for the Gran Sasso underground laboratory, where such a big detector cannot be hosted, by replacing it with a 100 Kton iron detector (that can be magnetized, to reduce backgrounds) [115–117] or with a 50 Kton T ASD [118]. It was later noticed that, when using high- Q ions with high- γ , the neutrino flux is peaked around the resonant energy for $\nu_e \rightarrow \nu_\mu$ conversion in Earth matter [119, 120]. This makes a high- Q high- γ beta-beam aiming to a very far 50 Kton iron detector (at $L \sim 7000$ Km) an extremely good experiment to measure the neutrino mass hierarchy. As a consequence, several two-baseline beta-beam

³ The SPS+, proposed at that time within the of maintenance and upgrade programme of the LHC.

Setup	γ	Ions	Fluxes [10^{18}]	Years	Baseline	Detector Technology
High- γ , 1 [113]	350	${}^6\text{He}$	2.9	5	700 km	500 Kton WC
		${}^{18}\text{Ne}$	1.1	5		
High- γ , 2 [118]	350	${}^6\text{He}$	2.9	2	700 km	50 Kton TASD
		${}^{18}\text{Ne}$	1.1	8		
Two baselines, 1 [121]	350	${}^8\text{Li}$	3	5	2000 km	50 Kton MIND
		${}^8\text{B}$	3	5	7000 km	50 Kton MIND
Two baselines, 2 [121]	350	${}^8\text{Li}$	5	5	2000 km	50 Kton MIND
		${}^8\text{B}$	5	5	7000 km	50 Kton MIND
Two baselines, 3 [121]	350	${}^8\text{Li}$	10	5	2000 km	50 Kton MIND
		${}^8\text{B}$	10	5	7000 km	50 Kton MIND
Cocktail, 1 [122]	390	${}^8\text{Li}$	0.6×3	2.5	7000 km	50 Kton MIND
	656	${}^8\text{B}$	0.6×3	2.5		
	350	${}^6\text{He}$	3	2.5	650 km	500 Kton WC
	350	${}^{18}\text{Ne}$	3	2.5		
Cocktail, 2 [124]	390	${}^8\text{Li}$	3	2.5	7000 km	50 Kton MIND
	656	${}^8\text{B}$	3	2.5		
	575	${}^6\text{He}$	3	2.5	650 km	50 Kton TASD
	575	${}^{18}\text{Ne}$	3	2.5		

Table V. Summary of the characteristics of the high- γ beta-beam setups that have been shown in the literature.

Setup	$(\sin^2 2\theta_{13})_{\min}$	CP discovery potential	
		CP – fraction for $\sin^2 2\theta_{13} = 0.1$	Sensitivity to $\text{sign}(\Delta m_{13}^2)$ CP – fraction for $\sin^2 2\theta_{13} = 0.1$
High- γ , 1	1.6×10^{-4}	93%	100%
High- γ , 2	5×10^{-4}	75%	85%
Two-baselines, 1	1×10^{-3}	44%	100%
Two-baselines, 2	3×10^{-4}	62%	100%
Two-baselines, 3	1.5×10^{-4}	74%	100%
Cocktail, 1	1.8×10^{-4}	81%	100%
Cocktail, 2	5×10^{-4}	73%	100%

Table VI. Summary of the performances of the $\gamma \geq 350$ beta-beam setups at 3σ in terms of: sensitivity to θ_{13} ; CP discovery potential; sensitivity to the neutrino mass hierarchy.

setups have been proposed, using a resonant beam aiming to $L = 7000$ Km and a second beam aiming to a moderate distance detector ($L \sim 2000$ Km when using Li/B [121], $L = 650$ Km when using He/Ne [122]; see also Refs. [123, 124]). These beams was shown to be competitive with the Neutrino Factory in most part of the parameter space. The characteristics of the high- γ setups are summarized in Tab. V. In Tab. VI we compare the performances of the high- γ beta-beam setups defined above.

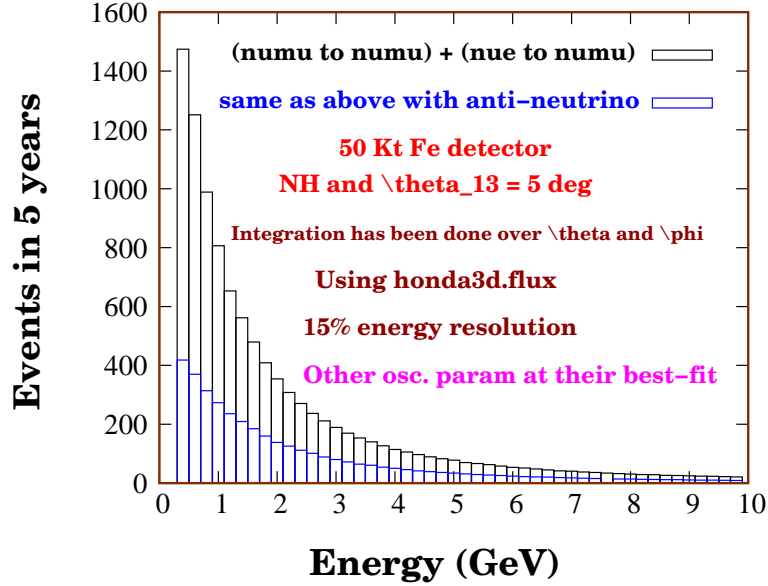


Figure 11. Atmospheric neutrino events in 50 Kton ICAL@INO detector in 5 years.

4.2. Atmospheric neutrino events at ICAL@INO and high Q β -beam [6]

1. Atmospheric events:

- First of all, we compute the expected number of atmospheric events in 50 kton ICAL@INO detector in 5 years. We have calculated separately the neutrino and anti-neutrino events. For neutrinos, we have considered $(\nu_\mu \rightarrow \nu_\mu + \nu_e \rightarrow \nu_\mu)$ oscillation channels. In case of anti-neutrinos, the considered channels are $(\bar{\nu}_\mu \rightarrow \bar{\nu}_\mu + \bar{\nu}_e \rightarrow \bar{\nu}_\mu)$. Fig. 1 shows the expected number of events as a function of neutrino energy at ICAL@INO detector in 5 years. Here we have done the integration over θ and ϕ in their entire range. All other details of the simulation have been mentioned on the body of the figure itself. Next, we will present these number of events in a tabular form (Table. 1 and 2).
- For beam studies, the atmospheric events which will occur along the beam direction and around it will serve as background. The zenith angle for CERN-INO baseline is 124° and in ICAL@INO detector, the angular resolution will be around 15° at most and with higher energies, the angular resolution improves a lot. Therefore, in our next study, we have considered a zenith angle range of 109° to 139° . In this zenith angle range, the atmospheric events that you expect at 50 kton ICAL@INO detector with 5 years of data taking is given in Table. 3.
- One can see from Table. 3 that the atmospheric neutrino flux falls steeply with energy and is expected to produce much fewer events for the energy range that we are interested in for CERN-INO beam study. Therefore, we need to see that how sensitivity will be affected in CERN-INO β -beam set-up with the increase in threshold.

Energy Bins GeV	ν events ($\nu_\mu \rightarrow \nu_\mu + \nu_e \rightarrow \nu_\mu$)	$\bar{\nu}$ events ($\bar{\nu}_\mu \rightarrow \bar{\nu}_\mu + \bar{\nu}_e \rightarrow \bar{\nu}_\mu$)
0.4 - 0.6	1474	418
0.6 - 0.8	1251	370
0.8 - 1	989	314
1 - 1.2	807	273
1.2 - 1.4	653	236
1.4 - 1.6	562	209
1.6 - 1.8	479	185
1.8 - 2	409	160
2 - 2.2	354	139
2.2 - 2.4	308	126
2.4 - 2.6	271	112
2.6 - 2.8	237	102
2.8 - 3	212	89
3 - 3.2	189	80
3.2 - 3.4	170	72
3.4 - 3.6	153	64
3.6 - 3.8	140	61
3.8 - 4	127	54
4 - 4.2	114	51
4.2 - 4.4	106	46
4.4 - 4.6	97	42
4.6 - 4.8	89	39
4.8 - 5	83	36

Table VII. Atmospheric neutrino events in 0.4 to 5 GeV range at 50 Kton ICAL@INO detector in 5 years.

Fig. 2 shows that the sensitivity of the experiment remains almost stable against the variation of the threshold energy upto 4 GeV. It means that we can work with a threshold of 4 GeV or so and in that way, we can reduce the atmospheric background a lot as can be seen from Table. 3.

- The fact that INO has charge identification capability further reduces the atmospheric background. The most important handle on the reduction of this background comes from the timing information of the ion bunches inside the storage ring. For 5T magnetic field and $\gamma = 650$ for ^8B ions, the total length of the storage ring turns out to be 19564 m. We have checked that with eight bunches inside this ring at any given time, a bunch size of about 40 ns would give an atmospheric background to *signal* ratio of about 10^{-2} , even for a very low $\sin^2 2\theta_{13}$ of 10^{-3} . For a smaller bunch span, this will go down even further. In addition, atmospheric neutrinos will be measured in INO during downtime and this can also be used to subtract them out.

Energy Bins GeV	ν events ($\nu_\mu \rightarrow \nu_\mu + \nu_e \rightarrow \nu_\mu$)	$\bar{\nu}$ events ($\bar{\nu}_\mu \rightarrow \bar{\nu}_\mu + \bar{\nu}_e \rightarrow \bar{\nu}_\mu$)
5 - 5.2	78	34
5.2 - 5.4	70	31
5.4 - 5.6	67	29
5.6 - 5.8	63	28
5.8 - 6	58	26
6 - 6.2	54	24
6.2 - 6.4	51	22
6.4 - 6.6	48	21
6.6 - 6.8	45	20
6.8 - 7	42	19
7 - 7.2	41	18
7.2 - 7.4	38	17
7.4 - 7.6	36	16
7.6 - 7.8	34	15
7.8 - 8	33	14
8 - 8.2	31	14
8.2 - 8.4	29	13
8.4 - 8.6	29	13
8.6 - 8.8	27	12
8.8 - 9	26	12
9 - 9.2	25	11
9.2 - 9.4	24	11
9.4 - 9.6	23	10
9.6 - 9.8	22	10
9.8 - 10	21	9

Table VIII. Atmospheric neutrino events in 5 to 10 GeV range at 50 Kton ICAL@INO detector in 5 years.

Energy range (GeV)	Total ν events	Total $\bar{\nu}$ events
1 - 12	214	94
2 - 12	155	69
3 - 12	114	48
4 - 12	90	39

Table IX. Atmospheric neutrino events at 50 Kton ICAL@INO detector in 5 years in the zenith angle range of 109° to 139° . Here full integration has been done over ϕ .

4.3. A minimal Beta Beam with high-Q ions to address leptonic CP violation [7]

The Beta-Beam concept and its different energy configurations have been discussed in details in [104, 125] and References therein. Here we focus on a Beta Beam designed with the aim of leveraging at

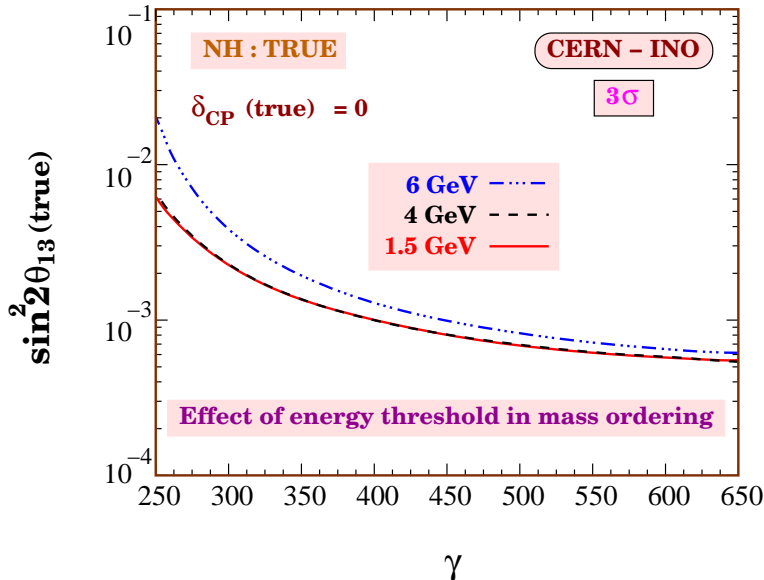


Figure 12. It shows the effect of changing the threshold energy of the detector. The sensitivity of the experiment remains almost stable against the variation of the threshold energy upto 4 GeV. Here we have used ${}^8\text{B}$ and ${}^8\text{Li}$ ions with 5 years of running and we have assumed 1.1×10^{18} (2.9×10^{18}) useful ions decays per year. This figure has been taken from [120].

most existing facilities and, in particular, the CERN acceleration complex. Beta Beams that are able to accelerate radioactive ions to high energies and produce multi-GeV ν_e and $\bar{\nu}_e$ allow for the use of high-density detectors, which, in turn, might be hosted in moderate-size underground laboratories. For a CERN-based Beta-Beam, the natural option to host the far detector is a laboratory located at a distance $O(600 - 700)$ Km from the neutrino source. The facility that *exploits at most existing European infrastructures* is a multi-GeV Beta-Beam based on the CERN-SPS accelerator pointing to a massive, high-density detector located in one of the experimental halls of the Gran Sasso laboratories [7]. The next cheapest alternative could be represented by the Canfranc Underground Laboratories in Spain, where some engineering would be however needed (albeit not so impressive as for a Mton class Water Čerenkov detector).

Beside the huge practical interest of exploiting in an optimal manner all European facilities without additional infrastructure investment [126], this detailed assessment is particularly relevant at present times: since 2009, machine studies for the Beta-Beam are concentrated on facilities that accelerate ions with Q-values larger than originally envisioned ($Q \sim 13$ MeV for ${}^8\text{Li}$ and ${}^8\text{B}$, to be compared with $Q \sim 3$ MeV for the ions considered in the original design, ${}^6\text{He}$ and ${}^{18}\text{Ne}$) using the existing SPS machine [20, 127]. This option ideally fits the “minimal” scheme mentioned above provided that neutrinos are pointed toward the underground halls of LNGS. Other options either based on low density detectors and/or on new terminal boosters at larger energies than the CERN-SPS have also been studied in literature: for details, we refer the reader to Ref. [125] and, in particular, to Refs. [105, 128, 129] for low-Q ions accelerated by the SPS, Refs. [113, 114, 116–118, 130, 131] for high- γ Beta Beams (using facilities different from the SPS to accelerate ions) and Refs. [106, 108, 109, 119–

124, 132–135] for high-Q Beta Beams (either at low- γ and high- γ).

The facility that we consider here does not differ from the baseline EURO ν [109, 136] design, but for a high density far detector located in a pre-existing hall at LNGS (for details on the facility and on the detector set-up and simulation we refer to [7, 116]).

The physics performance of the proposed setup have been studied in terms of two observables, defined as follows:

the CP discovery potential: for a given point in the parameter space, we will say that CP violation can be discovered if we can rule out the no CP violation hypothesis ($\delta = 0^\circ$ and 180°) at 3σ 1 d.o.f., after marginalizing over all the remaining parameters for both possible hierarchies.

the $\text{sgn}(\Delta m_{23}^2)$ reach: this is defined as the region of the $(\sin^2 2\theta_{13}, \delta)$ plane for which the wrong hierarchy can be eliminated at 3σ . Below this value of $\sin^2(2\theta_{13})$, the predictions for the wrong hierarchy cannot be distinguished from the data corresponding to the right hierarchy, at a statistical significance of 3σ .

For a far detector of 100 kton mass, a β^+ -emitters (^8B) flux of approximately 6×10^{18} useful decays per year⁴ is needed to observe CP violation in a large fraction of the parameter space (60%) for any value of θ_{13} that gives a positive signal at T2K ($\theta_{13} \gtrsim 3^\circ$). This sensitivity to δ is deteriorated for $\delta < 0$ due to the occurrence of the π -transit, as observed in other facilities. The ^8B flux must be accompanied by a ^8Li flux of $\sim 3 \times 10^{19}$ decays per year. Present studies on the ionization cooling technique or on ISOL-type targets indicate that such a large ^8Li flux could be feasible. Moreover, the former technique should produce β^+ and β^- emitters at a similar rate although ^8B ions interact stronger than ^8Li ions with materials in the target and in the recollection region. To achieve the fluxes above clearly represents the most challenging task for accelerator R&D but it is a viable option with respect to ^{18}Ne , where ISOL-type targets fall almost two orders of magnitude short of the goal.

In the same configuration, we find a non-negligible sensitivity to the neutrino mass hierarchy that extends up to $\theta_{13} \simeq 4^\circ$ for positive (negative) values of δ for normal (inverted) hierarchy. In the opposite parameter area, i.e. for negative (positive) values of δ and inverted (normal) hierarchy, the combination with atmospheric data collected during the Beta Beam run by the same magnetized detector further improves such sensitivity at large θ_{13} ($\simeq 6^\circ$). Combination of atmospheric data with Beta Beam-driven ones should also be able to solve part of the π -transit deterioration discussed above.

4.4. Update on the physics of Electron Capture neutrino beams [8]

Electron capture is a decay channel available to proton-rich nuclei that competes with positron decay in a manner that depends on the decay Q-value. Such decay channels are sources of mono-energetic neutrinos since there is no electron in the final state with which to share energy. It has been suggested [137–140] that ions with dominant electron capture channels can be used as an alternative to the standard Beta Beam ions to instead source an intense and collimated beam of mono-energetic

⁴ This is about three times the flux proposed for ^{18}Ne , where $F_0 \sim 2 \times 10^{18}$.

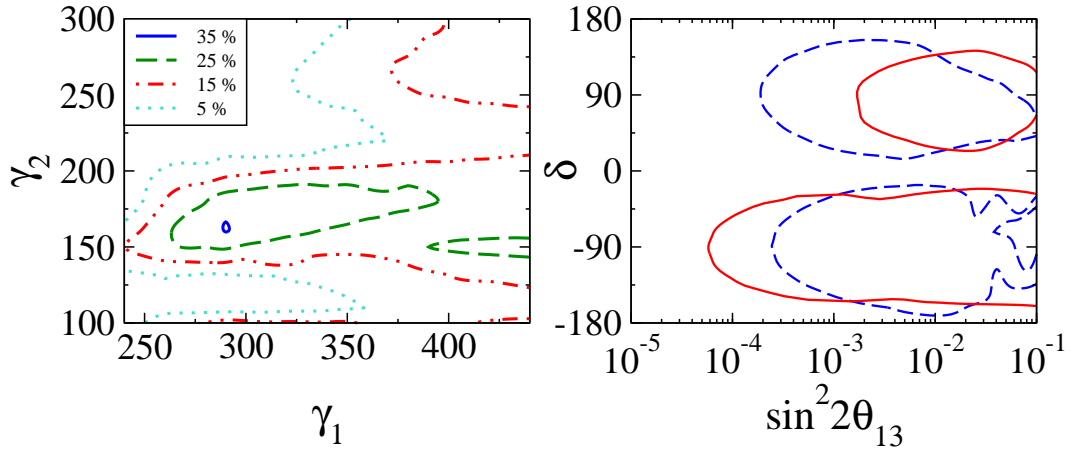


Figure 13. (Left panel) A discrete approximation to the integrated CP-fraction for a mono-energetic neutrino beam, sourced at CERN and directed at a 440 kton Water Čerenkov detector located at the Canfranc laboratory, as a function of the choice of boost pairings chosen. The plot shows the results for a run time ratio of low boost : high boost = 7 : 3. (Right panel) CP-violation discovery plots for the boost choices $(\gamma_1, \gamma_2) = (450, 150)$ (red solid lines) and $(280, 160)$ (blue dashed lines).

neutrinos. A neutrino beam of this type could be used to accurately probe the energy dependence of the $\nu_e \rightarrow \nu_\mu$ appearance probability: a means to observe CP-violation without the need for an anti-neutrino channel. However, since a single neutrino energy is insufficient to determine the unknown neutrino mixing parameters and resolve any degeneracy, it is necessary to include at least two ion boosts in any physics strategy. In a recent study [8], the previous works [137, 138] were extended to examine the physics reach of a ^{150}Dy electron capture beam sourced from CERN and directed towards a 440 kton fiducial mass Water Čerenkov detector 650 km distant to include the study of the choice of boost, the relative run times of each boost, the number of useful ion decays, and the number of atmospheric neutrino events.

In the first instance, the number of useful ion decays was fixed to 10^{18} per year, and atmospheric neutrino backgrounds were neglected so that the effect of altering the ion boosts and run times could be investigated. The results of this initial analysis is presented in the left panel of Fig. 13: for a choice of ion boosts (γ_1, γ_2) , the percentage of the parameter space $\sin^2 2\theta_{13} \in (10^{-5}, 10^{-1})$, $\delta \in (-180, 180)$ for which the existence of CP-violation can be demonstrated (referred to hereafter as CP-coverage) at 99 % confidence level is shown. (The procedure is outlined in detail in [8].) The results presented are for a low boost run taking 70 % of the whole experimental run. All results in this section use 2 degrees of freedom statistics. Little variation was found for the relative run times; however, two regions of the (γ_1, γ_2) plane returned large CP-coverage. The naive pairing of (almost) first and second oscillation maximum had a CP-coverage of approximately 35 % but was asymmetric in $\delta \rightarrow -\delta$ (right panel, red solid lines). For $\delta < 0$, this choice could rule out CP-conservation down to $\sin^2 2\theta_{13} = 10^{-4}$, but only $\sin^2 2\theta_{13} \sim 2 \cdot 10^{-3}$ for $\delta > 0$. There exists a slightly larger coverage for the pair $(280, 160)$. This

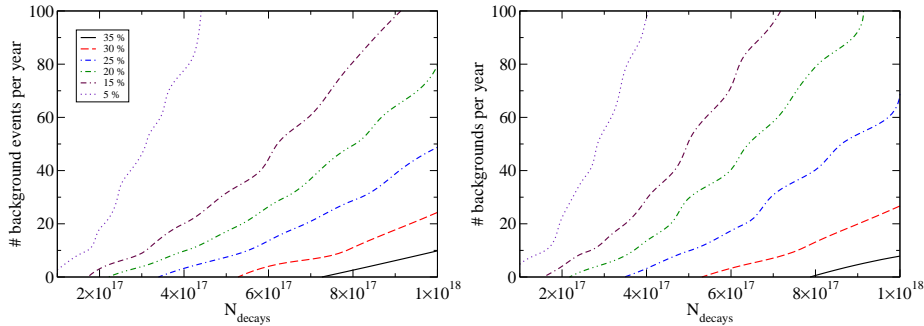


Figure 14. CP-violation coverage for $(\gamma_1, \gamma_2) = (280, 160)$ (left) and $(\gamma_1, \gamma_2) = (440, 150)$ (right) as a function of the number of useful decays and number of atmospheric backgrounds per year; both with γ_1 for 70 % of the experimental run time.

choice returned a (roughly) symmetrical CP-sensitivity region with CP-conservation ruled out down to $\sin^2 2\theta_{13} \sim 4 \cdot 10^{-4}$ (right panel, blue dashed lines).

However, no R&D has been carried out on the feasibility of sourcing 10^{18} useful decays per year for high proton number ions. A brief study adapting EURISOL Beta Beam codes [141] indicated that the decays are too slow and large tune-shifts would need to be accommodated. With existing technology, the number of useful decays is two orders of magnitude too small. At best, therefore, 10^{18} useful decays per year appears to be overly optimistic and should be considered as the hard limit on the yearly rate. To take this experimental fact into account, the ability to uncover CP-violation was investigated, for the two boost pairings identified above, as a function of the number of useful ion decays and the level of atmospheric neutrino background. The results are summarised in Fig. 14, again using the CP-coverage as an indicator. In both cases, the results were more volatile to small changes in the useful decay rate than the atmospheric background. It was found that drops in the total event rate can lead to degenerate solutions dropping below the required statistical significance of the test thus reducing the sensitivity in a manner beyond simply a scaling of the χ^2 [8]. The background merely reduces the χ^2 without interfering with its ability to rule out degenerate solutions. Its manifestation is simply to push the sensitivity contours inwards.

The feasibility of an electron capture beam remains open question; however, the most optimistic parameterisation considered in [8], and shown in Fig. 13, is likely to be beyond the hard limits imposed by available technology. It must be conceded that if θ_{13} were to be very small, the electron capture will not be a competitive facility, unless a fast decaying ion that can be produced in large quantities is found. This can be seen explicitly in Fig. 15 where the CP-discovery for the boost pairs (280,160) and (440,150), and 20 atmospheric events per year, are compared to the $\gamma = 350,350$ Beta Beam introduced in [114] with the baseline shortened to CERN-Canfranc, as in this study. The simulation used 1.1×10^{18} useful ^{18}Ne decays per year and 2.9×10^{18} useful ^6He decays year with an equal split between neutrino and anti-neutrino running for the Beta Beam.

We see that for a (440,150) electron capture facility, the physics return is poorer but relatively com-

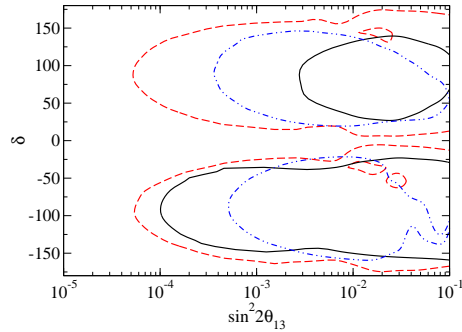


Figure 15. CP-violation sensitivity at 99 % confidence level for $N_{\text{atm}} = 20$ per year for $(\gamma_1, \gamma_2) = (440, 150)$ (black solid) and $(280, 160)$ (blue dot-dashed). The red dashed line displays the physics return for a standard Beta Beam directed along the CERN-Canfranc baseline with a boost $\gamma = 350$ for both neutrinos and anti-neutrinos.

petitive for $\delta < 0^\circ$. For these δ , the $(280, 160)$ facility is only competitive for $\sin^2 2\theta_{13} \in [10^{-3}, 10^{-2}]$. For $\delta > 0^\circ$, the $(440, 150)$ facility is outperformed by the standard Beta Beam by 2 orders of magnitude whilst, again the $(280, 160)$ facility is only competitive for $\sin^2 2\theta_{13} \in [10^{-3}, 10^{-2}]$. The physics reach of the electron capture machine is ultimately limited by the need to run for substantial periods at low energies where the appearance event rate is small. The availability of a mono-energetic anti-neutrino beam could resolve this issue. Ions that decay through bound beta decay could source such a beam; however, this is not possible from a practical point of view with available technology [8, 142].

4.5. High- γ Beta Beams within the LAGUNA design study [9]

Within the LAGUNA design study [143], seven candidate sites are being assessed for their feasibility to host a next-generation, very large neutrino observatory. Such a detector will be expected to feature within a future European accelerator neutrino programme: Superbeam, Beta Beam or, if the detector is magnetised, a low energy Neutrino Factory. In [9], a high boost ^{18}Ne and ^6He Beta Beam sourced at CERN and directed towards a 50 kton Liquid Argon detector [144] located at the LAGUNA sites: Slanic ($L = 1570$ km) and Pyhäsalmi ($L = 2300$ km) was investigated. The study assumed the availability of an 1 TeV SPS, as envisaged in some LHC upgrade options [145]. Using boosts of $\gamma = 350$ for both neutrinos and anti-neutrinos run for 5 years each, the ability to distinguish θ_{13} from zero, rule out CP-conservation, and determine the correct neutrino mass ordering was tested for both baselines. The simulations were then repeated but with the boost for ^{18}Ne increased to $\gamma = 570$. At present, no detector response data is available for a Beta Beam neutrino flux incident on a large Liquid Argon detector; however, they are expected to possess excellent energy resolution for ν_μ appearance events and background reduction capabilities whilst maintaining a high detection efficiency. The results presented here take this optimism at face value and therefore should be considered near the limit of the possible physics reach of the two setups.

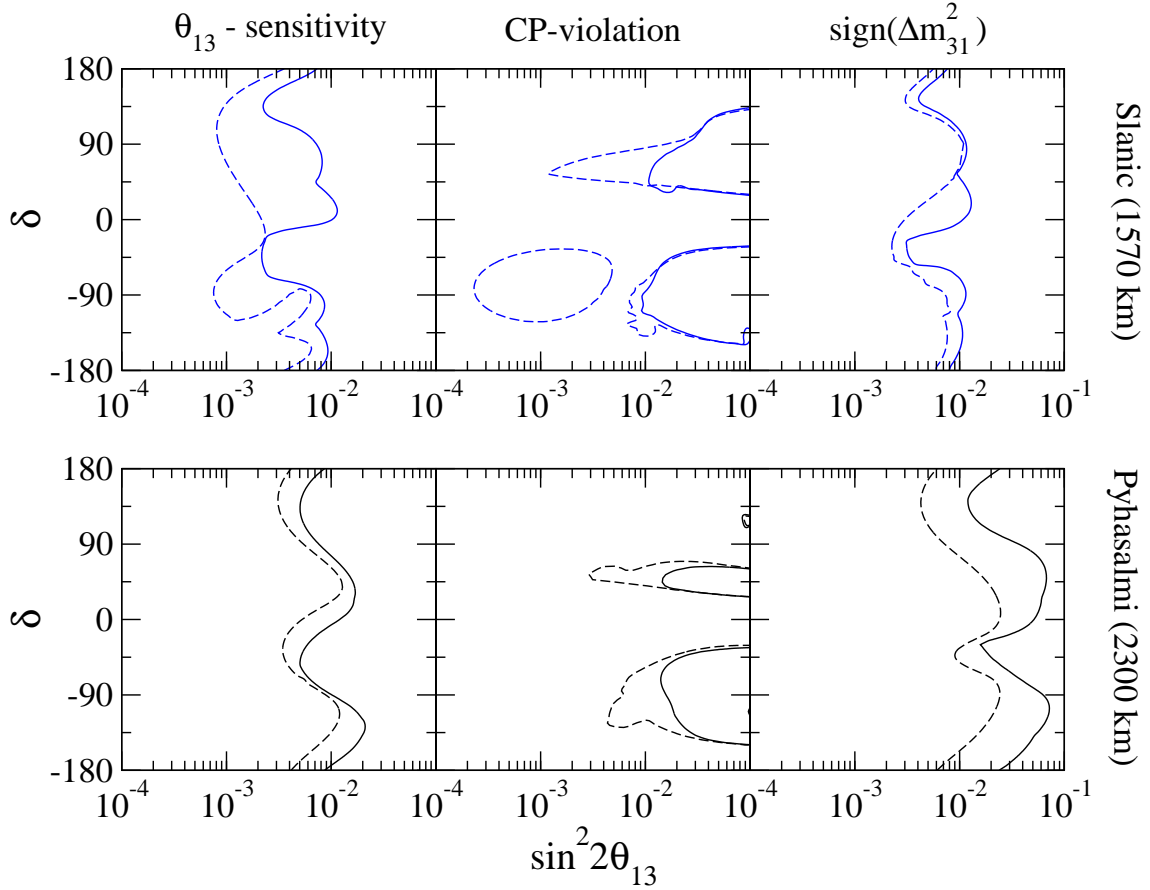


Figure 16. 3σ C.L. contours for discovery for non-zero θ_{13} (left), CP-violation (centre), and $\text{sign}(\Delta m_{31}^2)$ determination (right). In each plot, the solid line corresponds to a $\gamma = 350, 350$ ^{18}Ne and ^6He Beta Beam for a 50 kton Liquid Argon detector located at Slanic ($L = 1570$) (top line); and Pyhäsalmi ($L = 2300$ km) (bottom line). The dashed lines correspond to a $\gamma = 570, 350$ ^{18}Ne and ^6He Beta Beam.

The physics reach of the two baselines considered in summarised is Fig. 16. The results presented here have been simulated assuming 3×10^{18} useful decays per year for each ion. An energy threshold of 0.4 GeV is taken with energies up to 4 GeV considered with 12 energy bins and a $dE/E = 15\%$. ν_μ -appearance detection efficiency is flat at 80 % and neutral current backgrounds are taken at 0.1 % of the unoscillated flux. The LAGUNA study assumes a Liquid Argon detector of mass up to 100 kton. 50 kton is taken here to bring the simulations in line with other studies in the literature and to introduce some redundancy in the event that the parametrisation used here is too optimistic (e.g 1.5×10^{18} useful decays per year instead of 3×10^{18}).

The best sensitivity to non-zero θ_{13} and CP-violation is found for the CERN-Slanic baseline. This is to be expected since, with the same source, the flux is larger for this baseline. The weaker matter effect means that the $\text{sign}(\Delta m_{31}^2)$ degeneracy interferes less with these measurements. For the $\gamma = 570, 350$

boost pair, non-zero θ_{13} can be seen down to $\sin^2 2\theta \sim 10^{-3}$, and, for both boost pairs, at all values of δ for $\sin^2 2\theta_{13} > 10^{-2}$. However, there is a marked difference between the two boost pairings for sensitivity to CP-violation. For the $\gamma = 350, 350$ pair, the ability to rule out $\delta = 0^\circ$ or 180° is restricted to $\sin^2 2\theta_{13} > 10^{-2}$, but increasing the boost of the ^{18}Ne ions returns a large region of parameter space for $\delta < 0^\circ$ and centred on $\sin^2 2\theta_{13} = 10^{-3}$. There is little enhancement on the region for low boost pairing. This is suggestive that degeneracy is a problem for the $\gamma = 350, 350$ boost pairing; especially for $\sin^2 2\theta_{13} \sim 5 \cdot 10^{-3} - 1 \cdot 10^{-2}$ where there is a gap in CP-violation sensitivity. The lower event rates for the longer baselines mean that the data is insufficient to reduce the significance of some degenerate solutions. Although, the ability to rule out the incorrect mass ordering is poor relative to Neutrino Factories, for a Beta Beam it is not intrinsically bad. For the high boost run, the correct ordering can be indentified down to $\sin^2 2\theta_{13} = 2 \cdot 10^{-3}$, with determination for all values of δ for $\sin^2 2\theta_{13} > 10^{-2}$ in both cases. Although the increase in the ^{18}Ne boost improves the reach, it does not do so significantly. Increasing the boost makes data from higher energies available without significantly altering the event rate and composition at lower energies. Since European baselines make use of low and high energies in combination, improving the event rate in one region without the improving other need not, and has not, dramatically improved the physics return. The low event rate at low energies is still insufficient to break the degeneracy for small values of θ_{13} .

The physics return for the CERN-Pyhäsalmi baseline is weaker for each of the physics indicators, with little sensitivity for $\sin^2 2\theta_{13} < 10^{-2}$. Principally, this is due to the L^{-2} dependence of the unoscillated neutrino flux. In particular, the ability to determine the correct mass ordering is very poor even given the large matter effect at this baseline. The true and incorrect mass ordering solutions will be sufficiently separated in (θ_{13}, δ) space; however, the low event rate means that the solution regions at 3σ will be large and possibly merged together. When combined with a large solution region from the low energy bins (also owing to low event rates), the data is insufficient to break the degeneracy for small θ_{13} .

5. Physics at the Neutrino Factory

Neutrino factories have been studied as a mean to produce intense and collimated neutrino beams aiming at far detector(s) for the last ten years. Their impressive physics potential make them as the *ultimate* neutrino oscillation facility to improve our precision on known leptonic mixing matrix parameters and to measure the few remaining unknowns. The main activity in the field in 2010 focused on the possibility to "stage" a Neutrino Factory, so that at each upgrade a new physics program me is at hand [10]; on the physics potential of a "low-energy" Neutrino Factory that could optimize its capability to measure leptonic CP violation in case θ_{13} were large (as we now know it is the case); and, the study of an important source of background to the "golden channel" $\nu_e \rightarrow \nu_\mu$ oscillation that was previously overlooked (the τ -contamination problem, see [12]).

5.1. Neutrino Factory in stages [10]

Here we report on neutrino oscillation physics with a neutrino factory in stages, Ref. [10]. We include the possibility of upgrading the muon energy, adding another baseline, and increasing the detector mass within the same program. Two aspects are taken into account depending on the possible θ_{13} discovery by the next generation of experiments. For the large θ_{13} case ($\sin^2 2\theta_{13} \gtrsim 10^{-2}$), on the one hand, a low energy neutrino factory (LENF) with $E_\mu \simeq 4$ GeV to 5 GeV, discussed in Refs. [146–149], could be sufficient to discover CP violation (CPV) and the mass hierarchy (MH). We perform an optimization study of the physics reach, and we identify the "minimal" neutrino factory. On the other hand, we propose a staging scenario to chase θ_{13} if θ_{13} is smaller, i.e., $\sin^2 2\theta_{13} \lesssim 10^{-2}$. For details, see Ref. [10].

Minimal neutrino factory for the large θ_{13} . We investigate the minimal requirements for a neutrino factory suggested in Ref. [134]:

1. 5σ independent confirmation of $\sin^2 2\theta_{13} > 0$ (for any δ_{CP}).
2. 3σ determination of MH for *any* (true) δ_{CP} .
3. 3σ establishment of CPV for a certain fraction (such as 80%) of all (true) δ_{CP} .

We determine the minimal necessary luminosity as a function of baseline with respect to the above performance indicators in Fig. 17, where the requirement for θ_{13} can typically be easily met. The luminosity is expressed by a scale factor (SF) where SF=1 corresponds to $2.5 \cdot 10^{20}$ useful muon decays per year, which is the IDS-NF standard per baseline and polarity. For the LENF, the minimal baseline is determined by the MH reach, and the minimal SF by the CPV reach. The nominal luminosity SF=2.8, coming from the injection of all muons in the same storage ring and the re-optimization of the frontend, is sufficient for the CPV measurement for 80% of all true δ_{CP} and for the MH measurement for all δ_{CP} in the baseline window $1100 \text{ km} \lesssim L \lesssim 1400 \text{ km}$ for both values of $\sin^2 2\theta_{13}$ (left and right panel). One can read off these figures that luminosity is clearly an issue for large $\sin^2 2\theta_{13}$. If, for instance, only a lower SF can be achieved, the CPV discovery reach decreases accordingly. The "minimal" (optimal) LENF, *i.e.*, the one with the lowest SF, is in both panels at

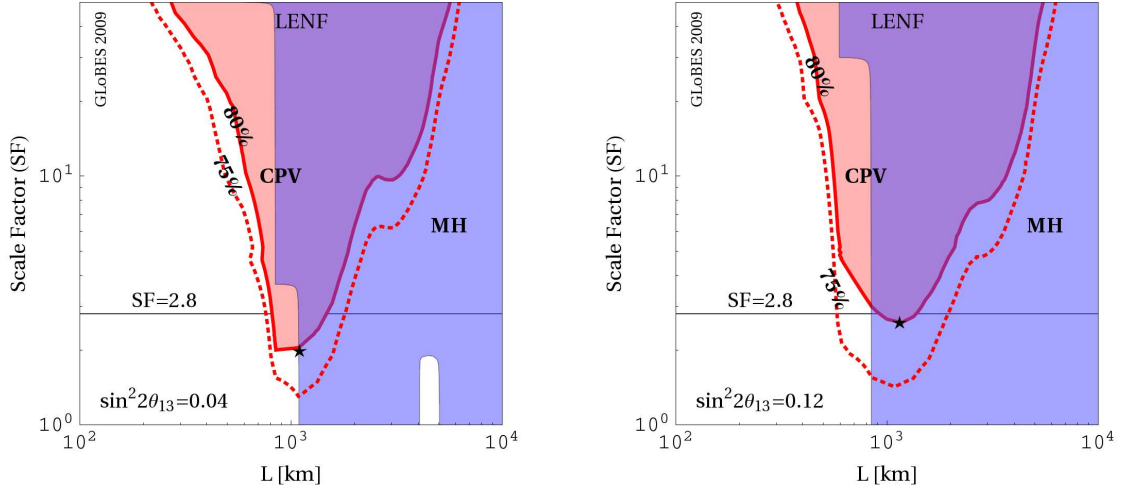


Figure 17. Discovery of CPV (dark/red) and MH (medium gray/light blue) for the one baseline (minimal) LENS as a function of baseline and luminosity scale factor SF. Discovery reach is given within the shaded regions at the 3σ CL, where for CPV a fraction of δ_{CP} of 75% or 80% is required (as indicated), and for the MH a fraction of δ_{CP} of 100%. The stars show the baseline with the minimal SF: in the left panel (1100 km, 2.0) and in the right panel (1150 km, 2.6). The nominal luminosity of the LENS is given by SF=2.8. Here the true value of $\sin^2 2\theta_{13}$ is chosen as given in the plot panels, and a normal hierarchy is assumed. The matter density uncertainty is assumed to be 2%. Figure taken from Ref. [10].

about $L \simeq 1100$ km, which is close to the FNAL-Homestake baseline $L = 1290$ km.

Staging for the small θ_{13} . After several years of data taking from Daya Bay and the other next generation experiments, we will know whether $\sin^2 2\theta_{13} \lesssim 0.01$ [150]. What has to be done if θ_{13} has not been found by these experiments? Here we propose a plausible staging scenario, starting with a low energy neutrino factory. Meanwhile, it is open to take three upgrade options increasing the muon energy, adding another baseline and increasing the detector mass. We proceed in three phases of data taking, five years each. As we show in Fig. 18 (5σ), phase I represents a low energy neutrino factory, phase II includes the energy upgrade to a high energy neutrino factory, and phase III considers additional upgrades, such as a larger detector or an additional baseline. In any phase, A combination of the data with the preceding phase is considered by default. We see the neutrino factory in stages for small $\sin^2 2\theta_{13}$, where a second baseline is used in phase III (solid curves) or the detector upgrade (dashed curves). At the 5σ confidence level, the strength of the magic baseline to resolve degeneracies becomes more important, especially for the mass hierarchy discovery reach. The largest increase in the discovery reaches just comes from the energy upgrade.

In summary, a realistic program may include components of LENS and HENS, even if $\sin^2 2\theta_{13}$ is small.

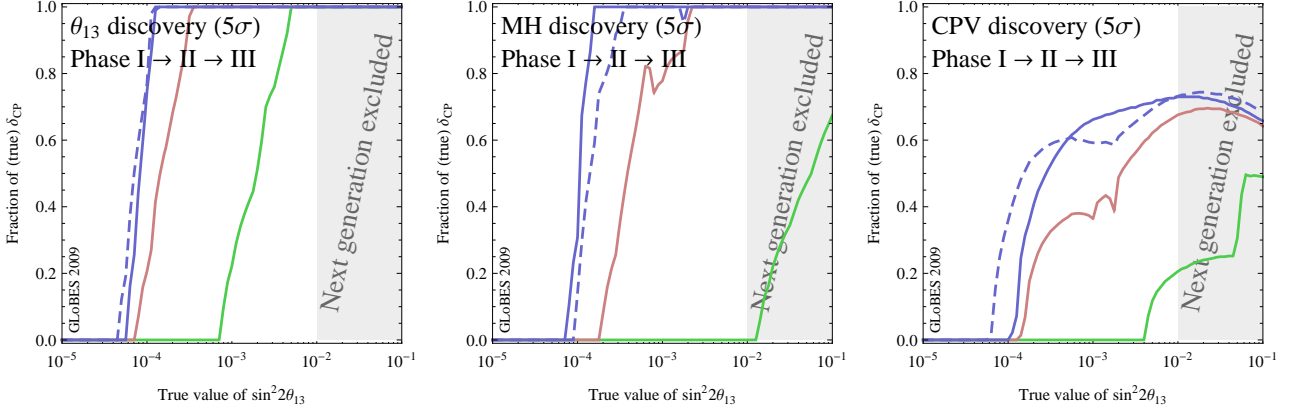


Figure 18. θ_{13} , MH, and CP discovery reaches for a neutrino factory in three phases: Phase I (light gray/green) is a low energy neutrino factory with a magnetized T ASD, phase II (medium gray/red) adds an energy upgrade with a MIND at the 4000 km baseline, and phase III (dark gray/blue) includes another (magic) baseline (solid curves) or a detector upgrade at the 4000 km baseline (dashed curves). 5σ confidence level. Figure taken from Ref. [10].

5.2. LENF Overview [11]

The low-energy neutrino factory (LENF), which uses muons of energy ~ 5 GeV and a baseline of ~ 1000 km, was first proposed in Ref. [146, 147]. Since then, developments to the accelerator and detector designs have enabled the experimental simulations to be refined and detailed optimisation studies to be performed [11]. The key finding was that given sufficiently high statistics, an optimised LENF can have excellent sensitivity to the standard oscillation parameters, competitive with, and even better than, the high energy neutrino factory for large θ_{13} ($\sin^2 2\theta_{13} \gtrsim 10^{-3}$). The possibility of observing the *platinum* channels ($\nu_\mu \rightarrow \nu_e$ and $\bar{\nu}_\mu \rightarrow \bar{\nu}_e$) in addition to the golden channels ($\nu_e \rightarrow \nu_\mu$ and $\bar{\nu}_e \rightarrow \bar{\nu}_\mu$) [151] was considered. It is found that the complementarity between these channels can be of great benefit if statistics are limited. There are also indications that the addition of these platinum channels is vital in order to resolve the degeneracy between standard oscillation parameters and non-standard interactions. Full details of the experiment can be found in Ref. [11]. In brief, we studied a setup having a baseline of 1300 km with a beam capable of delivering 1.4×10^{21} useful muon decays per year [152] for 5 years per polarity. For the detector we considered either a 20 kton totally active scintillating detector (T ASD) [153] and a 100 kton liquid argon (LAr) detector [154], both of which would be magnetised. These detectors would be capable of detecting and identifying the charges of both electrons and muons, providing access to multiple oscillation channels - the ν_μ ($\bar{\nu}_\mu$) disappearance channels, as well as the golden and platinum channels.

5.2.1. Sensitivity to standard oscillation parameters

The 3σ CP discovery potential and sensitivity to the mass hierarchy of the LENS with either a LAr detector or a TASD is shown in Fig. 19 (taken from Ref. [11]). We also show the sensitivities of the high energy neutrino factory (HENF) [155], various β -beams [104, 113, 114, 122], T2HK [155] and the wide-band beam (WBB) [156]. We see that a LENS with an optimistic LAr detector (left-hand edge of the blue band) has sensitivity to CP violation comparable to that of the HENF, for all values of θ_{13} . A TASD also performs competitively for $\sin^2(2\theta_{13}) \gtrsim 10^{-3}$. The sensitivity to the mass hierarchy is an order of magnitude better than that of the wide-band beam which uses the same 1300 km baseline.

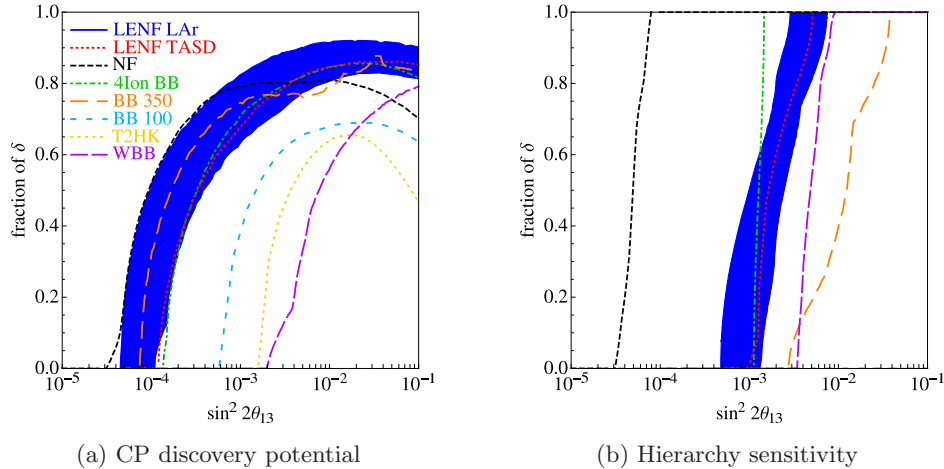


Figure 19. 3σ a) CP discovery potential and b) hierarchy sensitivity of the LENS with a 20 kton TASD and 100 kton LAr detector, the HENF, β -beams, T2HK, and the wide-band beam (WBB).

5.2.2. Sensitivity to non-standard interactions

Non-standard interactions (NSI's) can be parameterised by the parameters $\varepsilon_{\alpha\beta}$ [157, 158], which describe the rate of the transition $\nu_\alpha \rightarrow \nu_\beta$. The golden and platinum channels have leading order sensitivity to the parameters $\varepsilon_{e\mu}$ and $\varepsilon_{e\tau}$ [157, 158]. We show the sensitivity of the LENS with a 20 kton TASD to the NSI parameter $\varepsilon_{e\mu}$ [159], simulated by MonteCUBES [160]. We illustrate how the platinum channel enhances the sensitivity of the experiment, by showing the 68%, 90% and 95% allowed regions in the $\theta_{13} - \varepsilon_{e\mu}$ plane, both with the platinum channel (red solid lines) and without (blue dashed lines), for the case of $\varepsilon_{e\mu} = 0$ (Fig. 20a) and $\varepsilon_{e\mu} = 0.01$ (Fig. 20b). The current bound on $\varepsilon_{e\mu}$ is $O(1)$ [161]. Fig. 20a shows that the LENS could improve upon this and Fig. 20b shows that $\varepsilon_{e\mu} = 0$ could be excluded at $\sim 90\%$ confidence if $\varepsilon_{e\mu} \sim 0.01$. We find that this sensitivity is not affected much by statistics, unlike for the case of standard oscillations. This is an indication that if NSI's are present, then the experimental sensitivity is limited by the degeneracies between the oscillation and NSI parameters, not by statistics. Unless this degeneracy can be resolved, for

instance by including the platinum channels, then the sensitivity to both standard oscillation and NSI parameters will be severely limited.

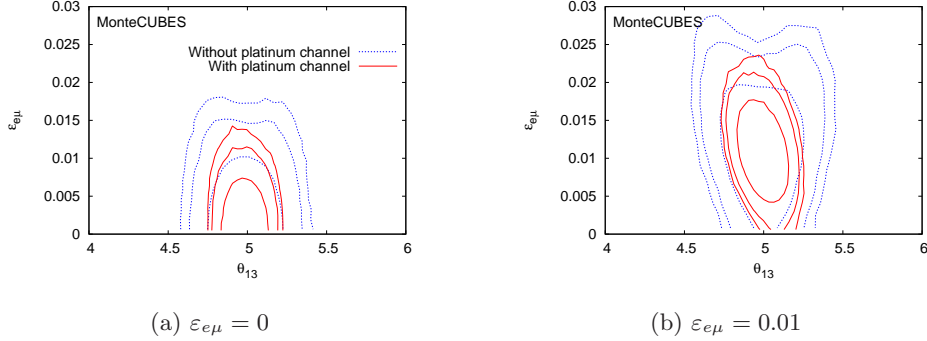


Figure 20. 68%, 90% and 95% allowed regions in the $\theta_{13} - \varepsilon_{e\mu}$ plane, with and without the platinum channel, for true values of a) $\varepsilon_{e\mu} = 0$ and b) $\varepsilon_{e\mu} = 0.01$.

5.3. The τ -contamination of the golden muon sample at the Neutrino Factory [12]

The problem of τ -contamination was first studied in Ref. [162] in the context of precision measurements of the atmospheric parameters $(\Delta m_{32}^2, \theta_{23})$ using the $\nu_\mu \rightarrow \nu_\mu$ channel at a Neutrino Factory. As it was shown in Ref. [163], it is useful to add all muons in the final state without muon charge identification, as the overall efficiency and threshold are much better and the backgrounds are still under control. The improved efficiency in the low-energy part of the neutrino spectrum, however, has the drawback that a previously irrelevant background becomes now potentially harmful. Oscillations into ν_τ 's, otherwise suppressed by low efficiency at low energy, enhance both the right- and wrong-sign muon samples⁵. Oscillations of $\nu_e, \nu_\mu \rightarrow \nu_\tau$ will produce τ 's through $\nu_\tau N$ CC interactions within the detector that will, eventually, decay into muons (approximately 17% of them). These muons from taus will, therefore, "contaminate" the "direct" muon samples (coming from $\nu_e, \nu_\mu \rightarrow \nu_\mu$ oscillations). Notice that muons from taus are not background but as good signal as the direct muons.

It is very hard to remove the muons from taus by applying kinematical cuts at an iron detector. Any cuts that attempt to do so drastically reduce the direct muon events as well and hence worsen the sensitivity to the oscillation parameters. They escape essentially all filters designed to kill the dominant backgrounds and directly add to the direct muon sample, see Ref. [162]. On the other hand, neglect of the tau contribution will lead to an incorrect conclusion about the precision achievable at the Neutrino Factory on a given observable. The τ -contamination must be added to the signal and it must be studied together with it.

The problem of τ -contamination of $\nu_e \rightarrow \nu_\mu$ was studied in detail in Ref. [12]. A good signal-to-background ratio is crucial to simultaneously determine with good precision θ_{13} and δ , since in

⁵ They actually contaminate the electron sample, also [164].

this channel we have a statistics of tens of events at most. To separate high-energy charged currents from the low-energy dominant neutral current background, is important a good reconstruction of the neutrino energy. For this reason, in the standard MIND analysis at the Neutrino Factory, the neutrino energy is reconstructed by adding the energy of the muon and that of the hadronic jet. This operation, however, yields a wrong result when the muon comes from a tau decay and it is detected at an iron calorimeter such as MIND, since no additional information regarding the neutrino missing energy in the $\tau \rightarrow \nu_\tau \bar{\nu}_\mu \mu^-$ decay can be provided⁶. The sample of wrong-sign muons from the decay of wrong-sign taus will be distributed erroneously in neutrino energy bins, thus contaminating the wrong-sign muon sample by events whose parent neutrino energy is reconstructed wrongly.

Consider a ν_τ of energy E_{ν_τ} , interacting in MIND and producing a wrongsign τ of energy E_τ together with a hadronic jet of energy E_h . After τ -decay, $E_{\nu_\tau} = E_\tau + E_h = (E_\mu + E_{miss}) + E_h$, where E_{miss} is the missing energy carried away by the two neutrinos in the τ -decay. Experimentally, we observe the secondary muon and a hadronic jet, a signal essentially indistinguishable from that of a wrongsign muon from CC ν_μ interactions. However, in this latter case, the addition of the (primary) muon energy E_μ and of the hadronic jet energy E_h results in the correct parent ν_μ energy, $E_{\nu_\mu} = E_\mu + E_h$. On the other hand, in the former case the addition of the (secondary) muon energy E_μ and of the hadronic jet energy E_h results in the wrongly reconstructed fake neutrino energy $E_{fake} = E_\mu + E_h = E_{\nu_\tau} + E_{miss}$. If we divide the τ three-body decay energy distribution in discrete fake neutrino energy bins, we find that for a monochromatic ν_τ beam of energy E_{ν_τ} , the final muon will be assigned to a given fake neutrino energy bin of energy E_j^μ with probability $V_j(E_{\nu_\tau})$, where $j = 1, \dots, N_{bin}^\mu$. We can compute the distribution of ν_τ of a given energy E_{ν_τ} and divide them into ν_τ energy bins of energy E_i^τ , where $i = 1, \dots, N_{bin}^\tau$. The ensemble of the probability vectors $V_j(E_i^\tau)$, for i and j running over all the ν_μ and ν_τ energy bins, is represented by the migration matrix M_{ij} , Fig. 21.

After having computed M_{ij} , the number of total wrong-sign muons in a given neutrino energy bin is given by

$$N_i(\theta_{13}, \delta) = \sum_{i=1, N_{bin}} \left[N_i^\mu(\theta_{13}, \delta) + \sum_{j=1, N_{bin}} M_{ij} N_j^\tau(\theta_{13}, \delta) \right]. \quad (19)$$

In Fig. 22 it is shown the fraction of muons coming from τ -decay that can be found in the wrong-sign muon sample⁷ after binning in the reconstructed neutrino energy, using the MIND efficiency [153] at $L = 4000$ Km (left) and $L = 7500$ Km (right). The data are shown for $\theta_{13} = 2^\circ$, $\delta = \pm 90^\circ$ (top and bottom, respectively) and the two possible neutrino mass hierarchies (red: normal hierarchy; blue: inverted hierarchy). In all cases, a significant τ -contamination can be observed below 5 GeV, ranging from a minimum of 10% (inverted hierarchy, $L = 4000$ Km, $\delta = 90^\circ$) to a maximum of 60% (normal hierarchy, $L = 7500$ Km, $\delta = 90^\circ$). For normal hierarchy, the contamination in the energy range $E_\nu \in [5, 10]$ GeV drops to the percent level (with the only exception of $L = 4000$ Km, $\delta = 90^\circ$). On

⁶ This would not be the case at ECC [165] or Liquid Argon detectors [144], capable of separating the $\nu_e \rightarrow \nu_\tau$ signal from the $\nu_e \rightarrow \nu_\mu$ one and to measure precisely the kinematic of the process under study (so that the neutrino energy can be reconstructed precisely even $\nu_e \rightarrow \nu_\tau \rightarrow \tau \rightarrow \mu$ transitions).

⁷ The setup is a 25 GeV Neutrino Factory with 5×10^{20} useful muon decays per year aiming at two 50 Kton MINDs located at $L = 4000, 7500$ Km, with 5 year of running time per muon polarity. An overall 2% systematic error has been considered.

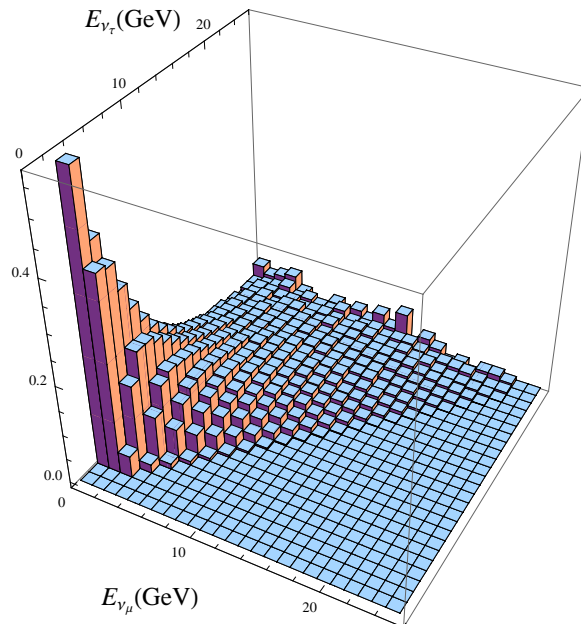


Figure 21. The migration matrix M_{ij} . M_{ij} has been statistically computed through a MonteCarlo simulation of the events, using the GENIE neutrino generator [166] with 10^6 simulated ν_τ s per neutrino energy bin and 25 bins in the range $E_{\nu_\tau} \in [0, 25]$ GeV. From Ref. [12].

the other hand, for inverted hierarchy the decrease of the τ -contamination with the neutrino energy is softer, being as large as 30% for $L = 7500$ Km, $\delta = 90^\circ$. Above 10 GeV, however, the contamination is at the percent level for both hierarchies (again, with the only exception of $L = 4000$ Km, $\delta = 90^\circ$ for inverted hierarchy).

The τ -contamination introduces, if not properly treated, an intolerable systematic error, in particular for large θ_{13} . Fig. 23 (left), from Ref. [12], shows that the test of the hypothesis that simulated data including the τ -contamination, $N_i(\theta_{13}, \delta)$, can be fitted using the direct wrong-sign muon distribution, $N_i^\mu(\theta_{13}, \delta)$, fails at more than 3σ for $\theta_{13} \geq 5^\circ$. For $\theta_{13} \in [1^\circ, 5^\circ]$, even if $N_i^\mu(\theta_{13}, \delta)$ can fit the τ -contaminated data (with a relatively poor χ^2 , though), the error in the joint measurement of θ_{13} and δ can be so large that it could actually prevent the use of the Neutrino Factory as a precision facility (see, again, Ref. [12] for a detailed analysis of the errors introduced by a wrong treatment of the τ -contamination). On the other hand, once M_{ij} has been statistically computed, experimental data distributed in reconstructed neutrino energy bins, can be fitted using the complete wrong-sign muons distribution $N_i(\theta_{13}, \delta)$, properly taking into account the τ -contamination of the golden muon sample. Using this procedure, the systematic error introduced by the muons from taus is completely removed. The remaining error is the statistical error of the migration matrix elements, that is under reasonable control.

It is worth noting that the τ -contamination of the wrong-sign muon sample, once properly treated, does not worsen the measurement of θ_{13} and δ , as it was the case for the atmospheric parameters measurement. Fig. 23(right) shows the comparison of the CP-fraction when only golden muons are

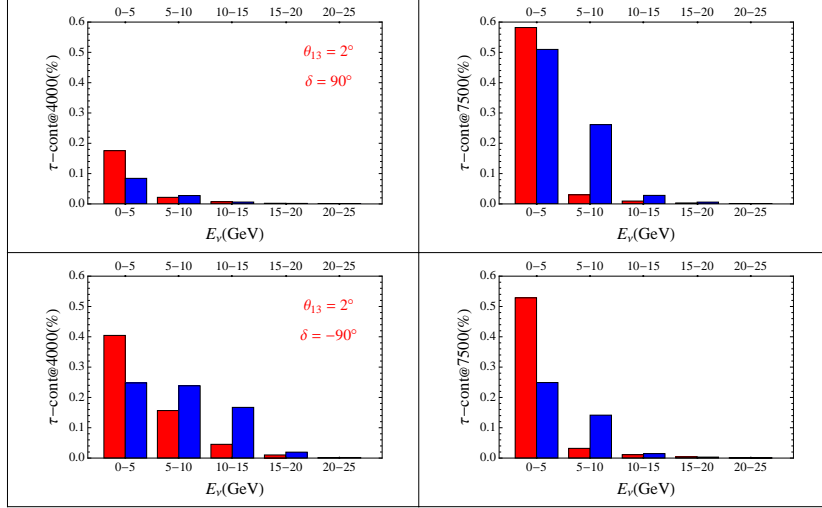


Figure 22. The fraction of τ -contamination of the golden muon sample as a function of the reconstructed neutrino energy, for $\theta_{13} = 2^\circ$. Left: L = 4000 Km; Right: L = 7500 Km. Top: $\delta = 90^\circ$; Bottom: $\delta = -90^\circ$. In red, we present the results obtained with normal hierarchy; in blue, with inverted hierarchy.

considered (solid blue line) or when the total wrong-sign muon signal is taken into account (dashed red line), as a function of $\sin^2 2\theta_{13}$. It can be seen that the only difference between the two lines is a slight displacement of the wiggles at $\sin^2 2\theta_{13} \sim 10^{-3}$ ($\theta_{13} \sim 1^\circ$). The wiggles are a consequence of the loss of sensitivity to CP violation introduced by the so-called sign clones for negative δ (a phenomenon known as π -transit, [167]). Since the location of the clones in the two samples differs, a small difference in the location of the wiggles is found when the two lines are compared. We can see, however, that once the τ -contamination is properly treated, no (significant) loss in the CP-fraction is found everywhere else. This is a consequence of the extremely low statistical weight of the τ -contamination in the golden channel. Since the signal is represented by tens of events, the τ -contamination amounts to a few events, at most. Once the problem of the wrong assignment of muons from taus into reconstructed energy bins is solved by means of the migration matrix approach, the residual statistical impact of the τ -contamination for $\theta_{13} \leq 10^\circ$ is marginal.

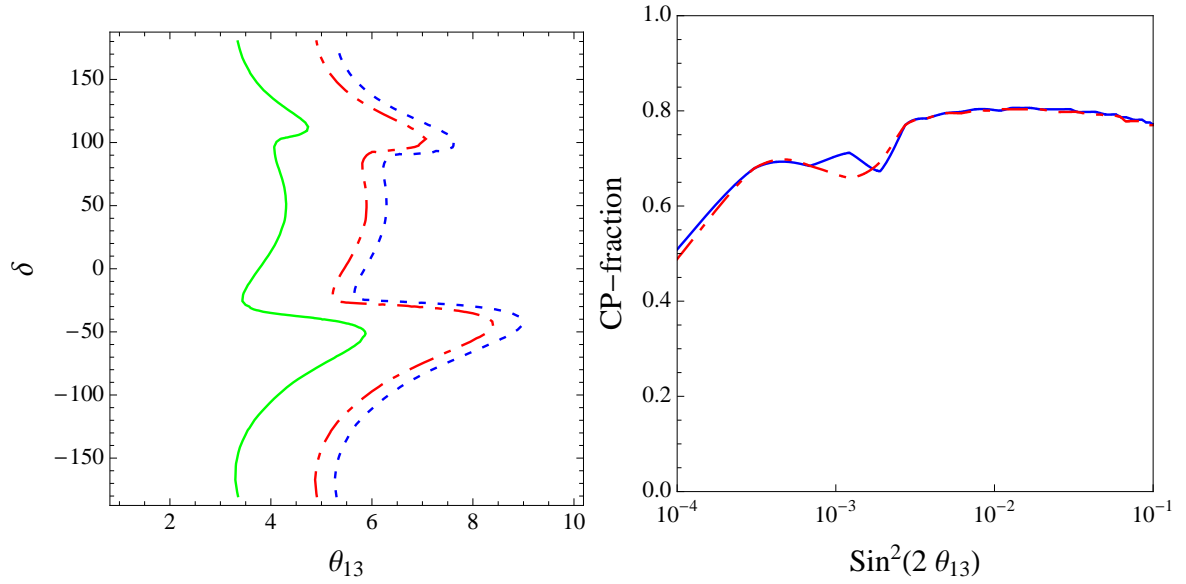


Figure 23. Left: Test of the hypothesis that a simulation of the data that includes the effect of the τ -contamination at $L = 4000$ km can be fitted with the golden muon theoretical distribution. In the regions to the right of the contour lines, the hypothesis can be rejected at 1, 2 or 3σ (from left to right), assuming the goodness-of-fit statistics follows the χ^2 distribution with $n = 8$ dof. From reference [12]. Right: Comparison of the CP-fraction achievable at the IDS-NF baseline Neutrino Factory when the τ -contamination is correctly taken into account (dashed red line) with respect to the ideal one in which no muons from taus are considered (solid blue line).

6. Physics beyond three-family oscillations

The new facilities proposed within EUROnu have some potential to look for new physics beyond the standard three-family oscillations, such as Non-Standard Interactions, violation of unitarity of the PMNS matrix and light sterile neutrinos. In this section we present the WP6 results on: neutrinoless double-beta decay [168]; sterile neutrinos as a solution to explain 2010 MiniBooNE data [13]; benefits of adding NSI's to sterile neutrinos to explain the 2010 MiniBooNE data [14]; the potential of the Neutrino Factory to search for sterile neutrinos [15]; the potential of the Neutrino Factory to distinguish NSI's from violation of unitarity of the PMNS matrix [16]; and, NSI's in the Zee-Babu model [17].

6.1. Neutrinoless double beta decay in seesaw models

Neutrino oscillations, implying the massive nature of neutrinos, constitute an evidence for physics beyond the Standard Model (SM). Thus, models accommodating this neutrino masses become an important component in the search for new physics. In this context, one of the most promising processes is the neutrinoless double beta decay ($0\nu\beta\beta$ decay), whose detection is the purpose of several ongoing and upcoming experiments [70]. Since this process is lepton number violating, its observation would imply that neutrinos are Majorana fermions [169].

Among the most popular models for neutrino masses, we find the different types of seesaw mechanisms: type-I [170–173], type-II [174–178], and type-III [179–182]. These are the extensions of the SM particle content that lead to the Weinberg $d = 5$ effective operator [183] after the extra mediators have been integrated out.

The extra degrees of freedom associated to the just mentioned models, and required to induce the Majorana nature of the SM neutrinos, can also contribute to the $0\nu\beta\beta$ decay. The effects of the SM neutrinos and these extra states, introduced to generate the neutrino masses, are usually analyzed as if they were independent (see, e.g., Refs. [184–188]). However, if the light neutrino masses are generated in the context of the model, important constraints between the light neutrino contribution and the one associated to the extra states arise. Here we will study the phenomenological implications of these correlations.

In order to take into account the extra neutrino contributions to the $0\nu\beta\beta$ decay rate in the most general type-I seesaw scenarios, we have computed the nuclear matrix element (NME) without any assumption on the mass of the neutrinos mediating the process. They are related to the observable $0\nu\beta\beta$ decay rate as follows:

$$\frac{\Gamma_{0\nu\beta\beta}}{\ln 2} = G_{01} \left| \sum_j U_{ej}^2 \frac{m_j}{m_e} M^{0\nu\beta\beta}(m_j) \right|^2, \quad (20)$$

where G_{01} is a well-known kinematical factor, m_e the electron mass, m_j the mass of the j neutrino, $M^{0\nu\beta\beta}(m_j)$ the NME, which contain the dependence on the neutrino propagator, and U_{ej} are elements of the neutrino mixing matrix.

The calculation was performed using Interacting Shell Model (ISM) nuclear wavefunctions, one of the most popular methods employed to obtain $0\nu\beta\beta$ decay NMEs [189]. The results show two distinct regions for the behaviour of the NME as a function of the virtual neutrino mass: almost constant up to $m_i \simeq 100$ MeV and then decreasing quadratically as the neutrino mass increases beyond 100 MeV. The transition mass 100 MeV is the typical momentum exchange of the decay, which is the momentum of the virtual neutrino $|\mathbf{p}|$. This scale is fixed by the typical distance between the two decaying nucleons, $r \simeq 1$ fm, and is sometimes referred as the nuclear scale.

The results of this computation are available at Ref. [190]. Different approximations are required in order to perform the calculation, both obtaining the wavefunctions and in the treatment of the two-body transition operator, and consequently some uncertainties are induced into the NMEs. These can be estimated in \sim_{-35}^{+25} % for light neutrino exchange ($m_j \leq 100$ MeV) and \sim_{-40}^{+35} % for heavy neutrinos ($m_j \geq 100$ MeV), more sensitive to the short range part of the transition operator.

Within the type-I seesaw, depending on whether the extra mass eigenstates fall in the light or heavy neutrino mass regimes we can split their respective contributions to the amplitude:

$$A \propto \sum_i^{\text{light}} m_i U_{ei}^2 M^{0\nu\beta\beta}(m_i) + \sum_I^{\text{light}} m_I U_{eI}^2 M^{0\nu\beta\beta}(m_I) + \sum_I^{\text{heavy}} m_I U_{eI}^2 M^{0\nu\beta\beta}(m_I), \quad (21)$$

where capital letters denote the mass index of the mostly sterile states and lowercase letters the mostly active SM states. Moreover, the diagonalization of the neutrino mass matrix provides an important constraint between the light and extra parameters:

$$\sum_I^{\text{light}} m_I U_{eI}^2 + \sum_I^{\text{light}} m_I U_{eI}^2 = 0. \quad (22)$$

This simple relation, stemming from the fact that a Majorana mass coupling for the active neutrinos is forbidden by the gauge symmetry of the SM, provides a useful constraint that should be always satisfied. We can now distinguish three cases exhibiting very different phenomenologies depending on the mass regime of the extra mass eigenstates:

All extra mass states are light. In this case Eq. (22) implies

$$A \approx - \sum_I^{\text{light}} m_I U_{eI}^2 \left(M^{0\nu\beta\beta}(0) - M^{0\nu\beta\beta}(m_I) \right). \quad (23)$$

Since in this regime the NMEs are basically independent of the neutrino mass, $M^{0\nu\beta\beta}(m_i) = M^{0\nu\beta\beta}(0) \simeq M^{0\nu\beta\beta}(m_I)$ the rate of $0\nu\beta\beta$ decay is very suppressed. Indeed, only the different neutrino masses in the NME prevent a full cancellation leading to a suppression driven by $\Delta m^2/p^2$ with $|p^2| \simeq (100 \text{ MeV})^2$. Therefore, in this regime, the $0\nu\beta\beta$ decay becomes experimentally inaccessible even being the neutrinos Majorana particles.

All extra mass states in the heavy regime. Now the NMEs for this extra states are very suppressed compared to the SM ones. Furthermore, Eq. (22) implies that

$$A \approx - \sum_I^{\text{heavy}} m_I U_{eI}^2 \left(M^{0\nu\beta\beta}(0) - M^{0\nu\beta\beta}(m_I) \right) \approx \sum_i^{\text{light}} m_i U_{ei}^2 M^{0\nu\beta\beta}(0). \quad (24)$$

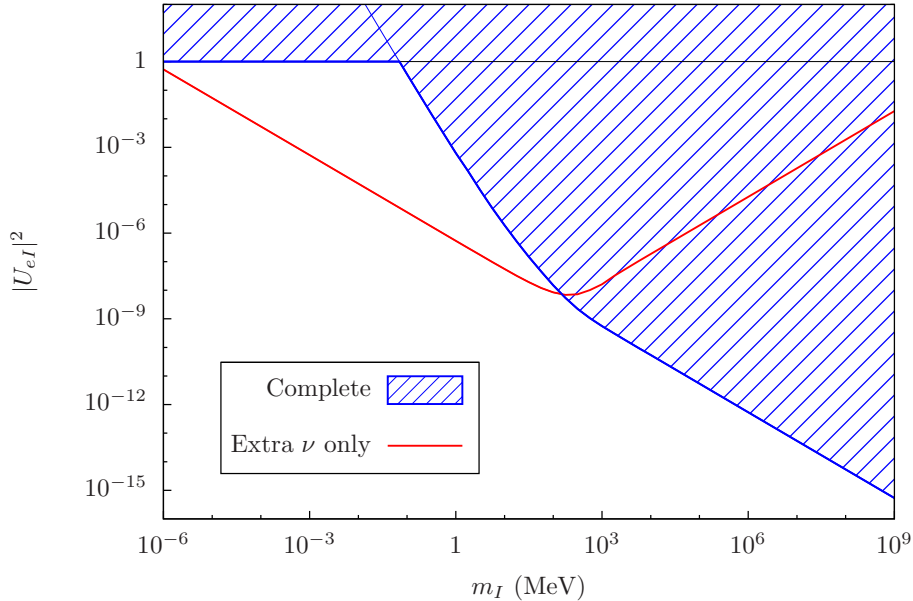


Figure 24. Bounds from CUORICINO on the extra neutrino mixing from $0\nu\beta\beta$ decay in ^{130}Te , with a 90 % CL half-life [191]. We have assumed the extra neutrinos are non hierarchical and show the bounds as a function of their common mass. We compare the case in which the contribution from the SM neutrinos is properly taken into account (striped area) to that in which only the extra contribution is considered (above the red line).

Thus, the contribution from the light active neutrinos (first term) dominates the transition rate. However, a much stronger bound on the mixing with the heavy neutrinos than the one usually shown in the literature can be extracted from it. This is shown in Fig. 24 using our calculation for the NME and the results from CUORICINO.

Extra mass states in the light and heavy regimes. In this scenario the leading terms stem from the light states:

$$A \propto \sum_i^{\text{light}} m_i U_{ei}^2 M^{0\nu\beta\beta}(m_i) + \sum_I^{\text{light}} m_I U_{eI}^2 M^{0\nu\beta\beta}(m_I). \quad (25)$$

Now it is possible to satisfy Eq. (22) even in a situation where $m_i U_{ei}^2 \ll m_I U_{eI}^2$, by canceling the contribution of the extra heavy states against that of the extra light ones while keeping the light neutrino masses small. In such a situation, the contribution of the light extra states could dominate over that of the active. As an example, if we consider the controversial Heidelberg-Moscow claim for a positive $0\nu\beta\beta$ decay signal [192], the accommodation of this signal through only SM neutrinos would require, using our ISM NMEs, $0.24 \text{ eV} < m_{\beta\beta} < 0.89 \text{ eV}$ at 2σ . The interpretation of this claim as light active SM neutrinos is very disfavoured by the constraints from cosmology and neutrino oscillation data [193–195]. However, this signal could be accommodated in a model with heavier

		MB	LS	MB+LS	KA	MB+LS+KA	Re	(MB+LS+KA)+Re
No Osc.	χ^2	17.8	15.0		6.8		51.0	
	NDF	16	5		8		56	
	GoF	0.33	0.010		0.55		0.66	
Osc.	χ_{\min}^2	10.6	1.4	13.3	6.4	24.1	48.5	75.6
	NDF	14	2	18	6	26	54	82
	GoF	0.71	0.51	0.77	0.38	0.57	0.69	0.68
	$\sin^2 2\vartheta_{\text{bf}}$	0.83	0.0058	0.0059	0.0010	0.89	0.042	0.013
	Δm_{bf}^2	0.069	8.13	4.57	6.76	0.055	1.86	0.46
PG	$\Delta\chi_{\min}^2$			1.30		5.80		2.94
	NDF			2		4		2
	GoF			0.52		0.21		0.23

Table X. Values of χ^2 , number of degrees of freedom (NDF), goodness-of-fit (GoF) and best-fit values $\sin^2 2\vartheta_{\text{bf}}$, Δm_{bf}^2 of the oscillation parameters obtained from the fit of various combinations of MiniBooNE (MB), LSND (LS), KARMEN (KA) and reactor Bugey and Chooz (Re) antineutrino data. The first three lines correspond to the case of no oscillations (No Osc.). The following five lines correspond to the case $\bar{\nu}_\mu \rightarrow \bar{\nu}_e$ oscillations (Osc.). The last three lines give the parameter goodness-of-fit (PG) [197]. The variations of $\sin^2 2\vartheta_{\text{bf}}$ and Δm_{bf}^2 depending on the fitted data sets are due to the oscillating character of $P_{\bar{\nu}_\mu \rightarrow \bar{\nu}_e}$ in Eq. (26). See Ref. [13] for details.

neutrinos (which are not bounded by cosmology) mediating the process. Indeed, we could reinterpret the result as $0.24 \text{ eV} < \left| \sum_I^{\text{heavy}} m_I U_{eI}^2 \right| < 0.89 \text{ eV}$.

As for the type-II and type-III seesaws, current bounds from accelerator experiments place the extra degrees of freedom in the heavy regime [196]. This effectively reduces the situation to that which appears for the type-I seesaw with only heavy extra states. In the same manner, mixed type-I and type-II/type-III seesaw models (with extra neutrinos below 100 MeV) resemble the situation of type-I seesaw with both light and heavy extra states.

6.2. Short-Baseline $\bar{\nu}_\mu \rightarrow \bar{\nu}_e$ Oscillations [13]

The MiniBooNE collaboration [198] recently reported the observation of a signal of short-baseline $\bar{\nu}_\mu \rightarrow \bar{\nu}_e$ transitions compatible with that observed in the LSND experiment [199]. The agreement of the MiniBooNE and LSND signals in favor of neutrino oscillations is remarkable, because the two experiments observed the signal of $\bar{\nu}_\mu \rightarrow \bar{\nu}_e$ transitions at different source-detector distances and different neutrino energy ranges. Since only the ratio of distance and energy is similar in the two experiments and neutrino oscillations depend just on this ratio (see Refs. [41, 55, 58, 200–204]), the neutrino oscillation explanation of the two signals is strongly favored. On the other hand, the MiniBooNE collaboration did not observe any signal of short-baseline $\nu_\mu \rightarrow \nu_e$ transitions [205] compatible with the MiniBooNE and LSND signals of $\bar{\nu}_\mu \rightarrow \bar{\nu}_e$ transitions. Therefore, it is possible that the effective parameters which govern neutrino and antineutrino oscillations are different, maybe because

of a violation of the CPT symmetry [206–224]. From a phenomenological point of view it is interesting to consider the neutrino and antineutrino sectors independently, especially in view of possible experimental checks of the short-baseline $\bar{\nu}_\mu \rightarrow \bar{\nu}_e$ signal [225–228]. Here we adopt this point of view [13] and we present the results of a combined fit of the MiniBooNE and LSND antineutrino data in favor of short-baseline $\bar{\nu}_\mu \rightarrow \bar{\nu}_e$ transitions, together with the constraints imposed by the data of the KARMEN experiment [229] in which the transitions have not been observed. We also take into account the constraints imposed by the absence of short-baseline $\bar{\nu}_e$ disappearance observed in reactor antineutrino experiments.

In the analysis of the data of $\bar{\nu}_\mu \rightarrow \bar{\nu}_e$ oscillation experiments we consider the simplest case of an effective two-neutrino-like short-baseline oscillation probability, similar to that obtained in the case of four-neutrino mixing (see Refs. [41, 58, 200, 203]),

$$P_{\bar{\nu}_\mu \rightarrow \bar{\nu}_e}(L/E) = \sin^2 2\vartheta \sin^2 \left(\frac{\Delta m^2 L}{4E} \right), \quad (26)$$

where Δm^2 is the relevant neutrino squared-mass difference and ϑ is the effective mixing angle for $\bar{\nu}_\mu \rightarrow \bar{\nu}_e$ transitions.

Tab. X shows the results of the fit of various combinations of MiniBooNE (MB), LSND (LS), KARMEN (KA) and reactor Bugey [230] and Chooz [54] (Re) antineutrino data.

The left panel in Fig. 25 shows a superposition of the 90% and 99% C.L. allowed regions in the $\sin^2 2\vartheta$ – Δm^2 plane obtained from the combined fit of MiniBooNE, LSND and KARMEN $\bar{\nu}_\mu \rightarrow \bar{\nu}_e$ data and the exclusion curves obtained in Ref. [231] from the fit of reactor Bugey and Chooz $\bar{\nu}_e \rightarrow \bar{\nu}_e$ data, which currently provide the most stringent constraints on short-baseline reactor $\bar{\nu}_e$ disappearance. The model-independent inequality

$$P_{\bar{\nu}_\mu \rightarrow \bar{\nu}_e} \leq 1 - P_{\bar{\nu}_e \rightarrow \bar{\nu}_e} \quad (27)$$

implies that in the left panel in Fig. 25 the large- $\sin^2 2\vartheta$ part of the straight region below $\Delta m^2 \approx 2 \text{ eV}^2$ allowed by the combined fit of MiniBooNE, LSND and KARMEN $\bar{\nu}_\mu \rightarrow \bar{\nu}_e$ data is excluded by the results of reactor antineutrino experiments. Quantitatively, only the parts with $\sin^2 2\vartheta \lesssim 3 \times 10^{-2}$ and $\sin^2 2\vartheta \lesssim 5 \times 10^{-2}$ are allowed at 90% and 99% C.L., respectively.

The right panel in Fig. 25 and the last column of Tab. X give the results of the combined fit of accelerator MiniBooNE, LSND and KARMEN $\bar{\nu}_\mu \rightarrow \bar{\nu}_e$ data and reactor Bugey and Chooz $\bar{\nu}_e \rightarrow \bar{\nu}_e$ data assuming an equality in Eq. (27). The value of the parameter goodness-of-fit in Tab. X shows that the accelerator and reactor data are compatible under the hypothesis of $\bar{\nu}_\mu \rightarrow \bar{\nu}_e$ oscillations.

From the right panel in Fig. 25 one can see that there is a favorite region at about 95% C.L. around the best-fit point for $2 \times 10^{-3} \lesssim \sin^2 2\vartheta \lesssim 5 \times 10^{-2}$ and $0.2 \lesssim \Delta m^2 \lesssim 2 \text{ eV}^2$. Larger values of Δm^2 are allowed only at more than about 95% C.L. for $5 \times 10^{-4} \lesssim \sin^2 2\vartheta \lesssim 5 \times 10^{-3}$.

This region is interesting for a study of the possibilities to check the LSND and MiniBooNE indication of short-baseline $\bar{\nu}_\mu \rightarrow \bar{\nu}_e$ oscillations with future experiments [225–228].

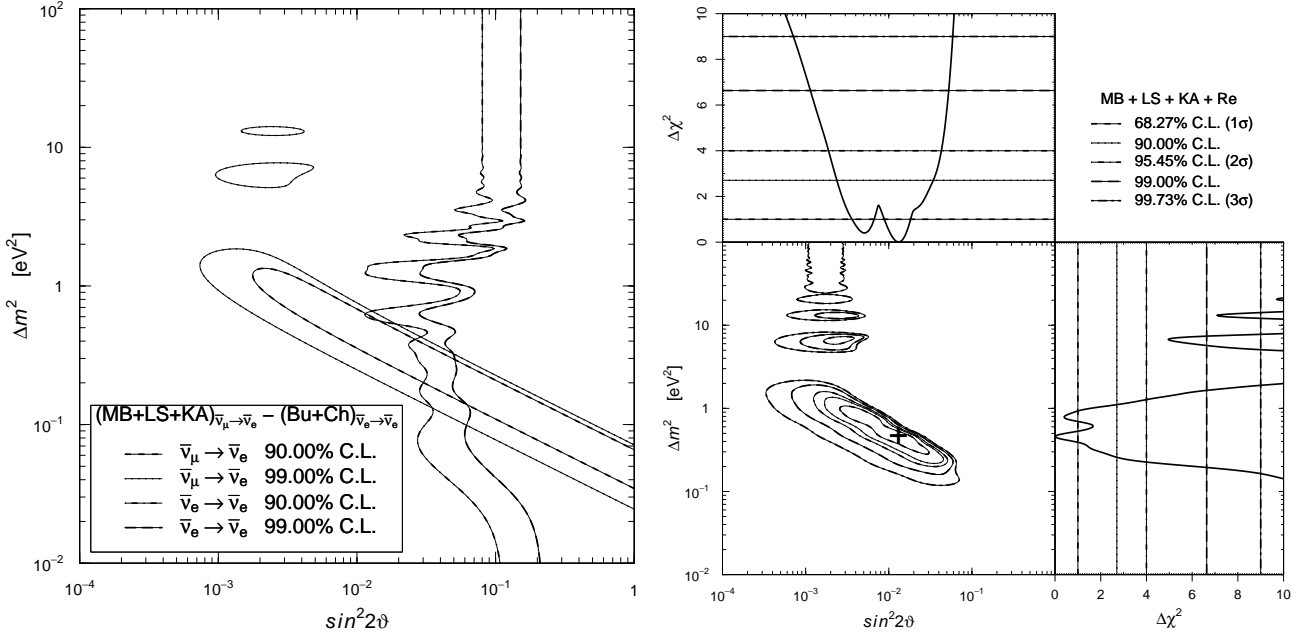


Figure 25. Left: superposition of the allowed regions in the $\sin^2 2\theta$ - Δm^2 plane obtained from the combined fit of MiniBooNE (MB), LSND (LS) and KARMEN (KA) $\bar{\nu}_\mu \rightarrow \bar{\nu}_e$ data and the exclusion curves obtained from the fit of reactor Bugey (Bu) and Chooz (Ch) $\bar{\nu}_e \rightarrow \bar{\nu}_e$ data. Right: allowed regions in the $\sin^2 2\theta$ - Δm^2 plane and marginal $\Delta\chi^2 = \chi^2 - \chi_{\min}^2$'s for $\sin^2 2\theta$ and Δm^2 obtained from the combined fit of MiniBooNE (MB), LSND (LS) and KARMEN (KA) $\bar{\nu}_\mu \rightarrow \bar{\nu}_e$ data and the exclusion curves obtained from the fit of reactor Bugey and Chooz (Re) $\bar{\nu}_e \rightarrow \bar{\nu}_e$ data. The best-fit point is indicated by a cross. See Ref. [13] for details.

6.3. MiniBooNE/LSND data: NSI's in a (3+1)-scheme vs. (3+2)-oscillations [14]

Recent MiniBooNE anti-neutrino data [198] indicate an excess of $\bar{\nu}_e$ events, in agreement with the LSND evidence [199] for $\bar{\nu}_\mu \rightarrow \bar{\nu}_e$ transitions. It is known that oscillations with one or more sterile neutrino(s) at the eV scale are not sufficient to explain the global data [232, 233]. The preprint EURONU-WP6-10-24, Ref. [14], investigated the possibility that in addition to a sterile neutrino there are some non-standard neutrino interactions (NSI), beyond the Standard Model weak interactions. Since matter effects are tiny for the short baselines relevant here, charged-current (CC) type NSI in the neutrino source and detector are considered. Thanks to the interference between NSI effects and oscillations with $\Delta m_{41}^2 \sim 1 \text{ eV}^2$ CP violation is obtained, even in the presence of only one mass scale. This effect is used to reconcile the indication for $\bar{\nu}_\mu \rightarrow \bar{\nu}_e$ in anti-neutrino experiments (LSND and MiniBooNE) with the absence of a signal in MiniBooNE neutrino data.

A general parameterisation of the relevant transition and survival probabilities in the presence of oscillations (within the one-mass scale approximation) and NSI is presented, and particular combinations of mixing matrix elements $U_{\alpha 4}$ and NSI parameters $\varepsilon_{\alpha\beta}$ entering in the probabilities are

identified. This drastically reduces the number of independent parameters and makes a general fit to global short-baseline data feasible.

Two versions of the (3+1) NSI model are considered. In the general case (denoted NSI^g) one makes use of the fact that the neutrino production mechanism in LSND (and in KARMEN) is muon decay (purely leptonic), whereas in all other experiments neutrino production and detection are semi-leptonic, involving transitions between u and d quarks. Therefore, in the presence of suitable NSI parameters one can decouple the transition probabilities in LSND and KARMEN from the rest of the data. In this case one obtains an excellent fit to the global data and the tension between appearance and disappearance experiments is resolved. In this case MiniBooNE does not provide a direct test of LSND, since different combinations of parameters are relevant for them. Also, in the global fit the excess observed in MiniBooNE anti-neutrino data is not reproduced.

For the second version of the (3+1) NSI model the assumption is adopted that NSI involving the charged muon can be neglected. In this case exactly the same NSI parameters are relevant for LSND and KARMEN as for all other experiments. In this constrained model (NSI^c) one makes use of the CP violation due to NSI-oscillation interference to reconcile neutrino and anti-neutrino data. It is shown that in the NSI^c model there is a factorisation between appearance and disappearance amplitudes, similar to that in the (3+1) oscillation scheme. Therefore, it is more difficult to satisfy constraints from disappearance experiments and some tension is left in the fit. However, also this model provides significant improvement of the global fit compared to the pure oscillation case.

The results of the fits are presented in terms of effective parameters, representing the specific combinations of NSI parameters entering in the transition probabilities. However, for both cases, NSI^c and NSI^g , examples are provided of how to realise the required parameters in terms of the fundamental mixing and NSI parameters. It is shown that values in safe agreement with bounds on the various ε 's can be found to realise the fits which require ε 's of order a few $\times 10^{-2}$.

The quality of the (3+1) NSI fits are compared to an updated fit in the (3+2) oscillation scheme, which also allows for CP violation due to the presence of two relevant mass scales. Similarly to (3+1) NSI, in (3+2) the appearance experiments can be described very well. However, as previously [232], for (3+2) oscillations significant tension remains in the global fit between appearance and disappearance experiments. The improvement of (3+2) compared to (3+1) is not significant, in terms of χ^2 gain per new parameter. None of the scenarios considered in [14] can explain the MiniBooNE low energy excess of events when disappearance data are taken into account. Therefore, the data below 475 MeV is excluded from the analysis, relying on a separate explanation for this anomaly.

The predictions of the model for future experiments depend on the detailed realization in terms of mixing and NSI parameters. In general one may expect some signals in searches for deviations from the standard three-flavour oscillation picture in both respects, sterile neutrino oscillations as well as NSI. Several proposals to search for sterile neutrinos at the eV scale have been presented recently, see for example [15, 221, 225, 227, 234, 235]. In [236] implications of sterile neutrinos for latest cosmological data have been investigated. Recent studies on NSI in the context of upcoming and far future experiments can be found, e.g., in [16, 157, 237, 238]. A specific prediction of the

scenario are zero-distance effects in appearance searches [16, 239, 240]. Hence, the observation of an energy independent appearance probability at very short distances is a characteristic signature from this kind of models.

The model may also provide a signature at the LHC. Typically, realising CC-like interactions as the ones considered here require a charged particle as mediator. The NSI parameters ε measure the strength of the new interactions relative to the standard weak interaction strength set by G_F . Therefore, from the fit results, $\varepsilon \sim 0.01$, one expects that the mass of a mediator for a dimension-6 operator should be roughly one order of magnitude larger than the W boson mass. Hence, one might expect charged particles to show up at the TeV scale, with good prospects to be observed at LHC. However, the results of [241, 242] suggest that NSI at the level of 0.01 are difficult to obtain from dimension-6 operators without being in conflict with bounds on charged-lepton processes. As discussed there, a possibility to obtain such large NSI would be to go to dimension-8 operators and allow for some fine tuning.

6.4. Sterile neutrinos beyond LSND at the Neutrino Factory [15]

In this section we will discuss the discovery reach for sterile neutrinos at the standard IDS-NF baseline. We consider the simplest scenario in which only one sterile neutrino is added to the three active neutrinos of the Standard Model in the so-called 3+1 scheme which recovers the standard picture in the case of small active-sterile mixings [15, 234, 243–248]. For the sake of simplicity, we just focus on the scheme where the fourth state is the heaviest and normal hierarchy is assumed in the standard sector. The numerical results on the discovery reach can be understood from the analytical expressions of the transition probabilities; we found particularly illuminating the following parameterization of the 4×4 unitary mixing matrix U :

$$U = R_{34}(\theta_{34}, 0) R_{24}(\theta_{24}, 0) R_{14}(\theta_{14}, 0) R_{23}(\theta_{23}, \delta_3) R_{13}(\theta_{13}, \delta_2) R_{12}(\theta_{12}, \delta_1), \quad (28)$$

where $R_{ij}(\theta_{ij}, \delta_l)$ are the complex rotation matrices in the ij -plane. In the short-baseline limit $|\Delta_{41}| = \Delta m_{41}^2 L/4E \sim \mathcal{O}(1) \gg |\Delta_{31}|$, the matter effects can be safely ignored, and the relevant probabilities read:

$$\mathcal{P}_{e\mu} = \mathcal{P}_{\mu e} = 4c_{14}^2 s_{14}^2 s_{24}^2 \sin^2 \Delta_{41} \quad (29)$$

$$\mathcal{P}_{ee} = 1 - \sin^2(2\theta_{14}) \sin^2 \Delta_{41} \quad (30)$$

$$\mathcal{P}_{\mu\tau} = 4c_{14}^4 c_{24}^2 s_{24}^2 s_{34}^2 \sin^2 \Delta_{41} \quad (31)$$

$$\mathcal{P}_{\mu\mu} = 1 - c_{14}^2 s_{24}^2 [3 + 2c_{14}^2 \cos(2\theta_{24}) - \cos(2\theta_{14})] \sin^2 \Delta_{41} \quad (32)$$

where we used the short-hand notation $\Delta_{ij} = \Delta m_{ij}^2 L/4E$. From these probabilities we can see that θ_{24} can be measured by $\mathcal{P}_{\mu\mu}$ and θ_{14} by \mathcal{P}_{ee} . On the other hand, θ_{34} only shows up in combination with the other small mixing angles. For long baselines, some of the relevant features of the probability transitions can be well understood using simple perturbative expansions: for $\Delta_{31} = \mathcal{O}(1) \ll \Delta_{41}$ and

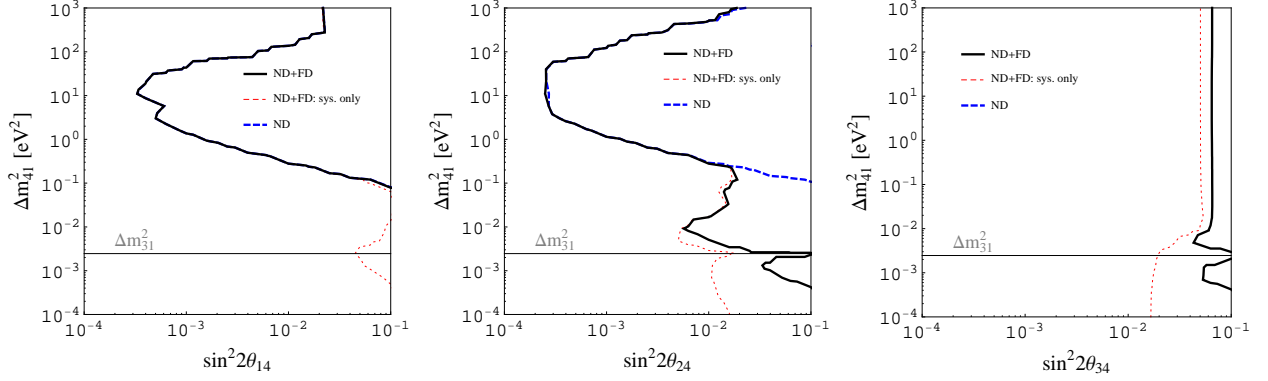


Figure 26. The exclusion limit at 90% CL (2 d.o.f) for $\sin^2 2\theta_{i4}-\Delta m_{41}^2$ ($i = 1, 2, 3$) (region on r.h.s. of curves excluded). Here gives results of the standard IDS-NF (4000 km and 7500 km) setup with near detectors (thick solid curves), and the impact of the near detectors is also shown separately (thick dashed curves). The thin dashed curves only consider systematics.

up to the second order in $s_{13}, s_{14}, s_{24}, s_{34}, \hat{s}_{23} = \sin \theta_{23} - \frac{1}{\sqrt{2}}$, and considering Δ_{21} as small as s_{ij}^2 , we obtain:

$$\begin{aligned} \mathcal{P}_{\mu\mu} = & \cos^2(\Delta_{31})(1 - 2s_{24}^2) + 8\hat{s}_{23}^2 \sin^2(\Delta_{31}) + c_{12}^2 \Delta_{12} \sin(2\Delta_{31}) + \\ & 2s_{24}s_{34} \cos \delta_3 \Delta_n \sin(2\Delta_{31}) - \\ & 2s_{13}^2 \Delta_{31} \cos(\Delta_{31}) \frac{(\Delta_{31} - \Delta_e) \Delta_e \sin(\Delta_{31}) - \Delta_{31} \sin(\Delta_{31} - \Delta_e) \sin(\Delta_e)}{(\Delta_{31} - \Delta_e)^2}, \end{aligned} \quad (33)$$

$$\begin{aligned} \mathcal{P}_{\mu\tau} = & \sin^2(\Delta_{31})(1 - 8\hat{s}_{23}^2 - s_{24}^2 - s_{34}^2) - c_{12}^2 \Delta_{12} \sin(2\Delta_{31}) - \\ & s_{24}s_{34} \sin(2\Delta_{31}) [2\Delta_n \cos \delta_3 - \sin \delta_3] - \\ & s_{13}^2 \Delta_{31} \sin \Delta_{31} \frac{\Delta_{31} \{\sin(\Delta_{31} - \Delta_e) + \sin(\Delta_e)\} - 2(\Delta_{31} - \Delta_e) \Delta_e \cos(\Delta_{31})}{(\Delta_{31} - \Delta_e)^2}. \end{aligned} \quad (34)$$

from which we learn that at the long baselines, θ_{24} is best accessible by $\mathcal{P}_{\mu\mu}$ with the first term proportional to $\cos^2(\Delta_{13})$. The leading sensitivity to θ_{34} can be expected from $\mathcal{P}_{\mu\tau}$ (the *discovery channel* as claimed by [234]). Notice also the dependence on the phase δ_3 in both probabilities which makes them useful to check whether other sources of CP violation beside the standard one (δ_2 in our parameterization) can be tested at the Neutrino Factory. Let us first discuss general constraints to the new mixing angles θ_{14} , θ_{24} , and θ_{34} and the additional mass squared difference Δm_{41}^2 without any additional assumptions [15]. The considered oscillation channels, simulated with a properly modified version of the GLoBES software, are electron to muon neutrino (appearance channels) and muon to muon neutrino (disappearance channels) oscillations. Beside the standard IDS-NF setup, we also considered near detectors with a fiducial mass of 32 t and a distance of $d = 2$ km from the end of the decay straight, which corresponds to the effective baseline of 2.28 km. We show three different exclusion planes $\theta_{i4}-\Delta m_{41}^2$ in Fig.6.4. The main sensitivity is obtained at about $\Delta m_{41}^2 \simeq 10 \text{ eV}^2$, which comes from the distance chosen for the near detectors. Since the efficiencies for muon neutrino detection

are typically better, the sensitivity to θ_{24} is slightly better than that to θ_{14} for our assumptions. As expected, there is no sensitivity to θ_{34} coming from the near detectors, because the ν_τ disappearance channel does not exist. For the effect at the long baselines, it is first of all useful to consider the thin dashed curves with systematics only. In all three panels, the sensitivity changes as a function of Δm_{41}^2 in the region where $\Delta m_{41}^2 \sim \Delta m_{31}^2$. It comes from the fact that the Neutrino Factory is sensitive to the atmospheric oscillation frequency, whereas for $\Delta m_{41}^2 \sim \Delta m_{21}^2$, no particular additional effects from the solar frequency can be found. As expected (see Eq. (33)), the main sensitivity is found for θ_{24} . However, there is also some sensitivity to θ_{14} , which vanishes after the marginalization, and some sensitivity to θ_{34} , which is even present for $\Delta m_{41}^2 = 0$ for systematics only. After marginalization (thick solid curves), only the sensitivities to θ_{24} and θ_{34} remain in the Δm_{41}^2 regions close to the atmospheric Δm_{31}^2 and above, where the effects of Δm_{41}^2 average out. Very interestingly, note that mixing angle correlations destroy the sensitivities for $\Delta m_{41}^2 = \Delta m_{31}^2$, where $m_4 = m_3$ and no additional Δm_{41}^2 is observable, leading to small gaps (see horizontal lines). We have tested that the sensitivity to θ_{34} is a matter potential-driven, statistic limited higher order effects present in the muon neutrino disappearance channels. In view of the three panels, it is not easy to disentangle the parameters for arbitrary massive sterile neutrinos. Parameter correlations lead to a pollution of the exclusion limit of a particular mixing angle with Δm_{41}^2 . In addition, there is a competition between Δm_{41}^2 and Δm_{31}^2 at the long baseline. Near detectors, on the other hand, have very good sensitivities to θ_{14} and θ_{24} but cannot measure θ_{34} . Nevertheless, the absolute values of the sensitivities are quite impressive. Especially, θ_{24} can be very well constrained close to the atmospheric mass squared difference range. This indicates that sterile neutrino bounds in that range should be also obtainable from current atmospheric neutrino oscillation experiments.

6.5. NSI's vs. non-unitary lepton flavor mixing at a neutrino factory [16]

Apart from the study of neutrino oscillation parameters, one of the most important tasks in future neutrino oscillation experiments, e.g., a neutrino factory (NF), is to search for non-standard effects stemming from the exchange of heavy fields presented in high-energy theories. In the language of the effective theory, the impacts of heavy particles can be parametrized in terms of a tower of higher dimensional non-renormalizable operators, e.g., the dimension-five operator $\mathcal{O}_W^5 = (\bar{L}^c i \tau^2 \phi) (\phi i \tau^2 L)$ responsible for the generation of neutrino masses. According to the nature of the heavy fields, the dimension-six operators can be classified into two categories, the scalar mediated operators and the fermion mediated operators (See discussions and references in, e.g., Refs. [17, 249, 250] on the possible theories behind these operators). These dimension-six operators typically suffer from severe experimental constraints on the lepton flavor violating processes, since $\ell \rightarrow \ell \ell \ell$ decays may be induced at tree level. However, there are two leptonic dimension-six operators which do not lead to charged lepton flavor violation,

$$\mathcal{O}^S = (\bar{L}^c \cdot L) (\bar{L} \cdot L^c) , \quad \mathcal{O}^F = (\bar{L}_\alpha \tilde{\phi}) i \not{\partial} (\tilde{\phi}^\dagger L_\beta) , \quad (35)$$

where L and ϕ stand for the Standard Model lepton doublets and the Higgs field. The scalar mediated operator \mathcal{O}^S leads to non-standard neutrino interactions (NSIs), whereas the fermion mediated operator \mathcal{O}^F results in non-unitarity (NU) effects. Note that, the NU effects are similar to these from NSIs, and therefore, both NSIs and NU can be described by using the same parametrization, i.e., the conventional ε^A parameters, where $A = s, m, d$ correspond to non-standard effects in the neutrino production, propagation, and detection processes, respectively.

The generic bounds on above two dimension-six operators come from rare lepton decays $\ell_\alpha \rightarrow \ell_\beta \gamma$, the invisible decay width of the Z -boson and the universality test of weak interactions, and can be found in Refs. [161, 241]. An important question to be answered is if we can distinguish these two operators at future neutrino oscillation experiments so as to find hints on the origin of non-standard effects. To this end, we remark that the NU effects are fundamental and process-independent, whereas the NSI effects are experiment-dependent. For example, \mathcal{O}^S does not affect the neutrino production process at a superbeam experiment since it is essentially a hadron decay process. We summarize in Tab. XI which non-standard effects are allowed for a neutrino factory and a superbeam if the origin are the discussed leptonic dimension-six operators. In addition, there exist non-trivial correlations

Table XI. *Allowed parameters from the discussed dimension-six effective operator classes in a neutrino factory (ν -factory) and a superbeam experiment (SB).*

	ν -factory		SB			ν -factory		SB			ν -factory		SB		
	\mathcal{O}^S	\mathcal{O}^F	\mathcal{O}^S	\mathcal{O}^F		\mathcal{O}^S	\mathcal{O}^F	\mathcal{O}^S	\mathcal{O}^F		\mathcal{O}^S	\mathcal{O}^F	\mathcal{O}^S	\mathcal{O}^F	
ε_{ee}^m		✓		✓	ε_{ee}^s	✓	✓	n/a	n/a	$\varepsilon_{\alpha\beta}^d$					
$\varepsilon_{e\mu}^m$					$\varepsilon_{e\mu}^s$	✓	✓	n/a	n/a						
$\varepsilon_{e\tau}^m$					$\varepsilon_{e\tau}^s$	✓	✓	n/a	n/a			✓		✓	
$\varepsilon_{\mu\mu}^m$	✓	✓	✓	✓	$\varepsilon_{\mu e}^s$		✓		✓						
$\varepsilon_{\mu\tau}^m$	✓	✓	✓	✓	$\varepsilon_{\mu\mu}^s$	✓	✓		✓						
$\varepsilon_{\tau\tau}^m$	✓	✓	✓	✓	$\varepsilon_{\mu\tau}^s$	✓	✓		✓						

between the source and matter non-standard effects for both \mathcal{O}^S and \mathcal{O}^F [242], i.e.,

$$\varepsilon_{\mu\tau}^m = -(\varepsilon_{\mu\tau}^{\text{NF}})^* \quad (\text{NSIs}), \quad \varepsilon_{\mu\tau}^m = -\varepsilon_{\mu\tau}^s \quad (\text{NU}), \quad (36)$$

which motivate us to investigate the possibility of distinguishing the origin of non-standard effects at a neutrino factory alone [16].

In the left column of Fig. 27, we illustrate the potential of discriminating \mathcal{O}^S from \mathcal{O}^F at an IDS-NF (International Design Study) with parent muon energy $E_\mu = 25$ GeV [251] (See also a detailed description of the experiment setups in Ref. [16]). In our numerical analysis, we make use of the “true” parameters in the case of \mathcal{O}^F (\mathcal{O}^S), and then fit the data with only \mathcal{O}^S (\mathcal{O}^F). For the IDS-NF neutrino factory combined with several different near detectors, the curves in the left column show that there is just a very small region beyond the bound at the 90 % C.L. on the \mathcal{O}^F operators, where the data generated with \mathcal{O}^F can be distinguished from the \mathcal{O}^S even if the OPERA-like near detector at the longer baseline is used. If \mathcal{O}^S is simulated, however, it can be distinguished from \mathcal{O}^F

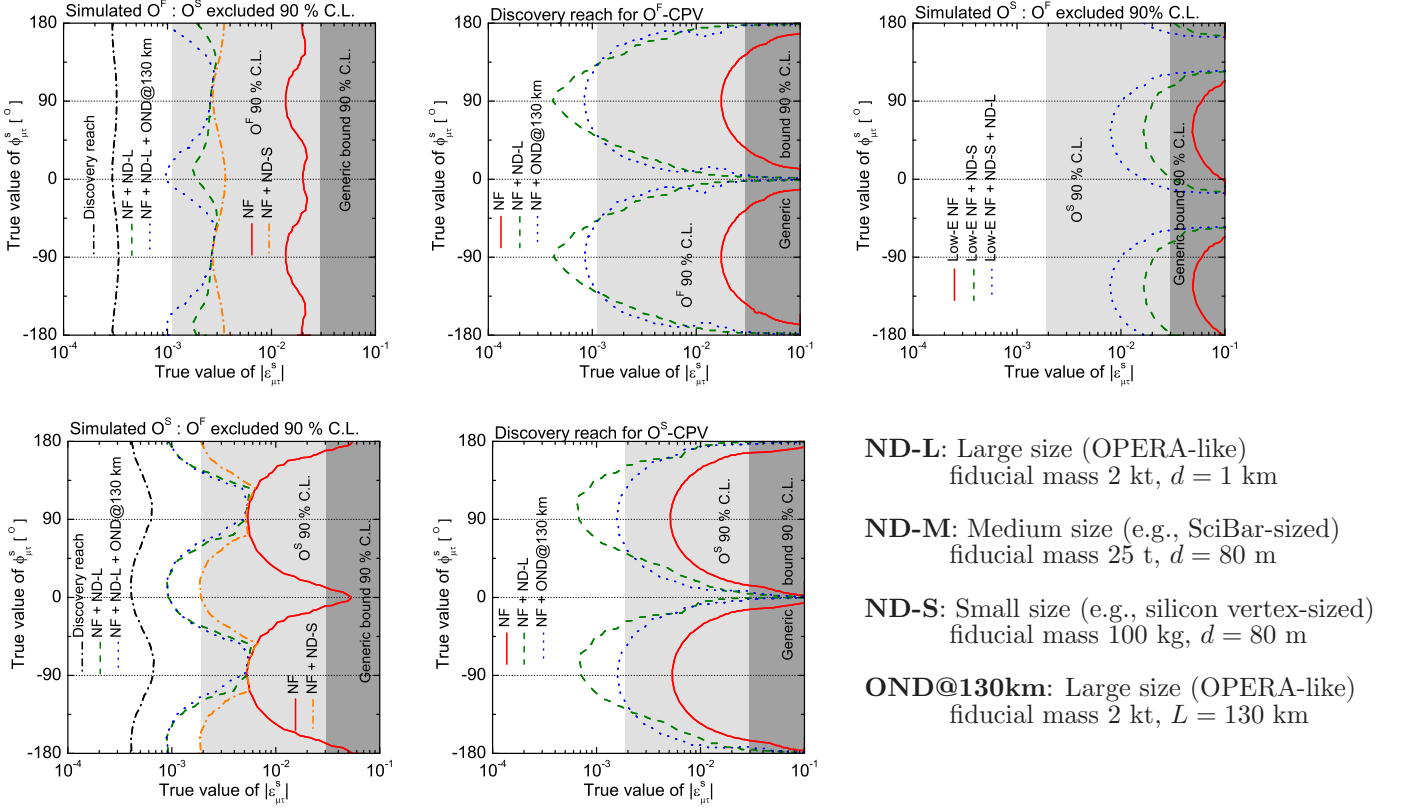


Figure 27. *Left column:* regions in the $(|\epsilon_{\mu\tau}^s| - \phi_{\mu\tau}^s)$ -plane where the simulated $\epsilon_{\mu\tau}^s$ induced by one type of operator can be uniquely established, i.e., the other type of operator is excluded at the 90 % C.L. (regions on the right-hand side of the curves) at an IDS-NF ($E_\mu = 25$ GeV). The discovery reach is also displayed in each plot. *Middle column:* 90 % C.L. of CP discovery potentials in the NU framework (upper plot) and NSI framework (lower panel) at an IDS-NF. *Right column:* same plot as the lower panel of the left column, but for a low-energy neutrino factory ($E_\mu = 4.5$ GeV) alone and in combination with the ND-S and ND-S+ND-L. Taken from [16].

for a part of the parameter space beyond the current bound with ND-L. In the middle column of Fig. 28, we plot the CP discovery potential for both \mathcal{O}^F (upper panel) and \mathcal{O}^S (lower plot) induced CP violations. This is defined as the ensemble of true values of $\phi_{\mu\tau}^s$ (phase of $\epsilon_{\mu\tau}^s$), which cannot be fitted with the CP-conserving values $\phi_{\mu\tau}^s = 0, \pm\pi$ at 90 % C.L. The combination of the standard IDS-NF neutrino factory with different large enough near detectors may discover CP violation, somewhat beyond the current bounds, especially for $\phi_{\mu\tau}^s \sim \pm\pi/2$. There are no qualitative differences between \mathcal{O}^F and \mathcal{O}^S . Finally, we show, in the right upper panel of Fig. 28, that a low-energy neutrino factory ($E_\mu = 4.5$ GeV) [147, 149] is not able to exclude the \mathcal{O}^F operator at 90 % C.L., since the exclusion regions are excluded by current limits already.

In conclusion, differentiating between NSIs and NU should be one of the key priorities of searches for new physics effects, since the nature of non-standard effect points towards the nature of the heavy mediator. The components necessary for this search are ν_τ detection at least in near detectors, both

at high-intensity superbeams and a neutrino factory. For the neutrino factory, a high enough muon energy is mandatory for the discussed non-standard effects searches, which means that the high-energy neutrino factory should at least be an upgrade option even for large θ_{13} . In addition, for non-standard effect searches, the size of the near detector is very important, which means that for all applications, large enough detectors are needed.

6.6. Non-standard neutrino interactions in the Zee–Babu model [17]

While the origin of neutrino masses emerges as one of the unsolved and fundamental problems in particle physics, the mechanism of radiative mass generation provides a natural method to obtain small neutrino masses. In such a framework, neutrino masses are exactly vanishing at tree level, and are induced as finite radiative corrections. The simplest version of this kind of models, i.e., the Zee model [252], cannot accommodate current experimental data, since the predicted leptonic mixing angle θ_{12} is too large. Alternatively, in the Zee–Babu model [253–255], two $SU(2)_L$ singlet scalars (one singly charged h^+ and one doubly charged h^{++}) are introduced besides the Standard Model (SM) particle content, and neutrino masses can be generated at two-loop level. In addition to the generation of neutrino masses, the exchange of heavy scalars also results in lepton flavor violating processes such as $\mu \rightarrow 3e$ and $\mu \rightarrow e\gamma$, which can be dramatically enhanced compared to those in the SM. Most interestingly, if kinematically accessible, the new scalars could be directly produced at the Large Hadron Collider or the future International Linear Collider, and the decay of the doubly charged Higgs may induce very clean like-sign bi-lepton events, which are basically free from SM background, and opening the possibility of collider tests of the neutrino mass generation mechanism.

Besides colliders, the next generation neutrino oscillation experiments, e.g., neutrino factories, will also help us to unveil the underlying physics behind neutrino masses, in particular, through exploring non-standard neutrino interactions (NSIs). Unfortunately, in most of the low-scale models [249], NSIs are typically linked to lepton flavor violating processes of charged leptons, yielding too tight bounds, see, e.g., Refs. [161, 241, 256]. However, in the case of the Zee–Babu model, the situation is more involved, since the masses of singly and doubly charged Higgs in principle can be well separated and a different set of Yukawa couplings controls charged lepton and neutrino interactions with the scalars. In the following we summarize the results of Ref. [17], where a detailed investigation of NSIs in the Zee–Babu model has been performed.

The Lagrangian of the minimal Zee–Babu model reads

$$\mathcal{L} = \mathcal{L}_{\text{SM}} + f_{\alpha\beta} L_{L\alpha}^T C i\sigma_2 L_{L\beta} h^+ + g_{\alpha\beta} \bar{e}_\alpha^c e_\beta k^{++} - \mu h^- h^- k^{++} + \text{h.c.} + V_H, \quad (37)$$

where L_L denote left-handed lepton doublets, e are the right-handed charged leptons, and the scalar potential V_H contains the couplings among scalar fields. f and g are antisymmetric and symmetric Yukawa couplings, respectively. Neutrino masses are generated at two-loop level as

$$m_\nu \simeq \frac{1}{48\pi^2} \frac{\mu}{M^2} \tilde{I} f D_e g^\dagger D_e f^T, \quad (38)$$

where $D_e = \text{diag}(m_e, m_\mu, m_\tau)$ contains the charged-lepton masses, $M = \max(m_k, m_h)$, and $\tilde{I}(r)$ is a dimensionless function of order unity [257]. Furthermore, the tree-level exchange of h^+ induces non-standard lepton interactions via dimension-six operators

$$\mathcal{L}_{d=6}^{\text{NSI}} = 4 \frac{f_{\alpha\beta} f_{\rho\sigma}^*}{m_h^2} (\bar{\ell}_\alpha^c P_L \nu_\beta) (\bar{\nu}_\sigma P_L \ell_\rho^c) = 2\sqrt{2} G_F \varepsilon_{\alpha\beta}^{\rho\sigma} (\bar{\nu}_\alpha \gamma^\mu P_L \nu_\beta) (\bar{\ell}_\rho \gamma_\mu P_L \ell_\sigma) , \quad (39)$$

where $\varepsilon_{\alpha\beta}^{\rho\sigma} \simeq 0.06 f_{\sigma\beta} f_{\rho\alpha}^* \left(\frac{m_h}{\text{TeV}}\right)^{-2}$ are the canonical NSI parameters. Using the conventional notation in the literature, e.g., Ref. [238], we find that the following NSI parameters are induced

$$\varepsilon_{\alpha\beta}^m = \varepsilon_{\alpha\beta}^{ee} = \frac{f_{e\beta} f_{e\alpha}^*}{\sqrt{2} G_F m_h^2} , \quad \varepsilon_{\mu\tau}^s = \varepsilon_{\tau e}^{e\mu} = \frac{f_{\mu e} f_{e\tau}^*}{\sqrt{2} G_F m_h^2} , \quad \varepsilon_{e\tau}^s = \varepsilon_{\mu\tau}^{e\mu} = \frac{f_{\mu\tau} f_{e\mu}^*}{\sqrt{2} G_F m_h^2} , \quad (40)$$

where the superscript m and s correspond to NSI effects in matter and in the neutrino source at a Neutrino Factory, respectively.

Equations (38) and (40) indicate that there exists a firm connection between neutrino parameters and NSI parameters. For example, in the of normal mass hierarchy ($m_1 \ll m_2 \ll m_3$, NH), the relation $f_{e\mu} \simeq f_{e\tau} \simeq f_{\mu\tau}/2$ approximately holds, while in the case of inverted mass hierarchy ($m_2 > m_1 \gg m_3$, IH), $|f_{e\mu}| \sim |f_{e\tau}|$ and $|f_{\mu\tau}| \sim |f_{e\tau}| s_{13}/s_{23}$ can be obtained. Taking into account the experimental constraints from the universality in $\ell_a \rightarrow \ell_b \bar{\nu} \nu$ decays [257], we can roughly estimate that $|f_{e\mu}| \sim |f_{e\tau}| \lesssim 0.05 (m_h/\text{TeV})$ and $|f_{\mu\tau}| \lesssim 0.1 (m_h/\text{TeV})$. Therefore, compared with Eq. (40), the important NSI parameters in the NH case is $\varepsilon_{e\tau}^s$, while in the IH case, $\varepsilon_{\mu\tau}^m$, $\varepsilon_{\mu\mu}^m$, $\varepsilon_{\tau\tau}^m$, and $\varepsilon_{\mu\tau}^s$ can be sizable.

Taking into account the experimental bounds summarized in Ref. [257], we present, in Fig. 28, the allowed regions of NSI parameters and $\sin\theta_{13}$ at 1σ , 2σ , and 3σ C.L. We find, from the left column, that $\varepsilon_{\mu\mu}^m$ and $\varepsilon_{\tau\tau}^m$ can only be sizable in the IH case, while the present long-baseline experiments are not very sensitive to these parameters. As for the source related NSI parameters, $\varepsilon_{e\tau}^s$ may reach values up to 10^{-3} for both hierarchies, whereas $\varepsilon_{\mu\tau}^s$ can be as large as few $\times 10^{-3}$ only in the IH case. In particular, for a scalar mass scale of 1 TeV, a non-trivial lower bound on the NSI parameters of order 10^{-4} is found, indicating that the model is rather constrained from the requirement of a correct neutrino mass matrix. The right column in Fig. 28 shows correlations between NSI parameters and the mixing angle θ_{13} . Especially, in the IH case, one obtains a quite strong prediction for θ_{13} , i.e., a lower bound $\sin^2\theta_{13} \gtrsim 10^{-2}$. Such a sizable lower bound is of particular interest, since it would guarantee a discovery at the forthcoming reactor or long-baseline experiments in the near future [150].

In conclusion, sizable NSIs can be accommodated in the Zee–Babu model in a natural way, and they depend on both the mass scale of the charged scalars and on the type of neutrino mass hierarchy, NH or IH. We further remark that, in addition to the NSIs, the singly and doubly charged scalars could be directly produced through the s -channel processes at the Tevatron and the LHC. Therefore, the interplay of the phenomenology at colliders, search for lepton flavor violation, and NSI effects at neutrino oscillation experiments could play a complementary role towards the goal of identifying the true mechanism of neutrino mass generation.

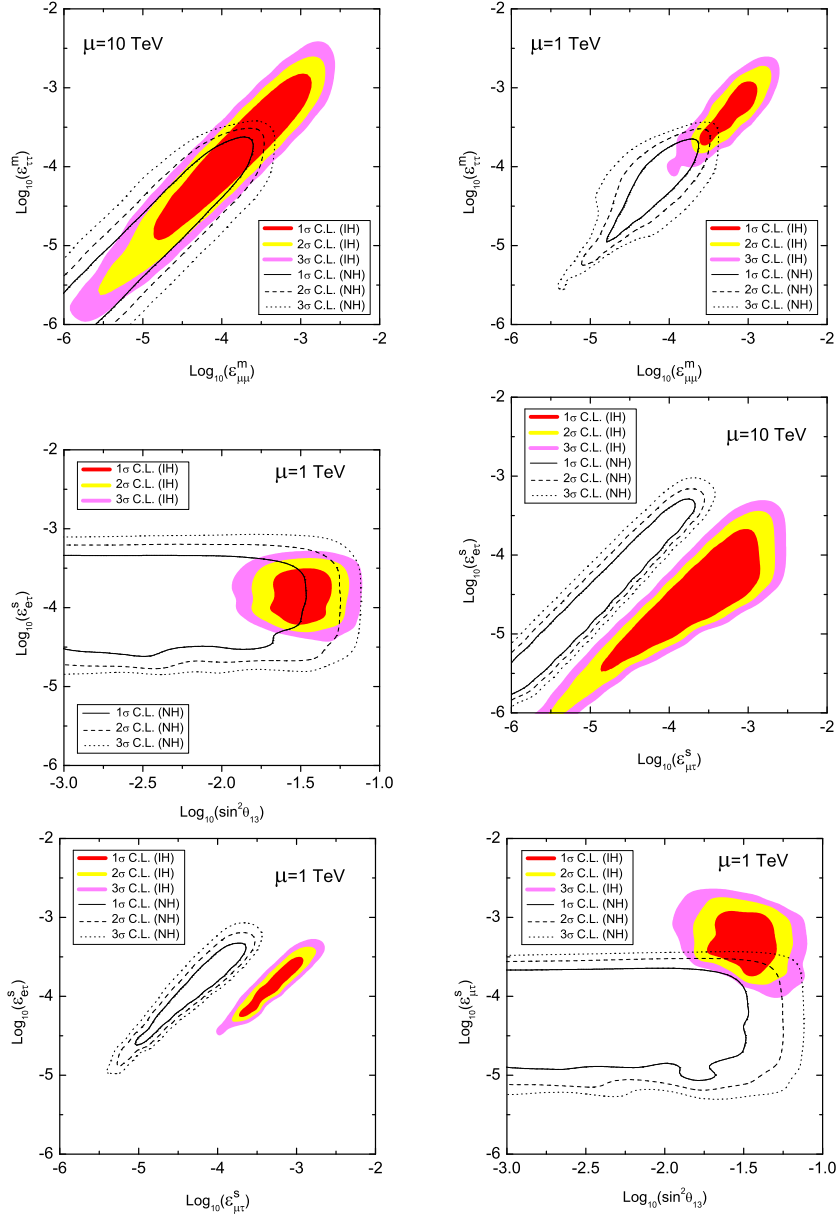


Figure 28. Allowed regions of NSI parameters and $\sin^2 \theta_{13}$ at 1σ , 2σ , and 3σ C.L. We take $m_h = m_k = \mu = 10$ TeV for the figures in the left column and $m_h = m_k = \mu = 1$ TeV for the figures in the middle and right column. Taken from [17].

7. Physics potential of EUROnu facilities as of April 2011 [18]

In Figs. 29-31 we present the comparison of the physics potential of the three EUROnu facilities (the 25 GeV Neutrino Factory, the $\gamma = 100$ Beta-Beam and the SPL Super-Beam) as shown at the Technical Review Meeting in Geneva, April 13th, 2011. Results for the $\gamma = 100$ beta-beam are shown for several values of the neutrino fluxes, as well as in combination with the SPL. In addition to the 25 GeV Neutrino Factory, results for the 10 GeV Low-Energy Neutrino Factory are also shown in case $\sin^2 2\theta_{13}$ were found to be larger than 10^{-2} (as it is indeed the case according to the recent results of T2K, MINOS, Daya Bay, RENO and Double Chooz experiments).

The three figures correspond to: (1) sensitivity to θ_{13} , Fig. 29; (2) CP discovery potential, Fig. 30; and, (3) sensitivity to the neutrino mass hierarchy, Fig. 31. The curves correspond to 3σ CL (1 dof). The other parameters have been fixed to $\Delta m_{31}^2 = 0.0024\text{eV}^2$, $\Delta m_{21}^2 = 8 \times 10^{-5} \text{ eV}^2$ and $\theta_{23} = 45^\circ$.

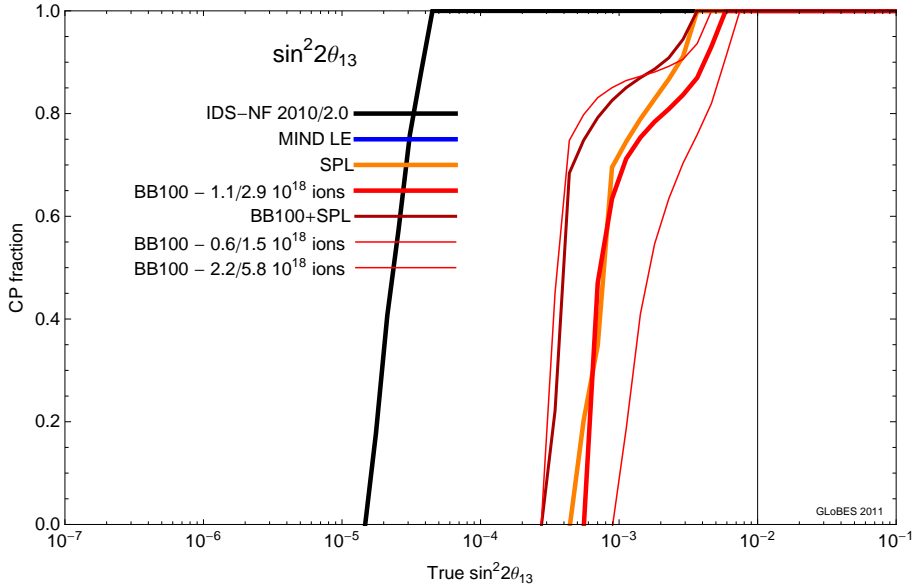


Figure 29. Comparison of the sensitivity to θ_{13} of different future facilities as a function of $\sin^2 2\theta_{13}$. Prepared by P. Huber for the EUROnu Technical Review, April 13th, 2011, using the GLOBES package [258, 259]. Curves are taken from [a] [103], [b] [260], [c] [122], [d] [150] and [e] [147].

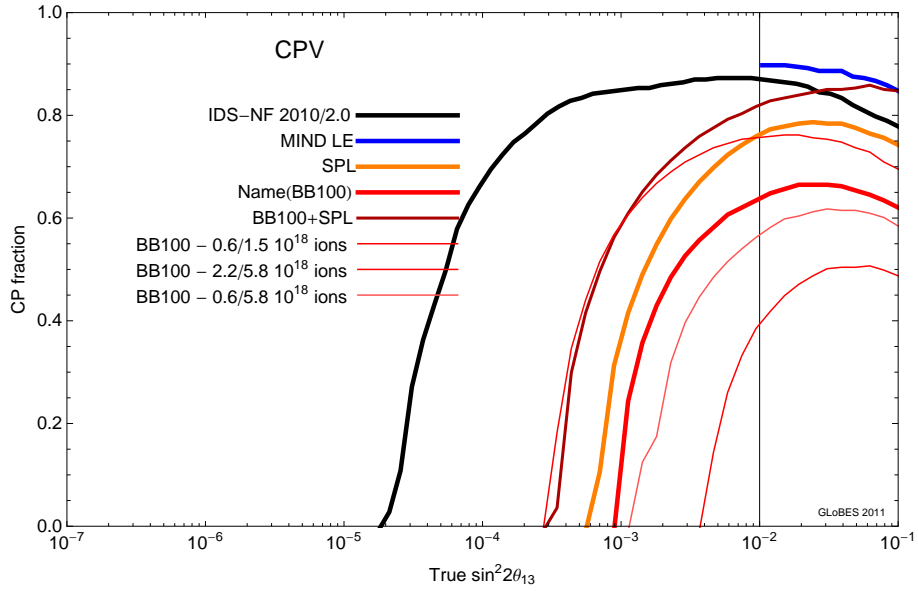


Figure 30. Comparison of the CP discovery potential of different future facilities as a function of $\sin^2 2\theta_{13}$. Prepared by P. Huber for the EUROnu Technical Review, April 13th, 2011, using the GLOBES package [258, 259]. Curves are taken from [a] [103], [b] [260], [c] [122], [d] [150] and [e] [147].

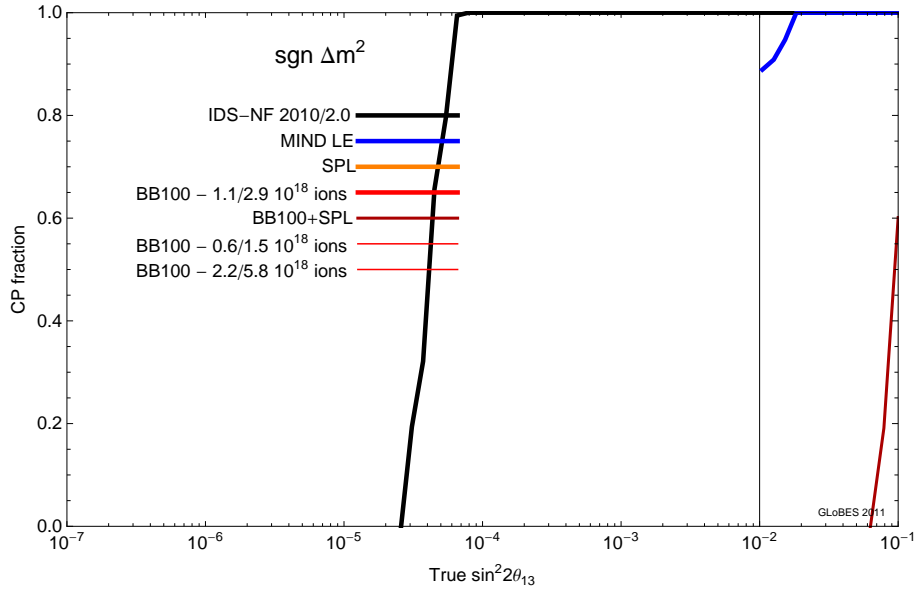


Figure 31. Comparison of the sensitivity to the neutrino mass hierarchy of different future facilities as a function of $\sin^2 2\theta_{13}$. Prepared by P. Huber for the EUROnu Technical Review, April 13th, 2011, using the GLOBES package [258, 259]. Curves are taken from [a] [103], [b] [260], [c] [122], [d] [150] and [e] [147].

8. Summary of the NuFlavour workshop [19]

In 8–10 June 2009, the workshop "Flavour physics in the era of precision neutrino experiments" at Coseners House, Abingdon, UK, focussed on a critical review of the physics case for neutrino physics and long baseline neutrino oscillations from a theoretical perspective. This workshop was organised with partial support from the European Community under the European Commission Framework Programme 7 Design Studies: EUROnu (Project Number 212372). The topics which were discussed included: i) lepton flavor violation (LFV) from grand unified theory (GUT) see-saw models and from TeV see-saw models, ii) Leptogenesis in the context of neutrino mass models, iii) A theoretical perspective on lepton flavor physics at the TeV scale within supersymmetric (SUSY) models and extra-dimension models, iv) Interplay between neutrino masses and other phenomenological signatures, v) Neutrino physics and cosmology/astroparticle physics, and finally vi) Performance indicators in long baseline neutrino oscillation experiments.

8.1. LFV from GUT see-saw models and from TeV see-saw models

See-saw models provide a natural solution to the smallness of neutrino masses and they can be embedded in Grand Unified Theories (talk by G. Ross) or emerge at the TeV scale, being testable at the LHC in the forecoming future (talk by E. Ma). All these models need also to account for the low energy flavor structure (talk by M. Schmidt). A series of theoretical questions emerged at the meeting: Is it possible to discriminate between GUT and TeV-scale see-saw models? How do these models inscribe into a more general theory? Where does the smallness of neutrino masses come from, and does it require fine-tuning anywhere? How can flavor mixing be implemented? Is it possible to define some "benchmark" scenarios? If so, which ones? Is it possible to have arguments for the precisions required for θ_{13} , δ , and the Majorana phases? What information on the origin of neutrino masses can be obtained from the mass hierarchy measurement? These questions were addressed in the discussion session lead by M. Frigerio. It was mainly emphasized that there are two aspects which need to be studied: the origin of neutrino masses and the rationale for the leptonic flavor structure. Three contributed talks were also given by A. Adulpravitchai on Non-abelian Discrete Flavor Symmetries from T^2/Z_N Orbifolds, by D. Hernandez on the Minimal Flavor Seesaw Models and by M. Satriawan on Possible mechanism for generating a very small Dirac neutrino mass.

8.2. Neutrino physics and the cosmology/astroparticle physics complementarity

The bath of relic cosmological neutrinos, which decoupled at $T \sim 1$ MeV, affects the evolution of the Universe, in particular Big Bang Nucleosynthesis, large scale structure formation and the Cosmic Microwave Background and allows to constrain neutrino masses, the number of neutrinos and the type of neutrino interactions (talk by S. Hannestad). Sterile neutrinos are the leading candidate for warm dark matter and can be tested in x-ray searches from dark matter overdensities, as the

center of the galaxy or nearby dwarf galaxies (talk by A. Kusenko). In the discussion session lead by P. Di Bari, various issues were discussed, in particular those related to the comparison between cosmological bounds and terrestrial ones, the estimation of systematic errors in the measurement of neutrino parameters from cosmological observations, and the impact of a non-standard evolution of the Early Universe.

8.3. A theoretical perspective on lepton flavor physics at the TeV scale within i) SUSY models ii) extra-dimension models

The origin of neutrino masses requires new particles and interactions which need to be embedded in a wider scheme to solve the hierarchy problem and explain the pattern of masses and mixing. Possible scenarios are supersymmetric (talks by S. Lavignac, S. Khalil and A. Teixeira), extra dimensions, and little Higgs models. One needs to consider how these models fit into a wider particle physics theory and if there are any model-independent signatures. These issues were discussed by A. Santamaria. Generically, the embedding of neutrino mass models in a wider scheme induces new signatures as LFV processes at low energy such as $\mu \rightarrow e\gamma$, $\mu - e$ conversion, and $\tau \rightarrow e\gamma$.

8.4. Leptogenesis in the context of neutrino mass models: model dependent versus model independent considerations

Leptogenesis (talk by A. Abada) is one of the favored mechanisms for the generation of the baryon asymmetry of the Universe and naturally takes place in see-saw models. In the presence of CP-violation the decays of heavy Majorana neutrinos in the Early Universe produce a lepton asymmetry which is partially washed-out and converted into a baryon asymmetry by sphaleron processes. Compelling questions arise (discussion session lead by E. Nardi): Under what conditions can a connection between low and high energy CP violation be established? Is it obvious to believe in leptogenesis if a low energy CP violation and lepton number violation is observed? In see-saw type I models, in general, there is not a direct connection between low energy parameters and high energy ones. This link arises if a theory of flavor is present, which explains the observed mixing pattern and reduces the number of free-parameters. For masses of the heaviest neutrino smaller than 10^{12} GeV, flavor effects play an important role. In this case, generically a connection between leptogenesis and low energy CP-violating phases can be obtained in the sense that if CP-violation is found in future neutrino experiments a lepton asymmetry needs to be generated in the Early Universe. Leptogenesis can also take place in other see-saw models, for example see-saw type II models and in other scenarios of neutrino mass generation.

8.5. Interplay between neutrino masses and other phenomenological signatures

Small neutrino masses require new physics beyond the Standard Model which can induce also other signatures at low energy. Additional sources of lepton flavor violation induce processes at low energy such as $\mu \rightarrow e\gamma$, $\mu - e$ conversion, $\tau \rightarrow e\gamma$ (talk by A. de Gouvea) at rates which could be close to present bounds. The LHC experiment will provide information on the physics at the TeV scale which might also be at the origin of neutrino masses (talk by T. Schwetz). Additional effects can arise in neutrino oscillations due to non-standard interactions of neutrinos with matter which can be tested in future long-baseline neutrino experiments (talk by E. Fernandez-Martinez). Neutrinoless double beta decay can be mediated not only by light Majorana neutrino masses but also by other mechanisms as heavy sterile neutrinos, supersymmetric R-parity violation. Once a positive signal is found, it will be critical to discriminate between the various mechanisms. S. Kom gave a contributed talk on LHC probes of SUSY neutrinoless double beta decay mechanism and C. Jackson on the issues related to understanding the mechanism of neutrinoless double beta decay with the SuperNEMO experiment. In the discussion session T. Ohlsson addressed the synergy and complementarity of these different experimental signatures in pinning down the mechanism at the origin of neutrino masses.

8.6. Discussion on performance indicators in long baseline experiments

Future long baseline neutrino oscillation experiments play a crucial role in determining the value of the unknown mixing angle θ_{13} , the type of neutrino mass hierarchy and the existence of CP-violation in the leptonic sector. A rich experimental program is under consideration for the near future: conventional and superbeam experiments (MINOS, OPERA, T2K, NOvA, LBNE) are already taking data, under construction or at the R&D phase while even more ambitious projects such as neutrino factories and beta-beams are studied. The sensitivity of the various setups is studied in detail. T. Li discussed the physics reach of the low energy neutrino factory and J. Lopez Pavon the search for 3+1 sterile neutrinos in contributed talks. It is necessary to compare the reach of different experiments in an objective way and with comparable assumptions. These issues were discussed in the round table lead by K. Long.

8.7. Conclusions

With the discovery of neutrino oscillations, neutrino physics has opened a new window on the physics BSM. This workshop has given the opportunity to review the status of the studies in neutrino phenomenology, theory and astroparticle physics with particular focus on the theoretical motivations for future precise neutrino oscillation experiments.

-
- [1] M. C. Gonzalez-Garcia, M. Maltoni, and J. Salvado, “Updated global fit to three neutrino mixing: status of the hints of $\theta_{13} > 0$,” *JHEP* **04** (2010) 056, [arXiv:1001.4524 \[hep-ph\]](#).
- [2] M. Mezzetto and T. Schwetz, “ θ_{13} : Phenomenology, present status and prospect,” *J.Phys.G* **37** (2010) 103001, [arXiv:1003.5800 \[hep-ph\]](#).
- [3] M. C. Gonzalez-Garcia, M. Maltoni, and J. Salvado, “Direct determination of the solar neutrino fluxes from solar neutrino data,” *JHEP* **05** (2010) 072, [arXiv:0910.4584 \[hep-ph\]](#).
- [4] A. Longhin, “A new design for the CERN-Fréjus neutrino Super Beam,” *Eur.Phys.J.* **C71** (2011) 1745, [arXiv:1106.1096 \[physics.acc-ph\]](#).
- [5] A. Donini, “Performances of Beta-beam setups as of January 2011,” 2011. EUROnu-WP6 internal note.
- [6] S. K. Agarwalla, “Atmospheric neutrino events at ICAL@INO and high Q β -beam,” 2011. EUROnu-WP6 internal note.
- [7] P. Coloma, A. Donini, P. Migliozi, L. S. Lavina, and F. Terranova, “A minimal Beta Beam with high-Q ions to address CP violation in the leptonic sector,” [arXiv:1004.3773 \[hep-ph\]](#).
- [8] C. Orme, “CP-violation reach of an electron capture neutrino beam,” *JHEP* **07** (2010) 049, [arXiv:0912.2676 \[hep-ph\]](#).
- [9] C. Orme, “High- γ Beta Beams within the LAGUNA design study,” [arXiv:1004.0939 \[hep-ph\]](#).
- [10] J. Tang and W. Winter, “Neutrino factory in stages: Low energy, high energy, off-axis,” *Phys. Rev. D* **81** (2010) 033005, [arXiv:0911.5052 \[hep-ph\]](#).
- [11] E. Fernandez Martinez, T. Li, S. Pascoli, and O. Mena, “Improvement of the low energy neutrino factory,” *Phys.Rev.* **D81** (2010) 073010, [arXiv:0911.3776 \[hep-ph\]](#).
- [12] A. Donini, J. J. Gomez Cadenas, and D. Meloni, “The τ -contamination of the golden muon sample at the Neutrino Factory,” *JHEP* **02** (2011) 95, [arXiv:1005.2275 \[hep-ph\]](#).
- [13] C. Giunti and M. Laveder, “Short-Baseline $\bar{\nu}_{\mu} \nu_e \rightarrow \bar{\nu}_{\mu} \nu_e$ Oscillations,” *Phys.Rev.* **D82** (2010) 093016, [arXiv:1010.1395 \[hep-ph\]](#).
- [14] E. Akhmedov and T. Schwetz, “MiniBooNE and LSND data: non-standard neutrino interactions in a (3+1) scheme versus (3+2) oscillations,” [arXiv:1007.4171 \[hep-ph\]](#).
- [15] D. Meloni, J. Tang, and W. Winter, “Sterile neutrinos beyond LSND at the Neutrino Factory,” [arXiv:1007.2419 \[hep-ph\]](#).
- [16] D. Meloni, T. Ohlsson, W. Winter, and H. Zhang, “Non-standard interactions versus non-unitary lepton flavor mixing at a neutrino factory,” *JHEP* **04** (2010) 041, [arXiv:0912.2735 \[hep-ph\]](#).
- [17] T. Ohlsson, T. Schwetz, and H. Zhang, “Non-standard neutrino interactions in the Zee-Babu model,” *Phys. Lett.* **B681** (2009) 269–275, [arXiv:0909.0455 \[hep-ph\]](#).
- [18] P. Huber, “Comparison of EUROnu facilities as of April 2011,” 2011. EUROnu-WP6 internal note.
- [19] S. Pascoli, “Summary of the NuFlavour workshop,” 2011. EUROnu-WP6 internal note.
- [20] J. Bernabeu *et al.*, “EURONU WP6 2009 yearly report: Update of the physics potential of Nufact, superbeams and betabeams,” [arXiv:1005.3146 \[hep-ph\]](#).
- [21] B. Pontecorvo, “Neutrino experiments and the question of leptonic-charge conservation,” *Sov. Phys. JETP* **26** (1968) 984–988.
- [22] V. N. Gribov and B. Pontecorvo, “Neutrino astronomy and lepton charge,” *Phys. Lett.* **B28** (1969) 493.
- [23] B. T. Cleveland *et al.*, “Measurement of the solar electron neutrino flux with the Homestake chlorine detector,” *Astrophys. J.* **496** (1998) 505–526.

- [24] F. Kaether, W. Hampel, G. Heusser, J. Kiko, and T. Kirsten, “Reanalysis of the GALLEX solar neutrino flux and source experiments,” *Phys. Lett. B* **685** (2010) 47–54, [arXiv:1001.2731 \[hep-ex\]](#).
- [25] **SAGE** Collaboration, J. N. Abdurashitov *et al.*, “Measurement of the solar neutrino capture rate with gallium metal. III: Results for the 2002–2007 data-taking period,” *Phys. Rev. C* **80** (2009) 015807, [arXiv:0901.2200 \[nucl-ex\]](#).
- [26] **Super-Kamiokande** Collaboration, J. Hosaka *et al.*, “Solar neutrino measurements in Super-Kamiokande-I,” *Phys. Rev. D* **73** (2006) 112001, [arXiv:0508053 \[hep-ex\]](#).
- [27] **SNO** Collaboration, B. Aharmim *et al.*, “Measurement of the ν/e and total B-8 solar neutrino fluxes with the Sudbury Neutrino Observatory phase I data set,” *Phys. Rev. C* **75** (2007) 045502, [arXiv:nucl-ex/0610020](#).
- [28] **SNO** Collaboration, B. Aharmim *et al.*, “Electron energy spectra, fluxes, and day-night asymmetries of B-8 solar neutrinos from the 391-day salt phase SNO data set,” *Phys. Rev. C* **72** (2005) 055502, [arXiv:nucl-ex/0502021](#).
- [29] **SNO** Collaboration, B. Aharmim *et al.*, “An Independent Measurement of the Total Active ^8B Solar Neutrino Flux Using an Array of ^3He Proportional Counters at the Sudbury Neutrino Observatory,” *Phys. Rev. Lett.* **101** (2008) 111301, [arXiv:0806.0989 \[nucl-ex\]](#).
- [30] **SNO** Collaboration, B. Aharmim *et al.*, “Low Energy Threshold Analysis of the Phase I and Phase II Data Sets of the Sudbury Neutrino Observatory,” *Phys. Rev. C* **81** (2010) 055504, [arXiv:0910.2984 \[nucl-ex\]](#).
- [31] **Borexino** Collaboration, C. Arpesella *et al.*, “Direct Measurement of the ^7Be Solar Neutrino Flux with 192 Days of Borexino Data,” *Phys. Rev. Lett.* **101** (2008) 091302, [arXiv:0805.3843 \[astro-ph\]](#).
- [32] **The Borexino** Collaboration, G. Bellini *et al.*, “Measurement of the solar ^8B neutrino rate with a liquid scintillator target and 3 MeV energy threshold in the Borexino detector,” *Phys. Rev. D* **82** (2010) 033006, [arXiv:0808.2868 \[astro-ph\]](#).
- [33] **Super-Kamiokande** Collaboration, Y. Ashie *et al.*, “A measurement of atmospheric neutrino oscillation parameters by super-kamiokande i,” *Phys. Rev. D* **71** (2005) 112005, [hep-ex/0501064](#).
- [34] **Super-Kamiokande** Collaboration, R. Wendell *et al.*, “Atmospheric neutrino oscillation analysis with sub-leading effects in Super-Kamiokande I, II, and III,” *Phys. Rev. D* **81** (2010) 092004, [arXiv:1002.3471 \[hep-ex\]](#).
- [35] **KamLAND** Collaboration, I. Shimizu, “KamLAND (anti-neutrino status),” *J. Phys. Conf. Ser.* **120** (2008) 052022.
- [36] **CHOOZ** Collaboration, M. Apollonio *et al.*, “Limits on Neutrino Oscillations from the CHOOZ Experiment,” *Phys. Lett. B* **466** (1999) 415–430, [arXiv:hep-ex/9907037](#).
- [37] **K2K** Collaboration, M. H. Ahn *et al.*, “Measurement of Neutrino Oscillation by the K2K Experiment,” *Phys. Rev. D* **74** (2006) 072003, [arXiv:hep-ex/0606032](#).
- [38] **MINOS** Collaboration, P. Adamson *et al.*, “Measurement of neutrino oscillations with the MINOS detectors in the NuMI beam,” *Phys. Rev. Lett.* **101** (2008) 131802, [arXiv:0806.2237 \[hep-ex\]](#).
- [39] **MINOS** Collaboration, P. Adamson *et al.*, “Search for muon-neutrino to electron-neutrino transitions in MINOS,” *Phys. Rev. Lett.* **103** (2009) 261802, [arXiv:0909.4996 \[hep-ex\]](#).
- [40] **MINOS** Collaboration, P. Adamson *et al.*, “New constraints on muon-neutrino to electron-neutrino transitions in MINOS,” *Phys. Rev. D* **82** (2010) 051102, [arXiv:1006.0996 \[hep-ex\]](#).
- [41] M. C. Gonzalez-Garcia and M. Maltoni, “Phenomenology with Massive Neutrinos,” *Phys. Rept.* **460** (2008) 1–129, [arXiv:0704.1800 \[hep-ph\]](#).
- [42] Z. Maki, M. Nakagawa, and S. Sakata, “Remarks on the unified model of elementary particles,” *Prog. Theor. Phys.* **28** (1962) 870–880.

- [43] M. Kobayashi and T. Maskawa, “CP Violation in the Renormalizable Theory of Weak Interaction,” *Prog. Theor. Phys.* **49** (1973) 652–657.
- [44] S. M. Bilenky, J. Hosek, and S. T. Petcov, “On Oscillations of Neutrinos with Dirac and Majorana Masses,” *Phys. Lett.* **B94** (1980) 495.
- [45] P. Langacker, S. T. Petcov, G. Steigman, and S. Toshev, “On the Mikheev-Smirnov-Wolfenstein (MSW) mechanism of amplification of neutrino oscillations in matter,” *Nucl. Phys.* **B282** (1987) 589.
- [46] G. L. Fogli, E. Lisi, A. Marrone, A. Palazzo, and A. M. Rotunno, “Neutrino masses and mixing: 2008 status,” *Nucl. Phys. Proc. Suppl.* **188** (2009) 27–30.
- [47] T. Schwetz, M. A. Tortola, and J. W. F. Valle, “Three-flavour neutrino oscillation update,” *New J. Phys.* **10** (2008) 113011, [arXiv:0808.2016 \[hep-ph\]](#).
- [48] M. Maltoni and T. Schwetz, “Three-flavour neutrino oscillation update and comments on possible hints for a non-zero θ_{13} ,” *Proc. of Science IDM* (2008) 072, [arXiv:0812.3161 \[hep-ph\]](#).
- [49] J. N. Bahcall, “Gallium solar neutrino experiments: Absorption cross sections, neutrino spectra, and predicted event rates,” *Phys. Rev.* **C56** (1997) 3391–3409, [arXiv:hep-ph/9710491](#).
- [50] P. Litchfield, “Review of atmospheric ν data.”. Talk given at the *XXII International Conference on Neutrino Physics*, Santa Fe, New Mexico, June 13–19, 2006.
- [51] R. Patterson, “New results for $\nu_\mu \rightarrow \nu_e$ oscillations in MINOS.”. Talk presented at the Fermilab National Accelerator Laboratory, April 9, 2010.
- [52] G. Pawloski, “New results for $\nu_\mu \rightarrow \nu_e$ oscillations in the MINOS experiment.”. Talk presented at the SLAC National Accelerator Laboratory, April 9, 2010.
- [53] A. Serenelli, S. Basu, J. W. Ferguson, and M. Asplund, “New Solar Composition: The Problem With Solar Models Revisited,” [arXiv:0909.2668 \[astro-ph.SR\]](#).
- [54] **CHOOZ** Collaboration, M. Apollonio *et al.*, “Search for neutrino oscillations on a long base-line at the CHOOZ nuclear power station,” *Eur. Phys. J. C* **27** (2003) 331–374, [arXiv:0301017 \[hep-ex\]](#).
- [55] G. L. Fogli, E. Lisi, A. Marrone, and A. Palazzo, “Global analysis of three-flavor neutrino masses and mixings,” *Prog. Part. Nucl. Phys.* **57** (2006) 742–795, [arXiv:0506083 \[hep-ph\]](#).
- [56] G. L. Fogli, E. Lisi, A. Marrone, A. Palazzo, and A. M. Rotunno, “Hints of $\theta_{13} > 0$ from global neutrino data analysis,” *Phys. Rev. Lett.* **101** (2008) 141801, [arXiv:0806.2649 \[hep-ph\]](#).
- [57] G. L. Fogli, E. Lisi, A. Marrone, A. Palazzo, and A. M. Rotunno, “SNO, KamLAND and neutrino oscillations: θ_{13} ,” [arXiv:0905.3549 \[hep-ph\]](#).
- [58] M. Maltoni, T. Schwetz, M. A. Tortola, and J. W. F. Valle, “Status of global fits to neutrino oscillations,” *New J. Phys.* **6** (2004) 122, [arXiv:0405172 \[hep-ph\]](#). Updated results in [hep-ph/0450172 \(v6\)](#).
- [59] S. Goswami and A. Y. Smirnov, “Solar neutrinos and 1-3 leptonic mixing,” *Phys. Rev. D* **72** (2005) 053011, [arXiv:0411359 \[hep-ph\]](#).
- [60] A. Balantekin and D. Yilmaz, “Contrasting solar and reactor neutrinos with a non-zero value of θ_{13} ,” *J. Phys. G* **35** (2008) 075007, [arXiv:0804.3345 \[hep-ph\]](#).
- [61] M. Maltoni, T. Schwetz, M. A. Tortola, and J. W. F. Valle, “Status of three-neutrino oscillations after the SNO-salt data,” *Phys. Rev. D* **68** (2003) 113010, [arXiv:0309130 \[hep-ph\]](#).
- [62] R. E. Shrock, “New tests for, and bounds on, neutrino masses and lepton mixing,” *Phys. Lett.* **B96** (1980) 159.
- [63] F. Vissani, “Non-oscillation searches of neutrino mass in the age of oscillations,” *Nucl. Phys. Proc. Suppl.* **100** (2001) 273–275, [arXiv:hep-ph/0012018](#).
- [64] Y. Farzan, O. L. G. Peres, and A. Y. Smirnov, “Neutrino mass spectrum and future beta decay experiments,” *Nucl. Phys.* **B612** (2001) 59–97, [arXiv:hep-ph/0105105](#).

- [65] J. Bonn *et al.*, “The Mainz neutrino mass experiment,” *Nucl. Phys. Proc. Suppl.* **91** (2001) 273–279.
- [66] V. M. Lobashev *et al.*, “Direct search for neutrino mass and anomaly in the tritium beta-spectrum: Status of ’Troitsk neutrino mass’ experiment,” *Nucl. Phys. Proc. Suppl.* **91** (2001) 280–286.
- [67] **KATRIN** Collaboration, A. Osipowicz *et al.*, “KATRIN: A next generation tritium beta decay experiment with sub-eV sensitivity for the electron neutrino mass,” [hep-ex/0109033](#).
- [68] H. V. Klapdor-Kleingrothaus *et al.*, “Latest Results from the Heidelberg-Moscow Double Beta Decay Experiment,” *Eur. Phys. J.* **A12** (2001) 147–154, [arXiv:hep-ph/0103062](#).
- [69] P. Vogel, “Neutrinoless double beta decay,” [arXiv:hep-ph/0611243](#).
- [70] F. T. Avignone, III, S. R. Elliott, and J. Engel, “Double Beta Decay, Majorana Neutrinos, and Neutrino Mass,” *Rev. Mod. Phys.* **80** (2008) 481–516, [arXiv:0708.1033 \[nucl-ex\]](#).
- [71] J. Lesgourgues and S. Pastor, “Massive neutrinos and cosmology,” *Phys. Rept.* **429** (2006) 307–379, [astro-ph/0603494](#).
- [72] R. Jimenez, T. Kitching, C. Pena-Garay, and L. Verde, “Can we measure the neutrino mass hierarchy in the sky?,” *JCAP* **1005** (2010) 035, [arXiv:arXiv:1003.5918 \[astro-ph.CO\]](#).
- [73] M. Gonzalez-Garcia, M. Maltoni, and J. Salvado, “Robust Cosmological Bounds on Neutrinos and their Combination with Oscillation Results,” *JHEP* **1008** (2010) 117, [arXiv:arXiv:1006.3795 \[hep-ph\]](#).
- [74] **Planck Collaboration** Collaboration, ESA, “The Scientific programme of Planck,” [arXiv:astro-ph/0604069 \[astro-ph\]](#).
- [75] **Daya-Bay** Collaboration, X. Guo *et al.*, “A precision measurement of the neutrino mixing angle θ_{13} using reactor antineutrinos at Daya Bay,” [arXiv:0701029 \[hep-ex\]](#).
- [76] **Double Chooz** Collaboration, F. Ardellier *et al.*, “Double Chooz: A Search for the neutrino mixing angle θ_{13} ,” [arXiv:hep-ex/0606025 \[hep-ex\]](#).
- [77] **RENO** Collaboration, J. K. Ahn *et al.*, “RENO: An Experiment for Neutrino Oscillation Parameter θ_{13} Using Reactor Neutrinos at Yonggwang,” [arXiv:1003.1391 \[hep-ex\]](#).
- [78] **NOvA** Collaboration, I. Ambats *et al.*, “Nova proposal to build a 30-kiloton off-axis detector to study neutrino oscillations in the fermilab numi beamline,” [hep-ex/0503053](#).
- [79] Y. Itow *et al.*, “The JHF-Kamioka neutrino project,” *Nucl. Phys. Proc. Suppl.* **111** (2001) 146–151, [arXiv:0106019 \[hep-ex\]](#).
- [80] A. de Gouvea and H. Murayama, “Statistical test of anarchy,” *Phys.Lett.* **B573** (2003) 94–100, [arXiv:hep-ph/0301050 \[hep-ph\]](#).
- [81] P. F. Harrison, D. H. Perkins, and W. G. Scott, “Tri-bimaximal mixing and the neutrino oscillation data,” *Phys. Lett. B* **530** (2002) 167, [arXiv:0202074 \[hep-ph\]](#).
- [82] V. D. Barger, S. Pakvasa, T. J. Weiler, and K. Whisnant, “Bimaximal mixing of three neutrinos,” *Phys.Lett.* **B437** (1998) 107–116, [arXiv:hep-ph/9806387 \[hep-ph\]](#).
- [83] G. Mention, T. Lasserre, and D. Motta, “A Unified analysis of the reactor neutrino program towards the measurement of the θ_{13} mixing angle,” *J.Phys.Conf.Ser.* **110** (2008) 082013, [arXiv:0704.0498 \[hep-ex\]](#).
- [84] M. Mezzetto, “Next Challenge in Neutrino Physics: The θ_{13} Angle,” [arXiv:0905.2842 \[hep-ph\]](#).
- [85] A. Suzuki, “ICFA report,” *PoS ICHEP2010* (2010) 564.
- [86] H. Bethe, “Energy production in stars,” *Phys.Rev.* **55** (1939) 434–456.
- [87] J. N. Bahcall, “NEUTRINO ASTROPHYSICS,”
- [88] J. N. Bahcall and R. K. Ulrich, “Solar Models, Neutrino Experiments and Helioseismology,” *Rev.Mod.Phys.* **60** (1988) 297–372.
- [89] S. Turck-Chieze, S. Cahen, M. Casse, and C. Doom, “Revisiting the standard solar model,” *Astrophys.J.* **335** (1988) 415–424.

- [90] J. N. Bahcall and M. Pinsonneault, “Standard solar models, with and without helium diffusion and the solar neutrino problem,” *Rev.Mod.Phys.* **64** (1992) 885–926.
- [91] J. N. Bahcall and M. Pinsonneault, “Solar models with helium and heavy element diffusion,” *Rev.Mod.Phys.* **67** (1995) 781–808, [arXiv:hep-ph/9505425](#) [hep-ph].
- [92] J. N. Bahcall, M. Pinsonneault, and S. Basu, “Solar models: Current epoch and time dependences, neutrinos, and helioseismological properties,” *Astrophys.J.* **555** (2001) 990–1012, [arXiv:astro-ph/0010346](#) [astro-ph].
- [93] J. N. Bahcall, A. M. Serenelli, and S. Basu, “New solar opacities, abundances, helioseismology, and neutrino fluxes,” *Astrophys.J.* **621** (2005) L85–L88, [arXiv:astro-ph/0412440](#) [astro-ph].
- [94] N. Grevesse and A. J. Sauval, “Standard Solar Composition,” *Space Sci.Rev.* **85** (1998) 161–174.
- [95] M. Asplund, N. Grevesse, and J. Sauval, “The Solar chemical composition,” *Nucl.Phys.* **A777** (2006) 1–4, [arXiv:astro-ph/0410214](#) [astro-ph].
- [96] M. Asplund, N. Grevesse, A. J. Sauval, and P. Scott, “The chemical composition of the Sun,” *Ann.Rev.Astron.Astrophys.* **47** (2009) 481–522, [arXiv:0909.0948](#) [astro-ph.SR].
- [97] J. N. Bahcall, S. Basu, M. Pinsonneault, and A. M. Serenelli, “Helioseismological implications of recent solar abundance determinations,” *Astrophys.J.* **618** (2005) 1049–1056, [arXiv:astro-ph/0407060](#) [astro-ph].
- [98] W. J. Chaplin, A. M. Serenelli, S. Basu, Y. Elsworth, R. New, *et al.*, “Solar heavy element abundance: constraints from frequency separation ratios of low-degree p modes,” *Astrophys.J.* **670** (2007) 872–884, [arXiv:0705.3154](#) [astro-ph].
- [99] S. Basu, W. J. Chaplin, Y. Elsworth, R. New, A. M. Serenelli, *et al.*, “Solar abundances and helioseismology: Fine structure spacings and separation ratios of low-degree p modes,” *Astrophys.J.* **655** (2007) 660–671, [arXiv:astro-ph/0610052](#) [astro-ph].
- [100] R. L. Hahn, “Radiochemical solar neutrino experiments, ‘successful and otherwise’,” *J.Phys.Conf.Ser.* **136** (2008) 022003.
- [101] **MINOS** Collaboration, P. Adamson *et al.*, “Search for muon-neutrino to electron-neutrino transitions in MINOS,” *Phys. Rev. Lett.* **103** (2009) 261802, [arXiv:0909.4996](#) [Unknown].
- [102] J. N. Bahcall, “The Luminosity constraint on solar neutrino fluxes,” *Phys.Rev.* **C65** (2002) 025801, [arXiv:hep-ph/0108148](#) [hep-ph].
- [103] J.-E. Campagne, M. Maltoni, M. Mezzetto, and T. Schwetz, “Physics potential of the CERN-MEMPHYS neutrino oscillation project,” *JHEP* **04** (2007) 003, [arXiv:hep-ph/0603172](#).
- [104] P. Zucchelli, “A novel concept for a $\bar{\nu}_e/\nu_e$ neutrino factory: The beta beam,” *Phys. Lett.* **B532** (2002) 166–172.
- [105] J. Bouchez, M. Lindroos, and M. Mezzetto, “Beta beams: Present design and expected performances,” *AIP Conf. Proc.* **721** (2004) 37–47, [hep-ex/0310059](#).
- [106] C. Rubbia, A. Ferrari, Y. Kadi, and V. Vlachoudis, “Beam cooling with ionisation losses,” *Nucl. Instrum. Meth.* **A568** (2006) 475–487, [hep-ph/0602032](#).
- [107] Y. Mori, “FFAG accelerators and their applications,” in *Proceedings of EPAC 2006, Edinburgh, Scotland*, pp. 950–954, EPAC. European Physical Society Accelerator Group, 2006.
- [108] A. Donini and E. Fernandez-Martinez, “Alternating ions in a beta-beam to solve degeneracies,” *Phys. Lett.* **B641** (2006) 432–439, [hep-ph/0603261](#).
- [109] E. Fernandez-Martinez, “The gamma = 100 beta-Beam revisited,” *Nucl.Phys.* **B833** (2010) 96–107, [arXiv:0912.3804](#) [hep-ph].
- [110] **DOUBLE-CHOOZ** Collaboration, Y. Abe *et al.*, “Indication for the disappearance of reactor electron antineutrinos in the Double Chooz experiment,” *Phys.Rev.Lett.* **108** (2012) 131801,

- arXiv:1112.6353 [hep-ex].
- [111] **DAYA-BAY Collaboration** Collaboration, F. An *et al.*, “Observation of electron-antineutrino disappearance at Daya Bay,” *Phys.Rev.Lett.* **108** (2012) 171803, arXiv:1203.1669 [hep-ex].
- [112] **RENO collaboration** Collaboration, J. Ahn *et al.*, “Observation of Reactor Electron Antineutrino Disappearance in the RENO Experiment,” *Phys.Rev.Lett.* **108** (2012) 191802, arXiv:1204.0626 [hep-ex].
- [113] J. Burguet-Castell, D. Casper, J. J. Gomez-Cadenas, P. Hernandez, and F. Sanchez, “Neutrino oscillation physics with a higher gamma beta-beam,” *Nucl. Phys.* **B695** (2004) 217–240, arXiv:hep-ph/0312068.
- [114] J. Burguet-Castell, D. Casper, E. Couce, J. J. Gomez-Cadenas, and P. Hernandez, “Optimal beta-beam at the CERN-SPS,” *Nucl. Phys.* **B725** (2005) 306–326, arXiv:hep-ph/0503021.
- [115] A. Donini, E. Fernandez, P. Migliozzi, S. Rigolin, L. Scotto Lavina, *et al.*, “Perspectives for a neutrino program based on the upgrades of the CERN accelerator complex,” arXiv:hep-ph/0511134 [hep-ph].
- [116] A. Donini *et al.*, “A beta beam complex based on the machine upgrades of the LHC,” *Eur. Phys. J.* **C48** (2006) 787–796, arXiv:hep-ph/0604229.
- [117] A. Donini, E. Fernandez-Martinez, P. Migliozzi, S. Rigolin, L. S. Lavina, *et al.*, “Neutrino hierarchy from CP-blind observables with high density magnetized detectors,” *Eur.Phys.J.* **C53** (2008) 599–606, arXiv:hep-ph/0703209 [HEP-PH].
- [118] P. Huber, M. Lindner, M. Rolinec, and W. Winter, “Physics and optimization of beta-beams: From low to very high gamma,” *Phys. Rev.* **D73** (2006) 053002, hep-ph/0506237.
- [119] S. K. Agarwalla, S. Choubey, and A. Raychaudhuri, “Neutrino mass hierarchy and θ_{13} with a magic baseline beta-beam experiment,” *Nucl. Phys. B* **771** (2007) 1–27, arXiv:hep-ph/0610333.
- [120] S. K. Agarwalla, S. Choubey, and A. Raychaudhuri, “Unraveling neutrino parameters with a magical beta-beam experiment at INO,” *Nucl.Phys.* **B798** (2008) 124–145, arXiv:0711.1459 [hep-ph].
- [121] P. Coloma, A. Donini, E. Fernandez-Martinez, and J. Lopez-Pavon, “ θ_{13} , δ and the neutrino mass hierarchy at a $\gamma = 350$ double baseline Li/B β -Beam,” *JHEP* **05** (2008) 050, arXiv:0712.0796 [hep-ph].
- [122] S. Choubey, P. Coloma, A. Donini, and E. Fernandez-Martinez, “Optimized Two-Baseline Beta-Beam Experiment,” *JHEP* **12** (2009) 020, arXiv:0907.2379 [hep-ph].
- [123] S. K. Agarwalla, S. Choubey, A. Raychaudhuri, and W. Winter, “Optimizing the greenfield beta-beam,” *JHEP* **06** (2008) 090, arXiv:0802.3621 [hep-ex].
- [124] S. K. Agarwalla, S. Choubey, and A. Raychaudhuri, “Exceptional sensitivity to neutrino parameters with a two baseline beta-beam set-up,” *Nucl. Phys. B* **805** (2008) 305–325, arXiv:0804.3007 [hep-ph].
- [125] M. Lindroos and M. Mezzetto, “Beta beams: Neutrino beams,”.
- [126] R. Battiston, M. Mezzetto, P. Migliozzi, and F. Terranova, “European facilities for accelerator neutrino physics: perspectives for the decade to come,” *Riv.Nuovo Cim.* **033** (2010) 313–343, arXiv:0912.3372 [hep-ex].
- [127] E. Wildner, “Beta Beams,” *Acta Phys. Polon.* **B41** (2010) 1525–1538.
- [128] A. Donini, E. Fernandez-Martinez, P. Migliozzi, S. Rigolin, and L. Scotto Lavina, “Study of the eightfold degeneracy with a standard beta-beam and a super-beam facility,” *Nucl. Phys.* **B710** (2005) 402–424, hep-ph/0406132.
- [129] A. Donini, E. Fernandez-Martinez, and S. Rigolin, “Appearance and disappearance signals at a beta-beam and a super-beam facility,” *Phys. Lett.* **B621** (2005) 276–287, hep-ph/0411402.

- [130] F. Terranova, A. Marotta, P. Migliozzi, and M. Spinetti, “High energy beta beams without massive detectors,” *Eur. Phys. J.* **C38** (2004) 69–77, [hep-ph/0405081](#).
- [131] S. K. Agarwalla, A. Raychaudhuri, and A. Samanta, “Exploration prospects of a long baseline beta beam neutrino experiment with an iron calorimeter detector,” [hep-ph/0505015](#).
- [132] C. Rubbia, “Ionization cooled ultra pure beta-beams for long distance $\nu/e \rightarrow \nu/\mu$ transitions, theta(13) phase and cp- violation,” [hep-ph/0609235](#).
- [133] A. Jansson, O. Mena, S. J. Parke, and N. Saoulidou, “Combining CPT-conjugate neutrino channels at Fermilab,” *Phys.Rev.* **D78** (2008) 053002, [arXiv:0711.1075 \[hep-ph\]](#).
- [134] W. Winter, “Minimal neutrino beta beam for large θ_{13} ,” *Phys. Rev.* **D78** (2008) 037101, [arXiv:0804.4000 \[hep-ph\]](#).
- [135] D. Meloni, O. Mena, C. Orme, S. Palomares-Ruiz, and S. Pascoli, “An Intermediate gamma beta-beam neutrino experiment with long baseline,” *JHEP* **0807** (2008) 115, [arXiv:0802.0255 \[hep-ph\]](#).
- [136] “EUROnu: A High Intensity Neutrino Oscillation Facility in Europe.” <http://www.euronu.org/>.
- [137] J. Bernabeu, J. Burguet-Castell, C. Espinoza, and M. Lindroos, “Monochromatic neutrino beams,” *JHEP* **12** (2005) 014, [arXiv:hep-ph/0505054](#).
- [138] J. Bernabeu and C. Espinoza, “Energy Dependence of CP-Violation Reach for Monochromatic Neutrino Beam,” *Phys. Lett.* **B664** (2008) 285–290, [arXiv:0712.1034 \[hep-ph\]](#).
- [139] J. Sato, “Monoenergetic neutrino beam for long baseline experiments,” *Phys. Rev. Lett.* **95** (2005) 131804, [arXiv:hep-ph/0503144](#).
- [140] M. Rolinec and J. Sato, “Neutrino beams from electron capture at high gamma,” *JHEP* **08** (2007) 079, [arXiv:hep-ph/0612148](#).
- [141] F. Matthew, “A survey of the introduction of rare-earth nuclei into the BETA-BEAM accelerator chain in order to attain a monochromatic neutrino beam,” 2007. EURISOL DS task note 12-25-2008-001.
- [142] C. Orme, “On the possibility of sourcing a mono-energetic $\bar{\nu}_e$ long baseline beta beam from bound beta decay,” [arXiv:0901.4287 \[hep-ph\]](#).
- [143] See <http://www.laguna-science.eu>.
- [144] A. Rubbia, “Experiments for CP-violation: A giant liquid argon scintillation, Cerenkov and charge imaging experiment?,” [arXiv:hep-ph/0402110](#).
- [145] O. B. *et. al.*, “Lhc luminosity and energy upgrade: A feasibility study,” 2002. CERN-LHC-PROJECT-REPORT-626, 2002.
- [146] S. Geer, O. Mena, and S. Pascoli, “A Low energy neutrino factory for large θ_{13} ,” *Phys. Rev.* **D75** (2007) 093001, [arXiv:hep-ph/0701258](#).
- [147] A. D. Bross, M. Ellis, S. Geer, O. Mena, and S. Pascoli, “A Neutrino factory for both large and small θ_{13} ,” *Phys. Rev.* **D77** (2008) 093012, [arXiv:0709.3889 \[hep-ph\]](#).
- [148] P. Huber and W. Winter, “Neutrino Factory Superbeam,” *Phys. Lett.* **B655** (2007) 251–256, [arXiv:0706.2862 \[hep-ph\]](#).
- [149] A. Bross *et al.*, “The multi-channel low energy neutrino factory,” [arXiv:0911.3776 \[hep-ph\]](#).
- [150] P. Huber, M. Lindner, T. Schwetz, and W. Winter, “First hint for CP violation in neutrino oscillations from upcoming superbeam and reactor experiments,” *JHEP* **11** (2009) 044, [arXiv:0907.1896 \[hep-ph\]](#).
- [151] A. Cervera *et al.*, “Golden measurements at a neutrino factory,” *Nucl. Phys.* **B579** (2000) 17–55, [arXiv:hep-ph/0002108](#).
- [152] C. Ankenbrandt *et al.*, “Low-energy neutrino factory design,” *Phys. Rev. ST Accel. Beams* **12** (2009) 070101.

- [153] **ISS Detector Working Group** Collaboration, T. Abe *et al.*, “Detectors and flux instrumentation for future neutrino facilities,” *JINST* **4** (2009) T05001, [arXiv:0712.4129](#) [[physics.ins-det](#)].
- [154] C. Rubbia, “The Liquid Argon Time Projection Chamber: A New Concept for Neutrino Detectors,” *CERN-EP-INT-77-08* (1977) .
- [155] **ISS Physics Working Group** Collaboration, A. Bandyopadhyay *et al.*, “Physics at a future Neutrino Factory and super-beam facility,” *Rept. Prog. Phys.* **72** (2009) 106201, [arXiv:0710.4947](#) [[hep-ph](#)].
- [156] V. Barger *et al.*, “Report of the US long baseline neutrino experiment study,” [arXiv:0705.4396](#) [[hep-ph](#)].
- [157] J. Kopp, T. Ota, and W. Winter, “Neutrino factory optimization for non-standard interactions,” *Phys. Rev.* **D78** (2008) 053007, [arXiv:0804.2261](#) [[hep-ph](#)].
- [158] A. M. Gago, H. Minakata, H. Nunokawa, S. Uchinami, and R. Zukanovich Funchal, “Resolving CP Violation by Standard and Nonstandard Interactions and Parameter Degeneracy in Neutrino Oscillations,” *JHEP* **01** (2010) 049, [arXiv:0904.3360](#) [[hep-ph](#)].
- [159] E. Fernández-Martínez, T. Li, O. Mena, and S. Pascoli. in preparation.
- [160] M. Blennow and E. Fernandez-Martinez, “Neutrino oscillation parameter sampling with MonteCUBES,” *Comput. Phys. Commun.* **181** (2010) 227–231, [arXiv:0903.3985](#) [[hep-ph](#)].
- [161] C. Biggio, M. Blennow, and E. Fernandez-Martinez, “General bounds on non-standard neutrino interactions,” *JHEP* **08** (2009) 090, [arXiv:0907.0097](#) [[hep-ph](#)].
- [162] D. Indumathi and N. Sinha, “Effect of tau neutrino contribution to muon signals at neutrino factories,” *Phys. Rev.* **D80** (2009) 113012, [arXiv:0910.2020](#) [[hep-ph](#)].
- [163] P. Huber, M. Lindner, M. Rolinec, and W. Winter, “Optimization of a neutrino factory oscillation experiment,” *Phys. Rev.* **D74** (2006) 073003, [arXiv:hep-ph/0606119](#).
- [164] R. Dutta, D. Indumathi, and N. Sinha, “Tau contamination in the platinum channel at neutrino factories,” *Phys.Rev.* **D85** (2012) 013003, [arXiv:1103.5578](#) [[hep-ph](#)].
- [165] **OPERA Collaboration** Collaboration, M. Guler *et al.*, “OPERA: An appearance experiment to search for ν_{μ} to ν_{τ} oscillations in the CNGS beam. Experimental proposal,”.
- [166] C. Andreopoulos *et al.*, “The GENIE Neutrino Monte Carlo Generator,” *Nucl. Instrum. Meth. A* **614** (2010) 87–104, [arXiv:0905.2517](#) [[hep-ph](#)].
- [167] P. Huber, M. Lindner, and W. Winter, “Superbeams versus neutrino factories,” *Nucl. Phys.* **B645** (2002) 3–48, [hep-ph/0204352](#).
- [168] M. Blennow, E. Fernandez-Martinez, J. Lopez-Pavon, and J. Menendez, “Neutrinoless double beta decay in seesaw models,” *JHEP* **1007** (2010) 096, [arXiv:1005.3240](#) [[hep-ph](#)].
- [169] J. Schechter and J. W. F. Valle, “Neutrinoless double-beta decay in $su(2) \times u(1)$ theories,” *Phys. Rev.* **D25** (1982) 2951.
- [170] P. Minkowski, “ $\mu \rightarrow e \gamma$ at a rate of one out of 1-billion μ on decays?,” *Phys. Lett.* **B67** (1977) 421.
- [171] T. Yanagida, “Horizontal gauge symmetry and masses of neutrinos.”. In Proceedings of the Workshop on the Baryon Number of the Universe and Unified Theories, Tsukuba, Japan, 13-14 Feb 1979.
- [172] R. N. Mohapatra and G. Senjanovic, “Neutrino mass and spontaneous parity nonconservation,” *Phys. Rev. Lett.* **44** (1980) 912.
- [173] M. Gell-Mann, P. Ramond, and R. Slansky, “COMPLEX SPINORS AND UNIFIED THEORIES,”. Print-80-0576 (CERN).
- [174] M. Magg and C. Wetterich, “Neutrino mass problem and gauge hierarchy,” *Phys. Lett.* **B94** (1980) 61.
- [175] J. Schechter and J. W. F. Valle, “Neutrino masses in $su(2) \times u(1)$ theories,” *Phys. Rev.* **D22** (1980) 2227.
- [176] C. Wetterich, “Neutrino masses and the scale of b-l violation,” *Nucl. Phys.* **B187** (1981) 343.

- [177] G. Lazarides, Q. Shafi, and C. Wetterich, “Proton lifetime and fermion masses in an so(10) model,” *Nucl. Phys.* **B181** (1981) 287.
- [178] R. N. Mohapatra and G. Senjanovic, “Neutrino Masses and Mixings in Gauge Models with Spontaneous Parity Violation,” *Phys. Rev.* **D23** (1981) 165.
- [179] R. Foot, H. Lew, X. G. He, and G. C. Joshi, “SEESAW NEUTRINO MASSES INDUCED BY A TRIPLET OF LEPTONS,” *Z. Phys.* **C44** (1989) 441.
- [180] E. Ma, “Pathways to Naturally Small Neutrino Masses,” *Phys. Rev. Lett.* **81** (1998) 1171–1174, [arXiv:hep-ph/9805219](#).
- [181] E. Ma and D. P. Roy, “Heavy triplet leptons and new gauge boson,” *Nucl. Phys.* **B644** (2002) 290–302, [arXiv:hep-ph/0206150](#).
- [182] T. Hambye, Y. Lin, A. Notari, M. Papucci, and A. Strumia, “Constraints on neutrino masses from leptogenesis models,” *Nucl. Phys.* **B695** (2004) 169–191, [arXiv:hep-ph/0312203](#).
- [183] S. Weinberg, “Baryon and Lepton Nonconserving Processes,” *Phys. Rev. Lett.* **43** (1979) 1566–1570.
- [184] P. Benes, A. Faessler, F. Simkovic, and S. Kovalenko, “Sterile neutrinos in neutrinoless double beta decay,” *Phys. Rev.* **D71** (2005) 077901, [arXiv:hep-ph/0501295](#).
- [185] A. Atre, T. Han, S. Pascoli, and B. Zhang, “The Search for Heavy Majorana Neutrinos,” *JHEP* **05** (2009) 030, [arXiv:0901.3589 \[hep-ph\]](#).
- [186] G. Belanger, F. Boudjema, D. London, and H. Nadeau, “Inverse neutrinoless double beta decay revisited,” *Phys. Rev.* **D53** (1996) 6292–6301, [arXiv:hep-ph/9508317](#).
- [187] F. Šimkovic, G. Pantis, J. D. Vergados, and A. Faessler, “Additional nucleon current contributions to neutrinoless double beta decay,” *Phys. Rev. C* **60** (1999) 055502, [hep-ph/9905509](#).
- [188] F. del Aguila and J. A. Aguilar-Saavedra, “Distinguishing seesaw models at LHC with multi-lepton signals,” *Nucl. Phys.* **B813** (2009) 22–90, [arXiv:0808.2468 \[hep-ph\]](#).
- [189] J. Menéndez, A. Poves, E. Caurier, and F. Nowacki, “Disassembling the Nuclear Matrix Elements of the Neutrinoless double beta Decay,” *Nucl. Phys. A* **818** (2009) 139–151, [arXiv:0801.3760 \[nucl-th\]](#).
- [190] M. Blennow, E. Fernandez-Martinez, J. Lopez-Pavon, and J. Menéndez, “Nuclear matrix elements as a function of the neutrino mass M_{ν} for the neutrinoless double beta decays of ^{48}Ca , ^{76}Ge , ^{82}Se , ^{124}Sn , ^{130}Te and ^{136}Xe ,” 2010. http://www.th.mppmu.mpg.de/members/blennow/nme_mnu.dat.
- [191] **CUORICINO** Collaboration, C. Arnaboldi *et al.*, “Results from a search for the $0\nu\beta\beta$ -decay of ^{130}Te ,” *Phys. Rev.* **C78** (2008) 035502, [arXiv:0802.3439 \[hep-ex\]](#).
- [192] H. V. Klapdor-Kleingrothaus and I. V. Krivosheina, “The evidence for the observation of $0\nu\beta\beta$ decay: The identification of $0\nu\beta\beta$ events from the full spectra,” *Mod. Phys. Lett.* **A21** (2006) 1547–1566.
- [193] G. Fogli *et al.*, “Observables sensitive to absolute neutrino masses. II.,” *Phys. Rev. D* **78** (2008) 033010, [arXiv:0805.2517 \[hep-ph\]](#).
- [194] S. Hannestad, A. Mirizzi, G. G. Raffelt, and Y. Y. Y. Wong, “Neutrino and axion hot dark matter bounds after WMAP-7,” *JCAP* **1008** (2010) 001, [arXiv:1004.0695 \[astro-ph.CO\]](#).
- [195] E. Komatsu *et al.*, “Seven-Year Wilkinson Microwave Anisotropy Probe (WMAP) Observations: Cosmological Interpretation,” [arXiv:1001.4538 \[astro-ph.CO\]](#).
- [196] **D0** Collaboration, V. Abazov *et al.*, “Search for pair production of doubly-charged Higgs bosons in the $H^{++}H^{--} \rightarrow \mu^+\mu^+\mu^-\mu^-$ final state at D0,” *Phys.Rev.Lett.* **101** (2008) 071803, [arXiv:0803.1534 \[hep-ex\]](#).
- [197] M. Maltoni and T. Schwetz, “Testing the statistical compatibility of independent data sets,” *Phys. Rev. D* **68** (2003) 033020, [arXiv:0304176 \[hep-ph\]](#).

- [198] **MiniBooNE** Collaboration, A. A. Aguilar-Arevalo *et al.*, “Observed event excess in the MiniBooNE search for $\bar{\nu}_\mu \rightarrow \bar{\nu}_e$ oscillations,” [arXiv:1007.1150](#) [[hep-ex](#)].
- [199] **LSND** Collaboration, A. Aguilar *et al.*, “Evidence for neutrino oscillations from the observation of $\bar{\nu}_e$ appearance in a $\bar{\nu}_\mu$ beam,” *Phys. Rev. D* **64** (2001) 112007, [arXiv:0104049](#) [[hep-ex](#)].
- [200] S. M. Bilenky, C. Giunti, and W. Grimus, “Phenomenology of neutrino oscillations,” *Prog. Part. Nucl. Phys.* **43** (1999) 1–86, [arXiv:hep-ph/9812360](#).
- [201] S. M. Bilenky, C. Giunti, J. A. Grifols, and E. Masso, “Absolute values of neutrino masses: Status and prospects,” *Phys. Rep.* **379** (2003) 69–148, [arXiv:hep-ph/0211462](#).
- [202] C. Giunti and M. Laveder, “Neutrino Mixing,” [arXiv:hep-ph/0310238](#). In “Developments in Quantum Physics – 2004”, p. 197-254, edited by F. Columbus and V. Krasnoholovets, Nova Science, Hauppauge, NY.
- [203] A. Strumia and F. Vissani, “Neutrino masses and mixings and...,” [arXiv:hep-ph/0606054](#).
- [204] C. Giunti and C. W. Kim, *Fundamentals of Neutrino Physics and Astrophysics*. Oxford University Press, Oxford, UK, 2007.
- [205] **MiniBooNE** Collaboration, A. A. Aguilar-Arevalo, “Unexplained Excess of Electron-Like Events From a 1-GeV Neutrino Beam,” *Phys. Rev. Lett.* **102** (2009) 101802, [arXiv:0812.2243](#) [[hep-ex](#)].
- [206] H. Murayama and T. Yanagida, “LSND, SN1987A, and CPT violation,” *Phys. Lett. B* **520** (2001) 263–268, [arXiv:0010178](#) [[hep-ph](#)].
- [207] G. Barenboim, L. Borisso, J. Lykken, and A. Y. Smirnov, “Neutrinos as the messengers of CPT violation,” *JHEP* **10** (2002) 001, [arXiv:hep-ph/0108199](#).
- [208] S. M. Bilenky, M. Freund, M. Lindner, T. Ohlsson, and W. Winter, “Tests of CPT invariance at neutrino factories,” *Phys. Rev.* **D65** (2002) 073024, [arXiv:hep-ph/0112226](#).
- [209] G. Barenboim, L. Borisso, and J. Lykken, “Neutrinos that violate CPT, and the experiments that love them,” *Phys. Lett.* **B534** (2002) 106–113, [arXiv:hep-ph/0201080](#).
- [210] A. Strumia, “Interpreting the lsnd anomaly: Sterile neutrinos or cpt- violation or...?,” *Phys. Lett.* **B539** (2002) 91–101, [hep-ph/0201134](#).
- [211] J. N. Bahcall, V. Barger, and D. Marfatia, “How accurately can one test cpt conservation with reactor and solar neutrino experiments?,” *Phys. Lett.* **B534** (2002) 120–123, [hep-ph/0201211](#).
- [212] H. Murayama, “CPT Tests: Kaon vs Neutrinos,” *Phys. Lett.* **B597** (2004) 73, [arXiv:hep-ph/0307127](#).
- [213] V. Barger, D. Marfatia, and K. Whisnant, “LSND anomaly from CPT violation in four-neutrino models,” *Phys. Lett. B* **576** (2003) 303–308, [arXiv:0308299](#) [[hep-ph](#)].
- [214] H. Minakata and S. Uchinami, “Testing CPT Symmetry with Supernova Neutrinos,” *Phys. Rev.* **D72** (2005) 105007, [arXiv:hep-ph/0505133](#).
- [215] M. C. Gonzalez-Garcia, M. Maltoni, and T. Schwetz, “Status of the CPT violating interpretations of the LSND signal,” *Phys. Rev. D* **68** (2003) 053007, [arXiv:0306226](#) [[hep-ph](#)].
- [216] M. Laveder, “Unbound neutrino roadmaps,” *Nucl. Phys. Proc. Suppl.* **168** (2007) 344–346. Talk presented at the Workshop on Neutrino Oscillation Physics (NOW 2006), Otranto, Lecce, Italy, 9-16 Sep 2006.
- [217] C. Giunti and M. Laveder, “ ν_e Disappearance in MiniBooNE,” *Phys. Rev.* **D77** (2008) 093002, [arXiv:0707.4593](#) [[hep-ph](#)].
- [218] S. Antusch and E. Fernandez-Martinez, “Signals of CPT Violation and Non-Locality in Future Neutrino Oscillation Experiments,” *Phys. Lett.* **B665** (2008) 190–196, [arXiv:0804.2820](#) [[hep-ph](#)].
- [219] C. Giunti and M. Laveder, “VSBL Electron Neutrino Disappearance,” *Phys. Rev.* **D80** (2009) 013005, [arXiv:0902.1992](#) [[hep-ph](#)].

- [220] A. D. Dolgov, “CPT violation and particle-antiparticle asymmetry in cosmology,” *Phys. Atom. Nucl.* **73** (2010) 588–592, [arXiv:0903.4318 \[hep-ph\]](#).
- [221] C. Giunti, M. Laveder, and W. Winter, “Short-Baseline Electron Neutrino Disappearance at a Neutrino Factory,” *Phys. Rev.* **D80** (2009) 073005, [arXiv:0907.5487 \[hep-ph\]](#).
- [222] G. Barenboim and J. D. Lykken, “Status of CPT-violating neutrinos,” *Phys. Rev.* **D80** (2009) 113008, [arXiv:0908.2993 \[hep-ph\]](#).
- [223] C. Giunti and M. Laveder, “Short-Baseline Electron Neutrino Disappearance, Tritium Beta Decay and Neutrinoless Double-Beta Decay,” [arXiv:1005.4599 \[hep-ph\]](#).
- [224] C. Giunti and M. Laveder, “Hint of CPT Violation in Short-Baseline Electron Neutrino Disappearance,” [arXiv:1008.4750 \[hep-ph\]](#).
- [225] B. Baibussinov *et al.*, “A new search for anomalous neutrino oscillations at the CERN-PS,” [arXiv:0909.0355 \[hep-ex\]](#).
- [226] I. Stancu *et al.*, “A Letter of Intent to Build a MiniBooNE Near Detector: BooNE,” [arXiv:0910.2698 \[hep-ex\]](#).
- [227] S. K. Agarwalla and P. Huber, “LSND reloaded,” [arXiv:1007.3228 \[hep-ph\]](#).
- [228] A. Rubbia, “Liquid Argon test module and test beam,” <http://indico.cern.ch/getFile.py/access?contribId=15&sessionId=2&resId=0&materialId=slides&confId=> Talk presented at NEU2012, 27-28 September 2010, CERN, Geneva, Switzerland.
- [229] **KARMEN** Collaboration, B. Armbruster *et al.*, “Upper limits for neutrino oscillations anti- ν / $\mu \rightarrow$ anti- ν / e from muon decay at rest,” *Phys. Rev.* **D65** (2002) 112001, [hep-ex/0203021](#).
- [230] **Bugey** Collaboration, B. Achkar *et al.*, “Search for neutrino oscillations at 15-meters, 40-meters, and 95-meters from a nuclear power reactor at Bugey,” *Nucl. Phys.* **B434** (1995) 503–534.
- [231] M. A. Acero, C. Giunti, and M. Laveder, “Limits on ν_e and $\bar{\nu}_e$ disappearance from Gallium and reactor experiments,” *Phys. Rev.* **D78** (2008) 073009, [arXiv:0711.4222 \[hep-ph\]](#).
- [232] M. Maltoni and T. Schwetz, “Sterile neutrino oscillations after first MiniBooNE results,” *Phys. Rev. D* **76** (2007) 093005, [arXiv:0705.0107 \[hep-ph\]](#).
- [233] G. Karagiorgi, Z. Djuric, J. M. Conrad, M. H. Shaevitz, and M. Sorel, “Viability of $\Delta m^2 \sim 1 \text{ eV}^2$ sterile neutrino mixing models in light of MiniBooNE electron neutrino and antineutrino data from the Booster and NuMI beamlines,” *Phys. Rev. D* **80** (2009) 073001, [arXiv:0906.1997 \[hep-ph\]](#).
- [234] A. Donini, K.-i. Fuki, J. Lopez-Pavon, D. Meloni, and O. Yasuda, “The discovery channel at the Neutrino Factory: $\nu_\mu \rightarrow \nu_\tau$ pointing to sterile neutrinos,” *JHEP* **08** (2009) 041, [arXiv:0812.3703 \[hep-ph\]](#).
- [235] S. K. Agarwalla, P. Huber, and J. M. Link, “Constraining sterile neutrinos with a low energy beta-beam,” *JHEP* **01** (2010) 071, [arXiv:0907.3145 \[hep-ph\]](#).
- [236] J. Hamann, S. Hannestad, G. G. Raffelt, I. Tamborra, and Y. Y. Wong, “Cosmology seeking friendship with sterile neutrinos,” [arXiv:1006.5276 \[hep-ph\]](#).
- [237] J. Kopp, M. Lindner, T. Ota, and J. Sato, “Non-standard neutrino interactions in reactor and superbeam experiments,” *Phys. Rev.* **D77** (2008) 013007, [arXiv:0708.0152 \[hep-ph\]](#).
- [238] T. Ohlsson and H. Zhang, “Non-Standard Interaction Effects at Reactor Neutrino Experiments,” *Phys. Lett.* **B671** (2009) 99–104, [arXiv:0809.4835 \[hep-ph\]](#).
- [239] P. Langacker and D. London, “Lepton number violation and massless nonorthogonal neutrinos,” *Phys. Rev.* **D38** (1988) 907.
- [240] E. Fernandez-Martinez, M. B. Gavela, J. Lopez-Pavon, and O. Yasuda, “CP-violation from non-unitary leptonic mixing,” *Phys. Lett.* **B649** (2007) 427–435, [arXiv:hep-ph/0703098](#).

- [241] S. Antusch, J. P. Baumann, and E. Fernandez-Martinez, “Non-Standard Neutrino Interactions with Matter from Physics Beyond the Standard Model,” *Nucl. Phys.* **B810** (2009) 369–388, [arXiv:0807.1003 \[hep-ph\]](#).
- [242] M. B. Gavela, D. Hernandez, T. Ota, and W. Winter, “Large gauge invariant non-standard neutrino interactions,” *Phys. Rev.* **D79** (2009) 013007, [arXiv:0809.3451 \[hep-ph\]](#).
- [243] A. Donini, M. Gavela, P. Hernandez, and S. Rigolin, “Neutrino mixing and CP violation,” *Nucl.Phys.* **B574** (2000) 23–42, [arXiv:hep-ph/9909254 \[hep-ph\]](#).
- [244] A. Kalliomaki, J. Maalampi, and M. Tanimoto, “Search for CP violation at a neutrino factory in a four neutrino model,” *Phys.Lett.* **B469** (1999) 179–187, [arXiv:hep-ph/9909301 \[hep-ph\]](#).
- [245] A. Donini, M. Lusignoli, and D. Meloni, “Telling three from four neutrinos at the neutrino factory,” *Nucl. Phys.* **B624** (2002) 405–422, [arXiv:hep-ph/0107231](#).
- [246] A. Donini and D. Meloni, “The 2+2 and 3+1 four-family neutrino mixing at the neutrino factory,” *Eur. Phys. J.* **C22** (2001) 179–186, [arXiv:hep-ph/0105089](#).
- [247] A. Dighe and S. Ray, “Signatures of heavy sterile neutrinos at long baseline experiments,” *Phys. Rev.* **D76** (2007) 113001, [arXiv:0709.0383 \[hep-ph\]](#).
- [248] S. Goswami and T. Ota, “Testing non-unitarity of neutrino mixing matrices at neutrino factories,” *Phys. Rev. D* **78** (2008) 033012, [arXiv:0802.1434 \[hep-ph\]](#).
- [249] M. Malinsky, T. Ohlsson, and H. Zhang, “Non-Standard Neutrino Interactions from a Triplet Seesaw Model,” *Phys. Rev.* **D79** (2009) 011301, [arXiv:0811.3346 \[hep-ph\]](#).
- [250] M. Malinsky, T. Ohlsson, and H. Zhang, “Non-unitarity effects in a realistic low-scale seesaw model,” [arXiv:0903.1961 \[hep-ph\]](#).
- [251] “International design study of the neutrino factory.” <http://www.ids-nf.org>.
- [252] A. Zee, “A theory of lepton number violation, neutrino majorana mass, and oscillation,” *Phys. Lett.* **B93** (1980) 389.
- [253] A. Zee, “Charged Scalar Field and Quantum Number Violations,” *Phys. Lett.* **B161** (1985) 141.
- [254] A. Zee, “QUANTUM NUMBERS OF MAJORANA NEUTRINO MASSES,” *Nucl. Phys.* **B264** (1986) 99.
- [255] K. S. Babu, “Model of ‘calculable’ majorana neutrino masses,” *Phys. Lett.* **B203** (1988) 132.
- [256] S. Davidson, C. Pena-Garay, N. Rius, and A. Santamaria, “Present and future bounds on non-standard neutrino interactions,” *JHEP* **03** (2003) 011, [arXiv:0302093 \[hep-ph\]](#).
- [257] M. Nebot, J. F. Oliver, D. Palao, and A. Santamaria, “Prospects for the Zee-Babu Model at the LHC and low energy experiments,” *Phys. Rev.* **D77** (2008) 093013, [arXiv:arXiv:0711.0483 \[hep-ph\]](#).
- [258] P. Huber, M. Lindner, and W. Winter, “Simulation of long-baseline neutrino oscillation experiments with GLoBES,” *Comput. Phys. Commun.* **167** (2005) 195, [hep-ph/0407333](#).
<http://www.mpi-hd.mpg.de/~globes>.
- [259] P. Huber, J. Kopp, M. Lindner, M. Rolinec, and W. Winter, “New features in the simulation of neutrino oscillation experiments with GLoBES 3.0,” *Comput. Phys. Commun.* **177** (2007) 432–438, [hep-ph/0701187](#). <http://www.mpi-hd.mpg.de/~globes>.
- [260] V. Barger, P. Huber, D. Marfatia, and W. Winter, “Which long-baseline neutrino experiments are preferable?,” *Phys. Rev. D* **76** (2007) 053005, [arXiv:0703029 \[hep-ph\]](#).